THESIS FOR THE DEGREE OF DOCTOR OF PHILOSOPHY

Millimeter-Waves Slot Array Antennas based on Gap Waveguide Technology

JINLIN LIU

CHALMERS

Department of Electrical Engineering
CHALMERS UNIVERSITY OF TECHNOLOGY

Göteborg, Sweden 2019

Millimeter-Waves Slot Array Antennas based on Gap Waveguide Technology

Jinlin Liu

Department of Electrical Engineering
Division of Communications and Antenna Systems
Chalmers University of Technology
SE–412 96 Göteborg
Sweden
Telephone: +46 (0)31 − 772 1000
Email: jinlin.liu@chalmers.se

Typeset by the author using LaTeX.

To my family

"Look deep into nature, and then you will understand everything better"

-Albert Einstein

Abstract

Recently, the gap waveguide technology is introduced as a promising guiding structure for millimeter-wave systems. The conception of the gap waveguide technology can be modeled for theoretical analysis by two parallel plates, a top perfect electric conductor layer and a bottom perfect magnetic conductor layer, and a wave guiding structure, such as a ridge, a groove waveguide or a microstrip line. This structure stops all other modes propagating in all directions except for a quasi-TEM mode along the guiding structure over a specific frequency band (stopband) when the gap between PEC and PMC plates is smaller than quarter wavelength at the operation frequency. Until now there are already four different versions of this novel concept—groove, ridge, inverted microstrip and microstrip ridge gap waveguides. The proposed thesis mainly focuses on array antenna design based on the gap waveguide technology. This thesis presents several low-profile single-layered and multilayer corporate-fed slot array antennas with high gain for the 60-GHz band and 140-GHz. The aim of this thesis is to demonstrate the advantages of the gap waveguide technology as an alternative to the conventional low-loss waveguide structure to overcome the problem of non-stable and non-guaranteed electrical contact in the conventional waveguide technology due to mechanical assembly. Measurement results and experimental validation are provided for the presented antenna designs.

Keywords: metallic pins, perfect magnetic conductor, inverted microstrip gap waveguide, ridge gap waveguide, slots array antenna, 60-GHz and 140-GHz.

Preface

This thesis is in partial fulfillment for the Doctor of Philosophy at Chalmers University of Technology.

The work that has resulted in this thesis was carried out between September 2014 and July 2019 and has been performed within the Division of Communications and Antennas Systems at the Department of Electrical Engineering, Chalmers University of Technology. The late Professor Per-Simon Kildal (from September 2014 to April 2016), Professor Jian Yang (from May 2016 to February 2019) and Associate Professor Ashraf Uz Zaman (from March 2019 to now) have been the main supervisors. Professor Jian Yang has been the examiner.

iv

Acknowledgments

List of Publications

This thesis is based on the work contained in the following appended papers:

Paper 1
J. Liu, Jian Yang, and A. U. Zaman, "Analytical Solutions towards Inverted Microstrip Gap Waveguide for characteristic Impedance and Losses based on variational Method", *IEEE Transactions on Antennas and Propagation*, vol. 66, no. 12, pp. 7049-7057, December, 2018.

Paper 2
J. Liu, A. Vosoogh, A. U. Zaman, and Jian Yang, "Design and Fabrication of a High-Gain 60-GHz Cavity-backed Slot Antenna Array fed by Inverted Microstrip Gap Waveguide", *IEEE Transactions on Antennas and Propagation*, vol. 65, no. 4, pp. 2117-2122, April, 2017.

Paper 3
J. Liu, A. U. Zaman, and Jian Yang, "A Low Sidelobe Double-Layer Corporate-Feed Array Antenna by Inverted Microstrip Gap Waveguide at 28 GHz", *International Symposium on Antennas and Propagation(ISAP)*, Oct. 28-31, 2019.

Paper 4
J. Liu, Jian Yang, and A. U. Zaman, "Design of Wideband Slot Array Antenna by Groove Gap Waveguide in Millimeter Waves", *IEEE-APS Topical Conference on Antennas and Propagation in Wireless Communications(APWC)*, Sept. 10-14, 2018.

Paper 5
J. Liu, A. U. Zaman, and Jian Yang, "A Slot Array Antenna With Single-Layered Corporate-Feed Based on Ridge Gap Waveguide in the 60-GHz Band", *IEEE Transactions on Antennas and Propagation*, vol. 67, no. 3, pp. 1650-1658, March, 2019.

Paper 6
J. Liu, A. U. Zaman, and Jian Yang, "Design and Fabrication of a 32×32-element Slot Array Antenna based on Ridge Gap Waveguide in D-Band", submitted to *IEEE Transactions on Antennas and Propagation*.

Other Publications

Additional related publications by the author, but not included in this thesis. The contents of these publications partially either overlap with the appended papers or are out of the scope of the thesis.

Paper A

J. Liu, A. Vosoogh, A. Uz Zaman and P.-S. Kildal, "Design of a Cavity-backed Slot Array Unit Cell on Inverted Microstrip Gap Waveguide", *Antennas and Propagation (ISAP), 2015 International Symposium on*, 24-28, October, 2015.

Paper B

J. Liu, A. Uz Zaman and P.-S. Kildal, "Optimizing the numerical port for inverted microstrip gap waveguide in full-wave simulators", *Antennas and Propagation (EU-CAP), Proceedings of the 10th European Conference on*, 10-15, April, 2016.

Paper C

J. Liu, A. Uz Zaman and P.-S. Kildal, "Design of transition from WR-15 to inverted microstrip gap waveguide," *2016 Global Symposium on Millimeter Waves (GSMM) Technology and Applications*, 6-8, June, 2016.

Paper D

J. Liu, A. Vosoogh, A. Uz Zaman and P.-S. Kildal, "Design of 8×8 slot array antenna based on inverted microstrip gap waveguide," *Antennas and Propagation (ISAP), 2016 International Symposium on*, 24-28, October, 2016.

Paper E

J. Liu, A. Vosoogh, A. Uz Zaman and Jian Yang, "A High-Gain High-Efficiency Corporate-Fed Slot Array Antenna directly Fed by Ridge Gap Waveguide at 60-GHz," *Antennas and Propagation (ISAP), 2017 International Symposium on*, 27-30, October, 2017. Best Paper Award 1st place

Paper F

J. Liu, A. Vosoogh, A. Uz Zaman and Jian Yang, "Slot Antenna Array Unit Cell Directly Fed by Inverted Microstrip Gap Waveguide," *Antennas and Propagation (ISAP), 2017 International Symposium on*, 27-30, October, 2017.

Paper G

J. Liu, A. Uz Zaman and Jian Yang, "Design of A Wideband Array Antenna Prototype with Gap Waveguide for W-Band Wireless Links," *Antennas and Propagation (EUCAP), Proceedings of the 12th European Conference on*, 8-12, April, 2018.

Paper H

J. Liu, A. Uz Zaman and Jian Yang, "Comparison among Microstrip, Covered Microstrip and Inverted Microstrip Gap Waveguide in Losses based on Variational Method in Millimeter Waves "*Swedish Microwave Days 2018*, 8th, July, 2018.

Paper I

J. Liu, A. Uz Zaman and Jian Yang, "Study of Dielectric Loss and Conductor Loss among Microstrip, Covered Microstrip and Inverted Microstrip Gap Waveguide Utilizing Variational Method in Millimeter Waves, "*Antennas and Propagation (ISAP), 2018 International Symposium on*, 24-28, October, 2018.

Paper J

J. Liu, A. Uz Zaman and Jian Yang, "Design of a 32 by 32 Slot Array Antenna based on Ridge Gap Waveguide at 140 GHz, "*The Cross Strait Quad-Regional Radio Science and Wireless Technology Conference*, 18-22, July, 2019.

Paper K

J. Liu, A. Uz Zaman and Jian Yang, "Two Types of High Gain Slot Array Antennas based on Ridge Gap Waveguide in the D-Band, "*IEEE-APS Topical Conference on Antennas and Propagation in Wireless Communications (APWC)*, 12-16, September, 2019.

Paper L

J. Liu, A. Uz Zaman and Jian Yang, "Double-layer corporate-fed Slot Array Antenna with Taylor-Distribution Synthesis by unequal Power Divider based on Inverted Microstrip Gap Waveguide at Ka-Band, to be submitted to *IEEE Transactions on Antennas and Propagation*, 2019.

x

List of Acronyms

5G	Fifth Generation
mmWs	Millimeter Waves
AMC	Artificial Magnetic Conductor
PEC	Perfect Electric Conductor
PMC	Perfect Magnetic Conductor
PNA	Performance Network Analyzer
IMGW	Inverted Microstrip Gap Waveguide
TEM	Transverse Electromagnetic
RF	Radio Frequency
RGW	Ridge Gap Waveguide
RX	Receiver
SIW	Substrate Integrated Waveguide
TE	Transverse Electric
TM	Transverse Magnetic
TX	Transmitter
VNA	Vector Network Analyzer
CNC	Computer Numerical Control
EDM	Electric Discharge Machining
ETSI	European Telecommunications Standards Institute
FCC	Federal Communications Commission
GGW	Groove Gap Waveguide
LTCC	Low Temperature Co-fired Ceramic
MEMS	Micro-Electro-Mechanical Systems
MMIC	Monolithic Microwave Integrated Circuit
PCB	Printed Circuited Broad
VSWR	Voltage Standing Wave Ratio

Contents

I   Introductory Chapters

Part I

Introductory Chapters

Chapter 1

Introduction of Gap Waveguide Technology and the Thesis

Communication technology has developed so fast in the past half century. In general, the communication technology has profound influences in the modern society. Today coordination and knowledge among people are facilitated by the rapid advancement of wireless and mobile communications. Wi-Fi and base station networks are now spread almost everywhere allowing people to access anytime with the mobile terminals. In 2020 the number of users will be exceeding five billion and expected to rise even more in the next decades. Potential commercial applications for wireless system include point to multi-point services, chip to chip high speed links, satellite communications, automotive radars, imaging and security systems. However, the current saturation of spectrum at microwave frequencies below 10 GHz is the major challenge.Thereby, it is necessary to explore new frequency bands in higher frequencies. Currently, considerable attention has been paid to millimeter and sub-millimeter wave communications [1]. However, wireless communications at such frequency bands are easily affected by the propagation loss and strong atmospheric absorption according to fundamental principles of electromagnetic field theory [2]. Therefore, waveguide
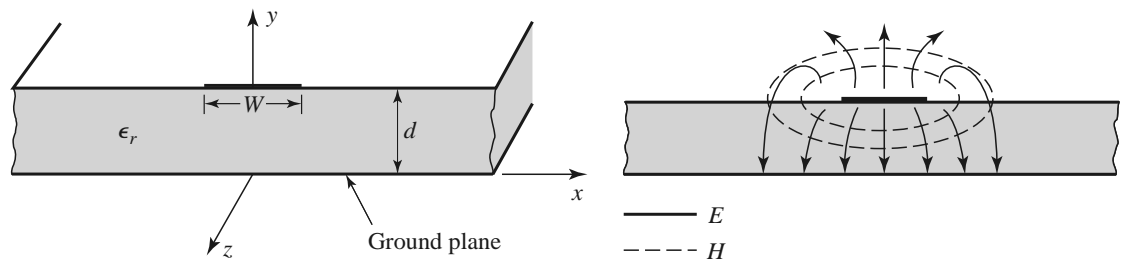
Figure 1.1: Microstrip Transmission Line.
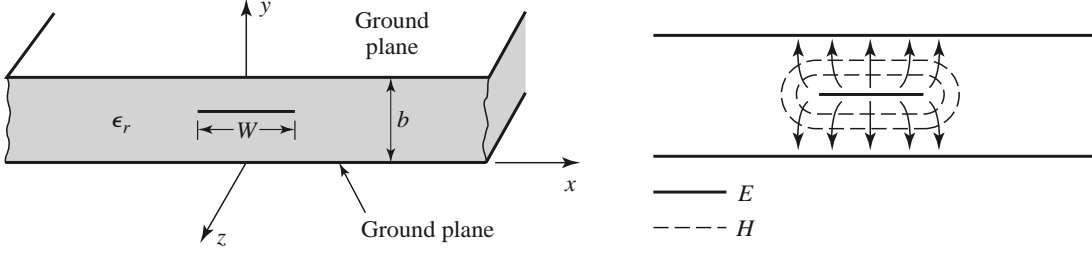
Figure 1.2: Stripline Transmission Line.

structures with low loss property and high gain antennas are required for such kinds of wireless systems.

As is well-known, different transmission lines are frequently utilized for communications systems. For example, specialized cable structures carry alternate current in a radio frequency (RF) system. In reality, transmission lines are used with the purposes such as connecting circuits for transmitter(TX), Receiver(RX) and antennas, distributed television cable and high speed bus system in a computer. The most common types of transmission lines in RF applications are microstrip line and stripline. A microstrip line is the most popular transmission line, as illustrated in Figure 1.1. A good conductor which is usually copper of width W is printed on a thin, grounded dielectric substrate of thickness d and relative permittivity ε_r. A regular sketch of the corresponding E- and H-fields is also shown in Figure 1.1. Similarly, the geometry of a stripline is depicted in Figure 1.2. A thin conducting strip of width W is centered between two wide conducting ground planes of separation b, the area between the ground planes is filled with a dielectric material. In reality, stripline is usually constructed by etching the center conductor on a grounded dielectric substrate of thickness $b/2$ and then covering with another grounded substrate.

Generally, the total loss of energy in a RF system consists of dielectric, conduction and radiation losses. Considering that those aforementioned two wave-guided structures suffer from dielectric substrate, the dielectric loss is unavoidable in them. The stripline and the microstrip line are typical applied topologies based on parallel-plate transmission line. Theoretically, the dielectric loss can be expressed as the multiplication of the frequency and loss tangent of the materials. Therefore, the corresponding dielectric loss squarely increases versus the frequency. The high dielectric loss is one of the main problems in transmission lines at millimeter waves(mmWs) frequency bands for planar array technologies.

The waveguide structure usually refers to the rectangular and circular waveguide. A typical geometry of rectangular waveguide is depicted in Figure 1.3. The hollow waveguide has characteristics of high power handling capability, good isolation, and can be used for large gain/high efficiency array antennas or high-Q filters. However,
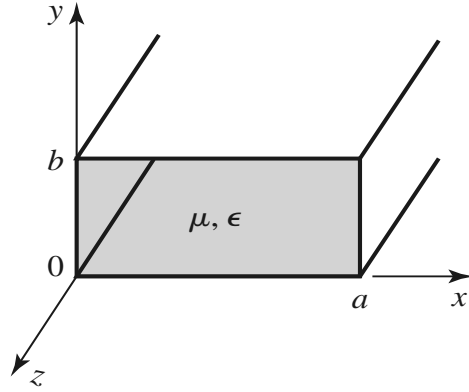
Figure 1.3: The geometry of a rectangular waveguide.

the fabrication cost of hollow waveguide is considered as a hinder in mmWs frequency bands. Until now we have several methods to fabricate waveguide structures, such as Computerized Numerical Control(CNC) machining and Electric Discharging Machining(EDM). Generally, the waveguide structures are typically manufactured in split-blocks and then connected by screwing, diffusion bonding or deep-brazing techniques. In mmWs frequency bands the split-blocks are very small so that the manufacture and the assembly outcomes are usually not accurate and perfect.

Substrate integrated waveguide (SIW) technology [3] has shown big advantages over both standard rectangular waveguide and printed circuit based transmission lines in mmWs. Geometrically, SIW is a compact planar printed circuit in which two rows of metallic via holes are embedded within a substrate material between two metallic plates, as illustrated in Figure 1.4. The electromagnetic behaviors of SIW is similar to those of rectangular waveguides with filled dielectrics [4]. The difference is that the electromagnetic waves propagate between two rows of metallic via holes
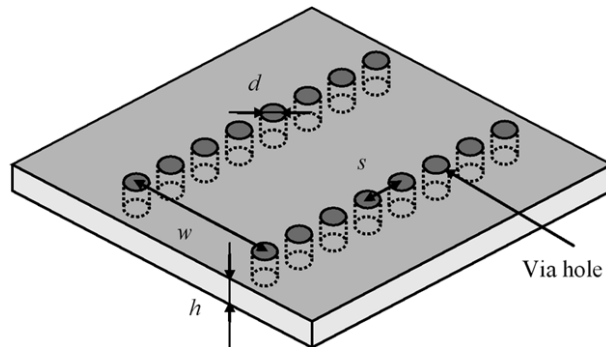
Figure 1.4: The geometry of a rectangular waveguide.

instead of metallic walls in rectangular waveguide. A large number of various array antennas fed by SIW distribution networks have been reported, such as in [5–12]. Moreover, SIW has an outstanding profile which facilities its easy integration with active RF components, such as low noise amplifier, power amplifier and mixer [13]. Nevertheless, SIW still has dielectric loss like normal microstrip lines due to the use of the substrate [14]. Applying low loss substrate materials is a choice to fabricate the SIW structure, but the dielectric loss still exists and its cost might increase. Another critical point to the overall loss in SIW is the leakage of energy through the gaps between metallic via holes when these are not properly organized or the operation frequencies are above 100 GHz [15]. Thereby, the dimensions of metallic via holes, the periodic space and the contact between two plates might increase the design complexity and the cost.

The recently introduced gap waveguide technology [16] constitutes a new type of wave guiding structure which presents lots of potentials to overcome the problems existing in conventional technologies mentioned before. The gap waveguide technology is based on the research results of soft- and hard- surfaces [17], which states the cutoff of electromagnetic fields when a metal plate is placed parallel to a textured artificial magnetic conductor (AMC) and their distance is smaller than quarter wavelength. The AMC surface is able to establish a high impedance surface boundary condition
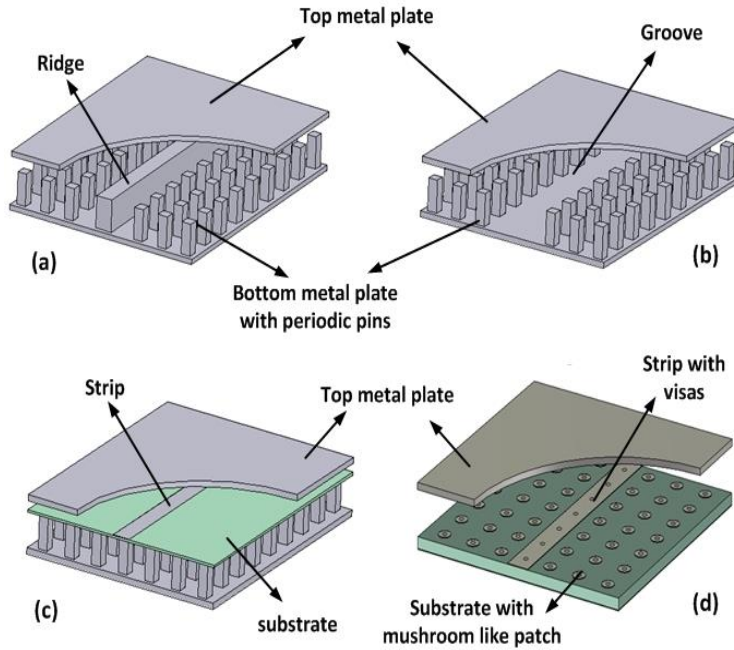
Figure 1.5: Four realized different gap waveguide geometries. (a) Ridge Gap Waveguide(RGW). (b) Groove Gap Waveguide(GGW). (c) Inverted Microstrip Gap Waveguide (IMGW). (d) Microstrip-Ridged Gap Waveguide.

that ensures together with the metal plate in a gap smaller than a quarter wavelength, the removal of any parallel-plate mode, cavity mode and surface waves within a certain frequency band (called as stopband). Usually this AMC is realized by the periodic structure of metallic pins or mushrooms. Then only a quasi-TEM mode is allowed to propagate confined within the air gap and along a desired path defined by a metallic ridge, groove or microstrip embedded in the AMC layer. Therefore, the gap waveguide technology is able to control the wave propagation in the desired paths, and forbids propagation of waves in undesired directions. Thereby, the gap waveguide technology is a promising wave guiding structure alternative to counteract the limitations of conventional technologies mentioned before in this chapter. So far there are four different realized versions based on guiding-line, propagation characteristics and the band gap structure: ridge gap waveguide(RGW), groove gap waveguide(GGW), inverted microstrip gap waveguide(IMGW) [18] and microstrip-ridge gap waveguide [19], as depicted in Figure 1.5. The RGW guides a quasi-TEM mode along the metallic ridge surrounding by metallic pins and no dielectric is required in the structure. The GGW can propagate a TE_{10} mode along the periodic pins surface. No substrate material is involved in the geometry. The IMGW guides a quasi-TEM mode along a microstrip etched on a Printed Circuited Broad (PCB). This PCB can be either supported by an AMC surface or AMC itself embedded in the substrate materials. In IMGW the field is mainly confined in the air gap. The gap waveguide technology has interesting characteristics such as low loss [18], easy manufacturing [20], and cost-effective RF integration [21] in mmW frequencies. The reason for the gap waveguides with low loss is that the wave propagates in the air. For example, the ridge and groove gap waveguide does not contain any dielectrics so that they can totally avoid the dielectric loss. Furthermore, the gap waveguides are mechanically more flexible to be fabricated and assembled than normal hollow waveguide. In addition, electrical contact between the building blocks is not needed anymore in these novel structures [22]. Thereby, these advantages offer good opportunities for making mmW antennas and corporate feed networks [23–33]. In practice, gap waveguide geometries can be manufactured by the usage of low cost fabrication techniques such as injection molding, die pressing, plastic hot embossing or EDM.

Another useful advantage of the gap waveguide technology is that the metallic pins are able to stop the surface current which is the origin for the metallic loss. This characteristic can be utilized to package the integrated circuits [34–37] and passive elements [38–41]. Microstrips and coplanar waveguide transmission lines are of open structures and the final products need to be protected from interference and physical damages. The traditional method is using metallic shielding boxes. However, the metallic shielding boxes may produce the surface current which creates cavity resonances in the shielding boxes when the dimensions of the boxes are larger than half wavelength. It is possible to suppress these resonances by adding absorber materials, which however introduces additional losses. The new gap waveguide technology can

avoid such problems introduced by using traditional methods.

1.1   Goal and outline of the thesis

In previous paragraphs, some existing challenges in the mmW technologies have been discussed briefly. There exists a big performance gap between the planar transmission lines such as microstrips, coplanar waveguide, SIW, multilayer technology and traditional hollow waveguide. One of the main current research challenges is to find a new guiding structure with flexible, low cost manufacture and low loss at the same time. Taking the mmW antenna design as examples, hollow waveguide is able to realize a high efficiency antenna, but the manufacture cost is very high. Microstrip and SIW have low cost and easy manufacture, but they suffer from high loss and low efficiency. Nevertheless, it is possible to utilize gap waveguide technology to have an optimal trade-off between the advantages and disadvantages of the conventional technologies. In this thesis, several different planar slot array antennas based on GGW, RGW and IMGW in the V-Band, W-Band and D-Band will be presented. In Chapter 2, an overview of the state-of-the-art of the planer mmWs antenna technologies is presented. In Chapter 3, an analytical analysis of IMGW is first summarized. Then two slot array antennas fed by IMGW are described briefly. In Chapter 4, the design and development of an 8×8 slot array antenna based on GGW in the W-Band is summarized. In Chapter 5, the design and its background of a single-layered corporate-fed array antenna in V-Band and the design work of a double-layered corporate-fed array antenna in D-Band are summarized. In Chapter 6, the thesis is summarized and concluded. In Chapter 7, I present the detailed my contributions in the papers the thesis is based on, and some thoughts on future work in the topic of the thesis. Above mentioned four antennas demonstrate high-gain, high-efficiency, low profile and low-cost fabrication. Thereby, those performances state that the gap waveguide technology has advantages over microstrip, coplanar array, SIW and standard waveguides. In the future, the gap waveguides technology will be a very good alternative to the traditional wave-guided structures for its potential in mmW frequency bands.

Chapter 2

Overview of the Planar Array Antenna Technologies in mmWs

The design and the manufacture of high-gain, high-efficiency and low-profile antennas are critical issues for mmWs communication systems. A conventional high-gain and high-efficiency antenna for backhauling systems is a parabolic reflector antenna or a lens antenna fed by a horn. Nevertheless, the bulky size and large profile make the reflector or lens antenna not suitable for integration with front-end planar circuits in micro-base stations. Thereby, a suitable high-gain and high-efficiency low-profile antenna is needed for the mmWs wireless communications. Usually, planar array antennas are very popular and widely utilized because of their advantages such as flat structure and low profile. Moreover, the main beam direction can be controlled by electronic steering. These advantages make them attractive for many applications, such as satellite communications, automotive radar and future base station antennas.

Table 2.1 lists 5 different planar array antennas in mmWs. In [12], a 4×4 mmW
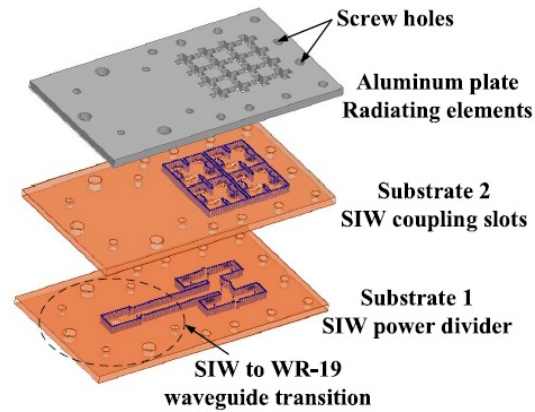
Figure 2.1: Geometry of the 4×4 array antenna with the SIW feeding network. Source: [12].

Table 2.1: Comparison among different Planar Array Antennas in mmW

Reference	[12]	[42]	[43]	[44]	[45]
Radiation Element	Metallic slot	Patch	Metallic slot	Patch	Metallic slot
Feed Networks	SIW	SIW/PCB	LTCC	SIW	Hollow Waveguide
No. of Elements	4×4	32×32	8×8	16×16	16×16
Sizes	3.84 mm × 3.84 mm	142 mm × 142 mm	47 mm × 31 mm	68 mm × 62 mm	72 mm × 67 mm
Frequency Band (GHz)	42-52	57-67	55-65	50-67	58-65
Input Impedance Bandwidth (-10 dB)	19%	16.7%	17%	27%	12.5%
Max.Gain (dBi)	19	34	23	34	32.5
Antenna efficiency	50%-60%	20%-30%	25%-35%	30%-40%	75%-85%

metallic slot array antenna has been reported. Figure 2.1 depicts the whole geometry of the array antenna, which consists of metallic slot radiation elements, the distribution feed network and the backed cavity layers by the surface SIW technology. The measured antenna gain is shown in Table 2.1. It can be observed that the realized maximal gain is only 19 dBi over 42 to 52 GHz, whereas the antenna efficiency is between 50% and 60%. Nevertheless, the array antenna is merely a small array, and it is not considered as a high-gain and high-efficiency antenna.
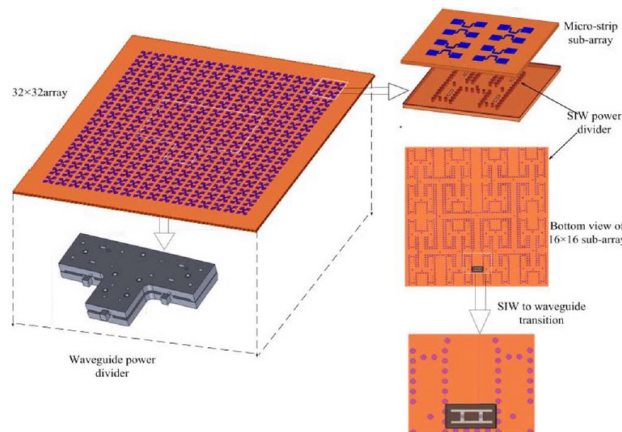
Figure 2.2: Geometry of the 32×32 patch array antenna with the SIW feeding network. Source: [42].
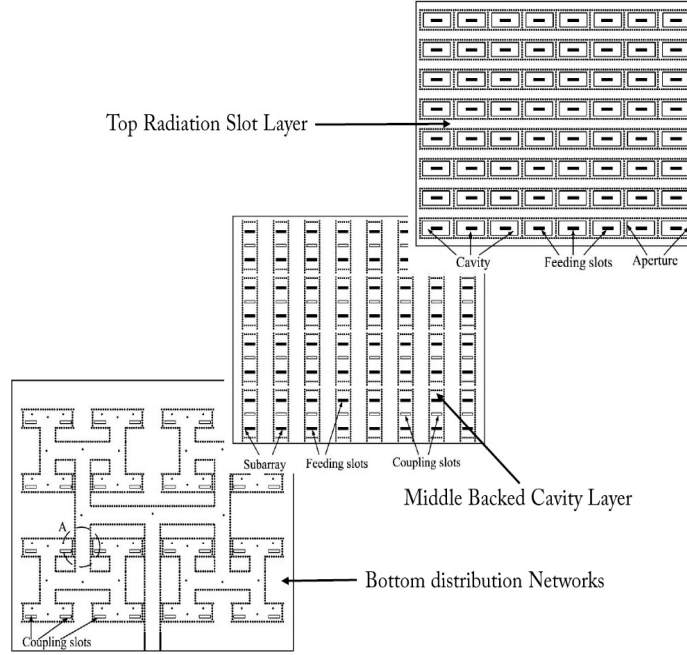
Figure 2.3: Geometry of the 8×8 slot array antenna with the LTCC feeding network. Source: [43].

In [42], a 32×32 patch array antenna with a SIW feeding network has been reported. Although the antenna array has low profile, it suffers from high dielectric and conducting ohmic losses in mmWs, which is a disadvantage for high-gain antenna applications. Figure 2.2 illustrates the geometry of the patch array antenna with the SIW feeding network. Table 2.1 shows the maximal gain of the array antenna in [42] is only 34 dBi with around 30% antenna efficiency.

Low-temperature co-firing ceramic(LTCC) technology can be defined as a multi-layer circuit fabricated by laminating substrates with printed conductor lines on the surface and firing them all together in one step. The big advantage of the LTCC system is the possibility to use low resistivity conductors like silver, gold, copper and alloys with palladium and platinum instead of tungsten and molybdenum. It is also possible to integrate passive elements like resistors, capacitors and inductors into the substrate. In [43], a full-corporate-fed slot array antenna with the backed cavity layer has been reported. Figure 2.3 depicts the configuration of the whole structure, which consists of classic three layers— the bottom distribution network layer, the middle backed-cavity layer and the top slot radiation layer. The measured gain reaches 23 dBi with 30% antenna efficiency. The disadvantages of the LTCC technology are also obvious. Firstly, the total losses from the fabrication tolerance and substrate are always unavoidable. Secondly, the cost of the fabrication process is very expensive in mmW.

Another SIW-fed patch array antenna has been reported in [44]. Figure 2.4 de-
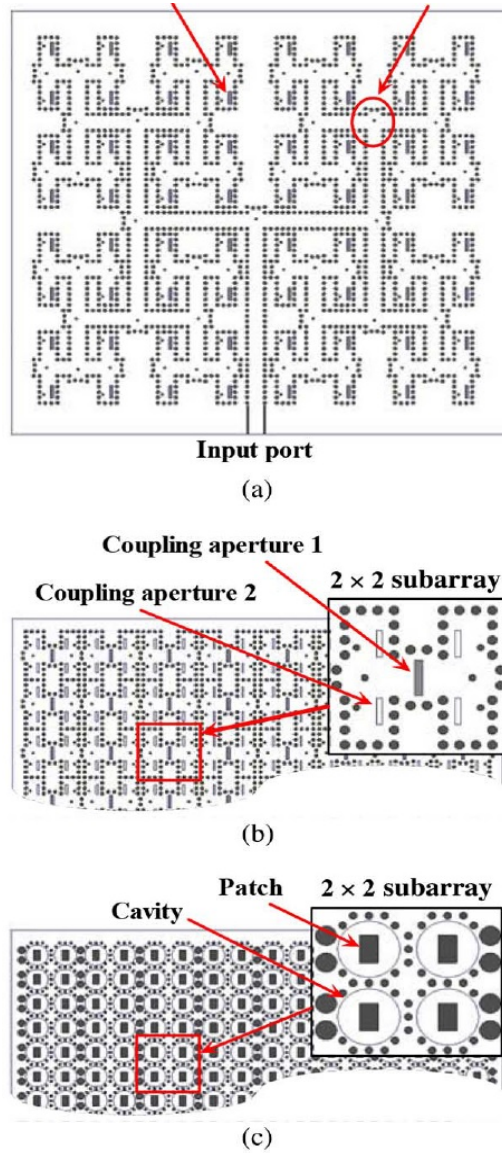
Figure 2.4: Geometry of the 16×16 patch array antenna with the SIW feeding network. Source: [44].

picts the configuration of the entire array antenna. In this design, a cylindrical cavity is adapted surrounding each radiation patch to improve the bandwidth of the entire array antenna. As stated in Table 2.1, the input impedance bandwidth is 27%, which is much broader than other designs. Nevertheless, the antenna efficiency is limited within 40%. For SIW-fed array antenna, high dielectric loss is always a critical issue. Probably, low-loss substrate materials are a choice for the antenna design. However, they are mechanically soft, and such a solution is usually very expensive.

Based on the analysis from above four examples, a high-gain array antenna

generally consists of a large number of sub-arrays, power dividers and transmission lines. Furthermore, every component requires very low loss so that the high-gain and high-efficiency properties can be achieved. Although microstrip and SIW arrays have low profile in geometry, dielectric and conducting ohmic losses are unavoidable, which is a huge disadvantage for high gain antenna applications in mmWs.

In [45], a classic double-layered corporate-fed slot array antenna at 60-GHz has been proposed. The entire geometry is depicted in Figure 2.5. As an example shown with the performance of the slot antenna in [45], slotted waveguide array antennas have been known for high-gain, high-efficiency, low-profile and high-power applications. However, the array antenna has been manufactured by diffusion bonding of laminated thin copper plates in order to achieve good electrical contact between all the plates. This fabrication technology is usually very expensive for mass production. Thereby, the manufacture of a complex waveguide structure is always a challenging task, especially above 30 GHz.

For mmWs array antenna design, the key issues, such as reducing the losses and
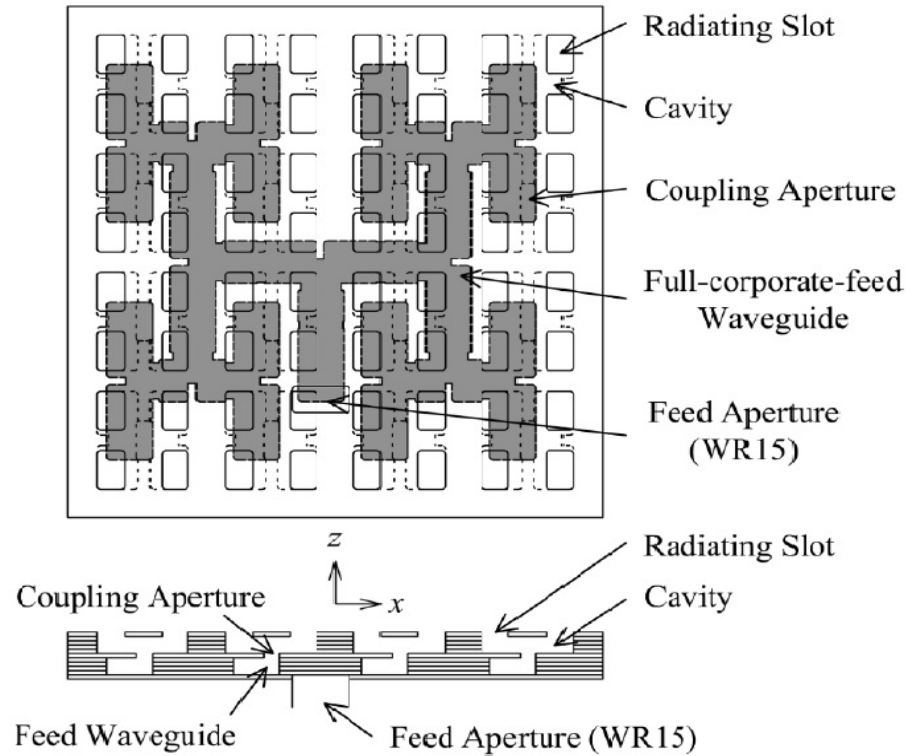
Figure 2.5: A typical configuration of 16×16 slot array antenna fed by hollow waveguide. Source: [45].

the manufacture cost, have been explored through our careful check for every technology. Dielectric and conductor losses always exist in substrate family—microstrip, strip line, covered microstrip, LTCC and SIW. The high dielectric loss in mmWs indicates that the transmission lines with substrate are not suitable for high-gain and high-efficiency planar arrays. On the other hand, the traditional hollow waveguides have the fabrication problems in mmWs even they provide low ohmic loss. Indeed, a hollow waveguide is usually manufactured in two parts and then joined together. This fabrication method usually suffers from problems of poor electrical contacts. This is even more critical if we want to fabricate a multilayer waveguide slot array antenna in mmWs where precise assembly is needed. Therefore, a new waveguide structure that can realize low loss property and avoid the non-stable and non- guaranteed electrical contact in mmWs is of interest. The research goal of my thesis project is to find solutions to the problems mentioned above.

Chapter 3

High-Gain Array Antennas based on IMGW

In chapter 2, the planar array antennas fed by microstrip, LTCC, SIW, and hollow waveguide have been carefully reviewed. The challenges of above mentioned transmission lines depend mainly on the high dielectric loss and fabrication complexity. In this chapter, my research work on a low loss transmission line with substrate - IMGW is summarized. First of all, the work that the classic variational method is applied for analyzing IMGW[paper 1] is summarized. The dielectric losses and the conductor losses among the microstrip, covered microstrip and IMGW in mmWs are analytically calculated based on the variational method. As a comparison reference, the conductor loss and the dielectric loss of SIW are included in this chapter. Secondly, the development of a high-gain array antenna based on IMGW is summarized in this chapter. The whole structure based on IMGW consists of radiation slots, groove gap cavity layer, distribution feeding network and a transition from standard WR-15 waveguide to IMGW. The complete antenna array is designed and fabricated using Electrical Discharging Machining (EDM) technology. The measurement shows that the antenna has 16.95% bandwidth covering 54-64 GHz frequency range. The measured gain of the antenna is more than 28 dBi with the efficiency higher than 40% covering 54-64 GHz frequency range. Compared with the slot array antennas introduced in [42] and [44], IMGW shows strong competitive strength in high-gain, high-efficiency array antennas. Lastly, the design work on a novel low sidelobe array antenna, which is fed by classic double-layer distribution networks based on IMGW is summarized. In order to achieve low sidelobe property, a classic Taylor synthesis method is adopted in this work. In the distribution network, a couple of unequal power dividers with identical output phases are applied for achieving low sibelobe in this work. The simulated radiation patterns show that the first sidelobe levels, front-back ratio of both E-plane and H-plane from 26.5 to 29.5 GHz are significantly improved compared with the equal amplitude and phase distribution networks. The input impedance bandwidth is about 12% with the reflection coefficient below -10
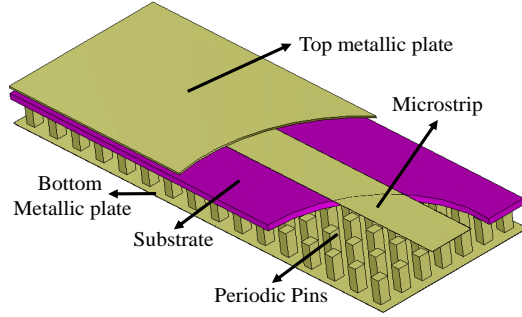
Figure 3.1: Brief geometry of the IMGW. Source: [Paper 3].

dB, and the gain is more than 29 dBi from 26.5 to 29.5 GHz.

3.1   Loss Comparison among various Transmission Lines in mmWs

The IMGW technology is based on the presence of a thin substrate that lies over a periodic pin pattern similar to the bed of nails. This bed of nails constitutes an artificial magnetic conductor(AMC) material and the combination with the upper metal lid prohibits any wave propagation within the air gap, also in the presence of the dielectric layer. Then, a wave guiding structure - the strip etched on the substrate is introduced to allow a quasi-TEM wave propagate only along the strip in the air gap between the strip and the upper metal. Figure 3.1 shows the basic layout of the IMGW. The main advantage of this IMGW is that wave is allowed to propagate only in the air gap. Thereby, the high dielectric loss in PCB is avoided. In addition, the pin plate with uniform pin period can be easily fabricated by low cost metal sawing or wire-cut technique.

As shown in Figure 3.2, the metallic textured pins surface can be modeled by an approximate Magnetic Conductor boundary condition according to the soft- and hard-surfaces theory [17]. The cross-section view of an IMGW, a covered microstrip line and a microstrip line are illustrated in Figure 3.3. The TEM mode in the above transmission lines can be described by a model of electrostatic fields as the dominant mode when the strip width is much smaller than a wavelength, even when a nonuniform medium is applied in the structure. Therefore, the TEM mode problem can be treated as an electrostatic model, namely solving a Poisson's equation or a Laplace's

Figure 3.2: The abstraction of the IMGW.
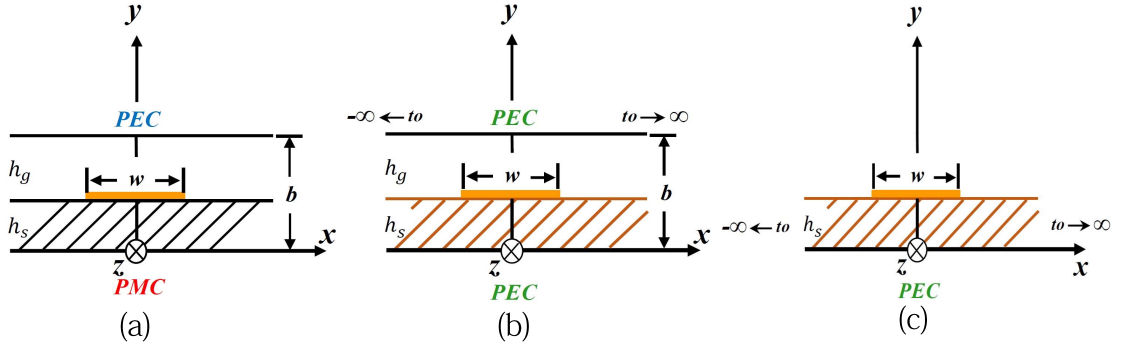
Figure 3.3: Cross-sectional view for (a) Inverted Microstrip Gap Waveguide, (b) Covered Microstrip, (c) Microstrip.

equation [paper 1]:

$$\nabla^2 \psi(x,y) = \frac{\partial^2 \psi(x,y)}{\partial x^2} + \frac{\partial^2 \psi(x,y)}{\partial y^2} = -\frac{\rho(x,y)}{\varepsilon}. \tag{3.1}$$

where ε is the permittivity of the substrate in the ideal IMGW. In reality, the thickness of microstrip is much smaller than the width w so that the microstrip can be considered as infinitesimally thin and $\rho(x,y)$ can be described by

$$\rho(x,y) = f(x)\delta(y - h_s) \tag{3.2}$$

where $\delta(y - h_s)$ is the Dirac's function and $f(x)$ the charge density distribution on the microstrip.

$$f(x) = 0.5 + \left|\frac{x}{w}\right|^3, |x| \leq \frac{w}{2} \quad and \quad 0.3 \ mm \leq w \leq 3 \ mm. \tag{3.3}$$

The Green's function G, regarded as the potential due to a unit charge in an infinitely small volume at (x', y'), is the solution to the equation of

$$\nabla^2 G(x, x'; y, y') = -\frac{1}{\varepsilon}\delta(x - x')\delta(y - y') \tag{3.4}$$

where $\delta(x - x')\delta(y - y')$ is the Dirac's function which expresses a unit charge. Once the Green's function G is obtained, the electric potential $\psi(x, y)$ due to the charge distribution $\rho(x', y')$ can be determined by the superposition principle expressed as:

$$\psi(x, y) = \int_{l'} G(x, x'; y, y')\rho(x', y')dl' \tag{3.5}$$

where the integral is defined over the conductor contour l' in 2-D cross sectional structure. Generally, it is very difficult to solve the Green's function. According to the differential property of the Fourier transform, namely, $\frac{\partial^2 \psi(x,y)}{\partial x^2} \Leftrightarrow (jk)^2 \widetilde{\psi}(k, y)$,

$$-k^2 \widetilde{\psi}(k, y) + \frac{\partial^2 \widetilde{\psi}(k, y)}{\partial y^2} = 0 \qquad (y \neq h_s). \tag{3.6}$$

In spectrum domain the solution of the potential distribution on the microstrip can be expressed as:

$$\widetilde{\psi}(k, y) = \widetilde{f}(k)\widetilde{G}(k, y), \tag{3.7}$$

where $\widetilde{f}(k)$ and $\widetilde{G}(k, y)$ are the charge density and the Green's function in spectrum domain. The corresponding Green's functions of microstrip, covered microstrip and IMGW are given by (3.8), (3.9) and (3.10), respectively,

$$\widetilde{G}_m(k, h_s) = \frac{sinh(kh_g)}{k[\varepsilon_0 cosh(kh_g) + \varepsilon_s sinh(kh_s)]}. \tag{3.8}$$

$$\widetilde{G}(k, h_s) = \frac{sinh(kh_g)sinh(kh_s)}{k[\varepsilon_0 sinh(kh_g)cosh(kh_s) + \varepsilon_s cosh(kh_g)sinh(kh_s)]}. \tag{3.9}$$

$$\widetilde{G}(k, h_s) = \frac{sinh(kh_g)cosh(kh_s)}{k[\varepsilon_0 cosh(kh_s)cosh(kh_g) + \varepsilon_s sinh(kh_s)sinh(kh_g)]}. \tag{3.10}$$

The conductor loss α_c is given by:

$$\alpha_c = \frac{R_s \int_l i_s^2 dl}{2\int_S v\varepsilon(\nabla\psi)^2 dS} \quad [Neper/Unit\ Length] \tag{3.11}$$

where $R_s = \sqrt{0.5\omega\mu_0/\sigma_c}$ is the surface resistance, σ_c the conductivity of the microstrip, $i_s = v\rho(x, h_s)$ the current density on the microstrip, and $v = c\sqrt{C_0/C}$ the propagation velocity. Similarly, the attenuation constant due to the dielectric loss can be calculated by :

$$\alpha_d = \frac{\sigma_d \int_S (\nabla\psi)^2 dS}{2\int_S v\varepsilon(\nabla\psi)^2 dS} \quad [Neper/Unit\ Length] \tag{3.12}$$

Table 3.1 summarizes the calculated dielectric loss and the conductor loss of microstrip, covered microstrip, IMGW and SIW [14]. For the analysis, we have selected the same dielectric materials Rogers 4003 with the identical thickness. From this

Table 3.1: The Loss Comparison among different Transmission Lines

Losses/Types	Microstrip	Covered Microstrip	Inverted Microstrip Gap Waveguide	SIW
Dielectric Loss	1.2 dB/cm	1.1 dB/cm	0.15 dB/cm	0.35 dB/cm
Conductor Loss	0.09 dB/cm	0.1 dB/cmB	0.1 dB/cm	0.1 dB/cm

table we can easily see that the dielectric loss is dominant and the conductor loss is almost identical among the various transmission lines in mmWs. The dielectric losses of microstrip and covered microstrip lines are almost 7 times higher than IMGW. The dielectric loss of the SIW is also lower than traditional microstrip and covered microstrip lines. Nevertheless, it is a big challenge for SIW to design and fabricate an array antenna gain larger than 30 dBi because it needs a large number of power divider and longer SIW transmission lines. According to the theory in this section, the unavoidable dielectric losses for SIW, microstrip, covered microstrip and IMGW are usually characterized by three factors, the electromagnetic field distributions in both the air gap and the substrate, the loss tangent value and the dimensions of the substrate. Thereby, the dielectric loss may be decreased by using thinner substrate materials. Furthermore, the application of substrate materials with low-loss tangent value is also a choice to decrease the dielectric loss, but the corresponding cost might be increased. Lastly, changing the distribution of the electromagnetic field is a better choice to reduce the dielectric loss and the inverted microsrip gap waveguide is introduced based on this idea. Applying high impedance surface at the bottom of substrate is able to make the electromagnetic wave to propagate in the air gap so that the dielectric loss is significantly decreased, as listed in Table 3.1.

3.2 A high-gain Slot Array Antenna on IMGW in the V-band

As mentioned in previous section, IMGW has low dielectric loss and it is suitable to be applied in high-gain planar array antennas in mmWs. Figure 3.4 depicts the configuration of a 16×16 slot array antenna fed by IMGW. The details of the antenna can be found in [Paper 2]. The metal block of the designed prototype is etched by recurring electric discharges between the workpiece and electrodes. The final designed array aperture dimension is 64×64 mm^2 (8 mm×8 mm× 64 elements). The simulated and measured input reflection coefficients of the proposed antenna are shown in Figure 3.5. The measured S_{11} is a bit higher than the simulation. However, it is still below -10 dB from 54.5 GHz to 66 GHz (19.2% impedance bandwidth). There are some differences between the simulated and measured results. As discussed in [Paper
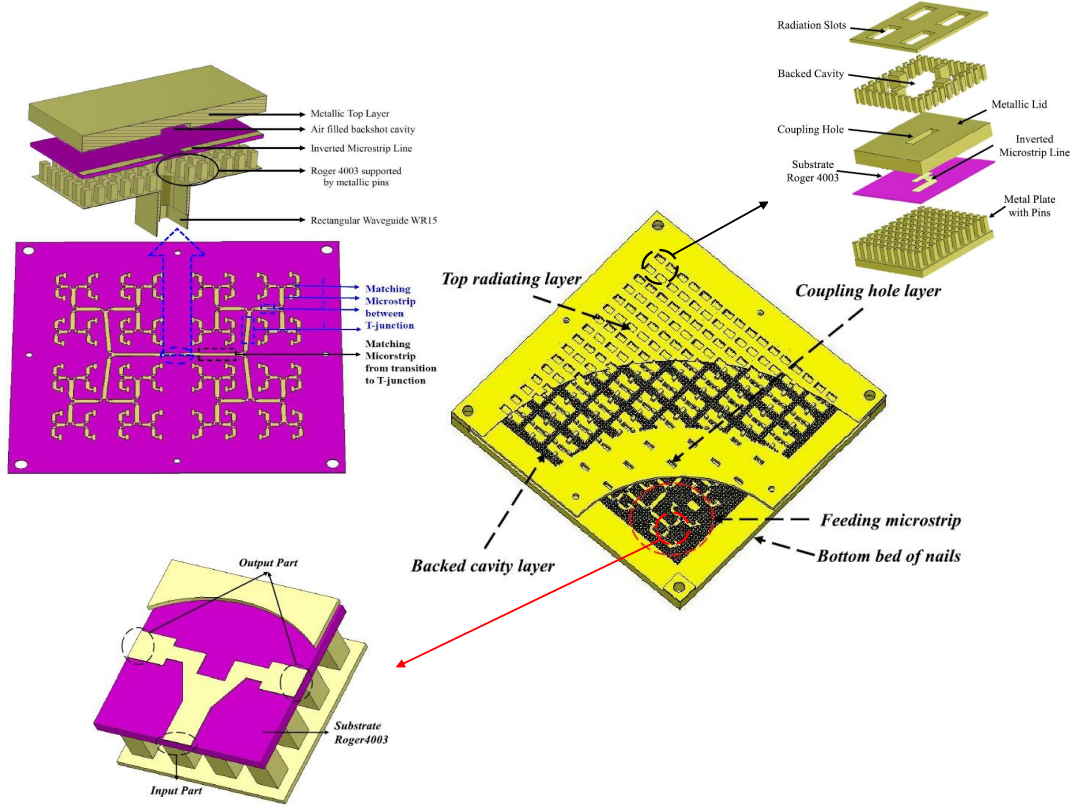
Figure 3.4: The configuration of the high-gain antenna on IMGW. The large array antenna consists of the 2×2 sub-arrays, the vertical hybrid transition and T-junction power dividers. Source: [Paper 2].

2], the dispersion diagram of whole structure is affected by dimensions of metallic pins, the thickness of substrate and the height of air gap. Therefore, any manufacture tolerances of bed of nails and the height change of air gap will cause a shift of the stopband. As reported in [46], there is always a frequency shift in reflection coefficient which drifts towards to lower or higher frequency. A consequence of the manufacture tolerances is that the PCB may not remain rigidly supported over the bed of pins, and there are some points in which the pins do not have a good contact with the substrate. Moreover, these untouched gap between substrate and pins automatically creates capacitance effect. This small shunt capacitor affects the dispersion diagram of IMGW.

The radiation pattern of proposed antenna is measured in an anechoic chamber. The simulated and measured normalized radiation patterns in the E- and H-plane at four different frequencies (57, 60, 61, 66 GHz) are shown in Figure 3.6 and Figure 3.7. The measured Co-polarization radiation patterns show a very good agreement with the simulated results. The simulated and measured radiation patterns are symmetrical, and the first side-lobe levels in both E- and H-planes are around -13 dB. The
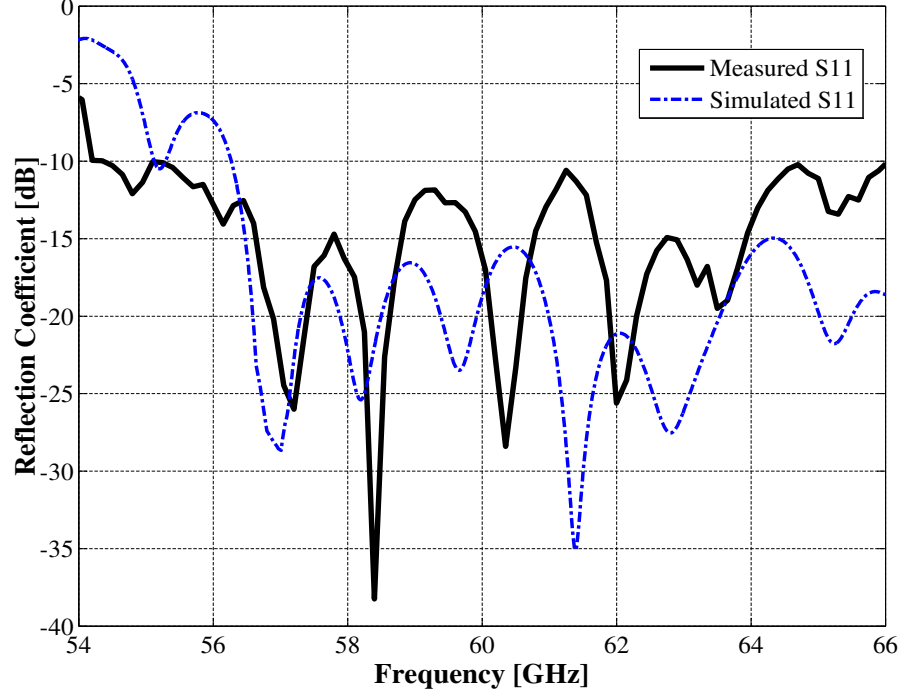
Figure 3.5: Comparison of simulated and measured reflection coefficient of the proposed 16×16 slot array antenna. Source: [Paper 2].

measured grating lobes of the fabricated array in both E- and H-planes are below -20 dB over the desired frequency band. The cross-polarization values are below -40 dB at all frequencies.

The simulated directivity and gain of proposed antenna are shown in Figure 3.8. The red solid line, which stand for simulated directivity, is above 80% aperture efficiency ($64{\times}64\ mm^2$). The pink dash line indicates the simulated gain after taking into account the modified loss tangent of substrate. The blue dash-dot line in Figure 3.8 shows the measured gain, illustrating above 40% aperture efficiency over the frequency band 54-64 GHz, higher than that of the arrays design by SIW and microstrip patch in [44] and [42].

Two engineering issues should be treated carefully in IMGW. Firstly, low loss tangent substrate, such as Rogers 3003, Rogers 5880 and Rogers 6002, are usually mechanically soft. Thereby, the corresponding PCB cannot be rigidly supported by the bed of nails and gets bends easily. As a result, there may be a tiny gap between the substrate and the metallic pins surface. This tiny gap may shift the frequency stopband towards higher frequencies. Secondly, the soft substrates are not easy to be kept flat and the conductor loss thereby increases a lot caused by bent microstrip.

(a)

(b)

(c)

(d)
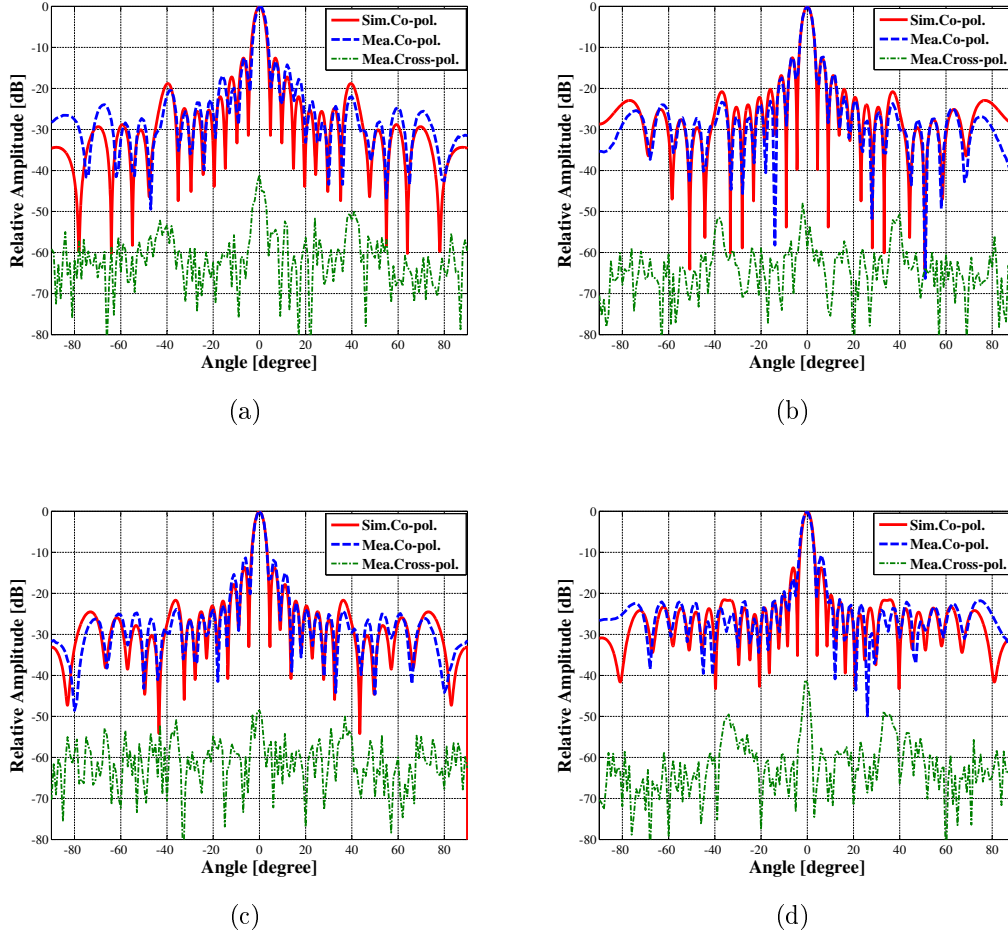
Figure 3.6: Measured and simulated radiation pattern of proposed array antenna on E-plane. (a) 57 GHz. (b) 60 GHz. (c) 61 GHz. (d) 66 GHz.

The rigid substrate, such as Rogers 4003 and FR4, on the other hand, can be used to avoid the above mechanical problem. However, their loss tangent values are usually higher than those of soft ones, thereby, the corresponding dielectric losses are also larger. Based on the experience of mine, the IMGW technology is optimal for high-gain antennas and beam steering antennas in Ka-band, because firstly, the loss tangent value of the rigid substrates is still small and thereby its dielectric loss is acceptable. And secondly, the wavelength in Ka-band is still centimeter level, the gap between the substrate and the metallic pins surface will be much smaller than the wavelength. Thereby, the frequency stopband is not sensitive to the tiny gap and the transmission performance will not be affected much by the mechanical problem. In addition, IMGW is able to integrate with active components, such as phase shifter and amplifiers. Thereby, this type transmission line is suitable to design steering beam active array antennas. Lastly, microstrip can be easily etched as any desired
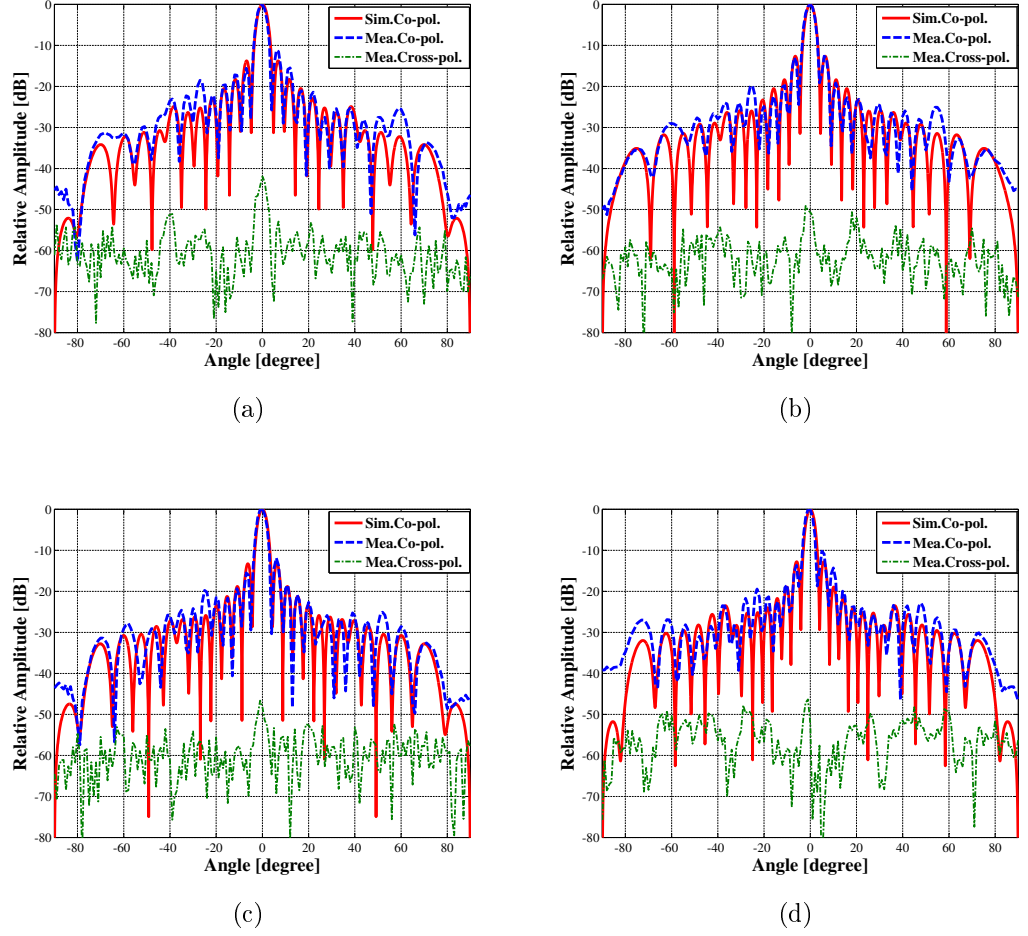
Figure 3.7: Measured and simulated radiation pattern of proposed array antenna on H-plane. (a) 57 GHz. (b) 60 GHz. (c) 61 GHz. (d) 66 GHz. Source: [Paper 2].

shapes, which is superior to metallic waveguide structures, such as hollow waveguide, RGW and GGW in this manufacturing aspect. In the next section, a novel unequal power divider designed by IMGW is reported and it is very practical to synthesize the low sidelobe array antenna. The obtained phase balance of the novel power divider is much better than those types by ridge or hollow wavegudie.

3.3 A low sidelobe Array Antenna on Inverted Microstrip Gap Waveguide in the Ka-band

Low sidelobe arrays are important components in the high-performance wireless communication systems to minimize interferences in the complex telecommunications network. Amplitude-taper methods are usually adopted in the synthesis of antenna
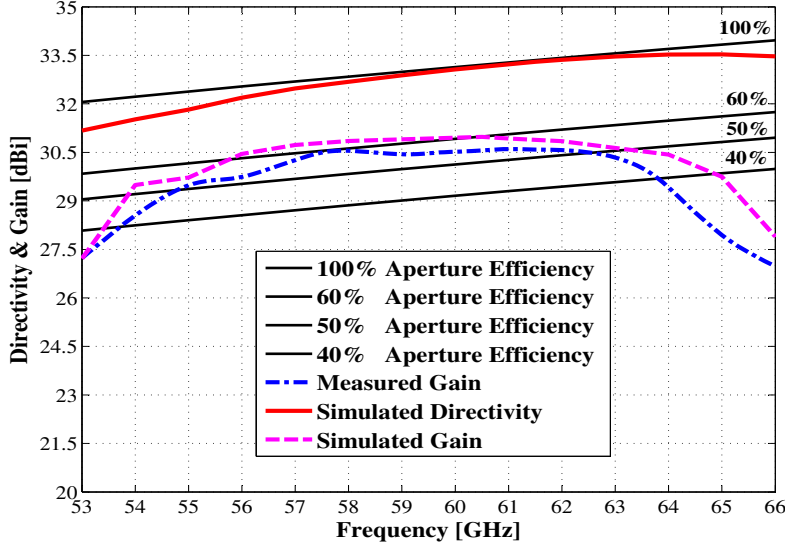
Figure 3.8: Measured gain and simulated directivity of present 16×16 slot array antenna. Source: [Paper 2].

arrays. Low sidelobe levels in far-field patterns are achieved by weighting the power applied to each element through a proper feed-network. The Taylor's distribution is a well-known analytical approach for low sidelobe array design. Hollow waveguide and ridge waveguide are usually low loss, and thereby they can be utilized for high-gain high-efficiency antenna [45]. Nevertheless, the waveguide structures occupy a large volume and lack design flexibility. It is difficult to design appropriate power-weighting waveguide feed-networks while considering amplitude tapering distributions and phase balance among antenna apertures. So far, most of the published works which implemented Taylor distribution are based on the microstrip planar arrays due to the ease of designing and manufacture on power-taper networks by microstrip lines [47] [48].

As discussed in the former section, IMGW has lower dielectric loss compared with microstrip, covered microstrip and SIW. Moreover, the manufacture and the design freedom of IMGW is more flexible than hollow waveguide and ridge waveguide. The work of the development of a low sidelobe array antenna based on IMGW at 28 GHz is summarized in this section. The details of the antenna can be found in [Paper 3]. Figure 3.9 shows the 3-D configuration of the entire 16×16 low sidelobe slot array antenna, and its layout of microstrip is depicted in Figure 3.10. In this low sidelobe array antenna, four types of unequal power dividers are required for the power distribution criterion: 2 dB, 5 dB, 7 dB and 10 dB. The 3-D view for the unequal power divider is shown in Figure 3.11. The detailed geometrical sizes of the unequal power divider is shown in Figure 3.12. For realizing the big power ratio, the proposed
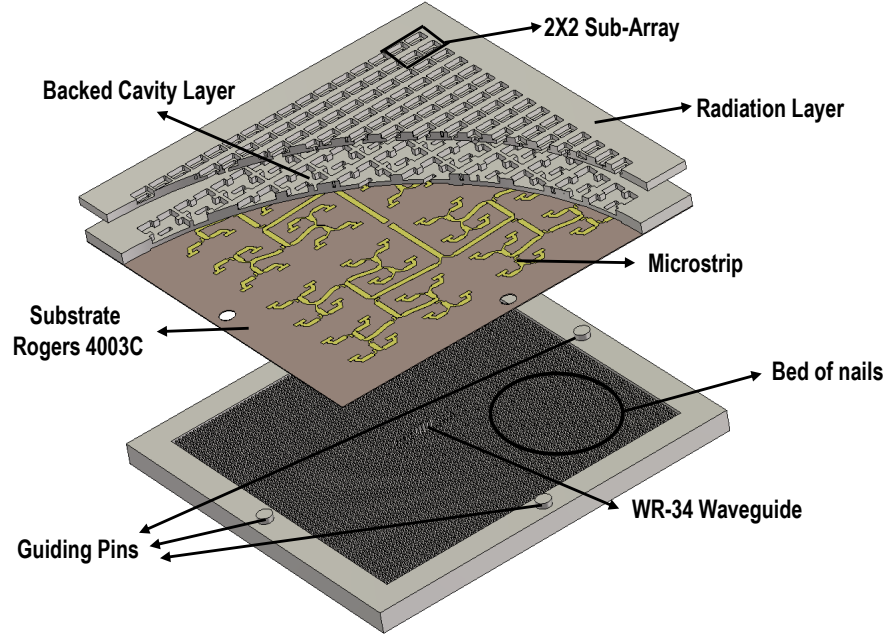
Figure 3.9: The 3-D configuration of present 16×16 low sidelobe slot array antenna. Source: [Paper 3].

unequal power divider is asymmetric. The required power ratios have been obtained by the offset value T_a. The phase balance between two output ports are mainly controlled by P_a. The input and the output impedance are mainly affected by the width of microstrip W. The width of microstrip at all ports are selected identical so that the matching networks between any two of them are avoided. The simulated results of the 10 dB power ratio divider is shown in Figure 3.13. As is depicted, the reflection coefficient is below -25 dB from 26 to 30 GHz, and the output phases are almost identical. Furthermore, the analysis of the power amplitude difference and the phase difference of two output ports is shown in Figure 3.14. The power ratio varies from 9 dB to 12 dB from 26 to 30 GHz. The Phase difference is very well controlled within 2 degrees from 26 to 30 GHz. The proposed unequal power divider characterizes much better reflection coefficient, larger power ratio of outputs and phases consistency. The simulated normalized radiation patterns in both E- and H-planes at three frequencies of 26.5, 28 and 29.5 GHz are shown in Figure 3.15. As is shown, the E-plane radiation patterns are very well improved. The first sidelobe levels are below -20 dB, and those values in [45] and [21] are -13.2 dB. Compared with previous radiation patterns with equal amplitude distribution networks, those value of the proposed low sidelobe array antenna are much better. Nevertheless, the relatively high sidelobes values are observed in the far-out region (40-50 degrees) on the H-planes. The major reason for this phenomenon is that it is not an accurate Taylor distribution on the H-plane.
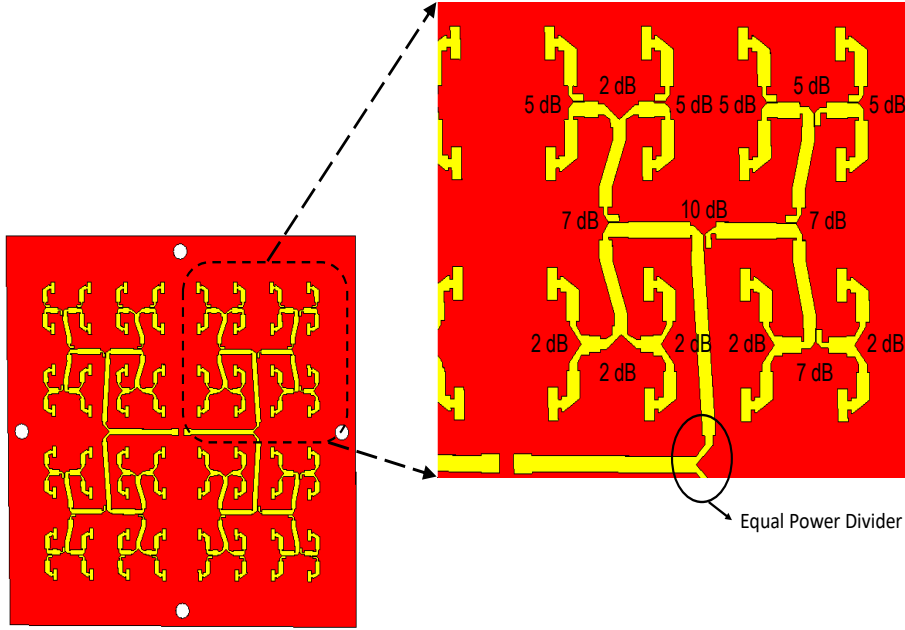
Figure 3.10: The configuration of the distribution networks of proposed low sidelobe array antenna. Source: [Paper 3].
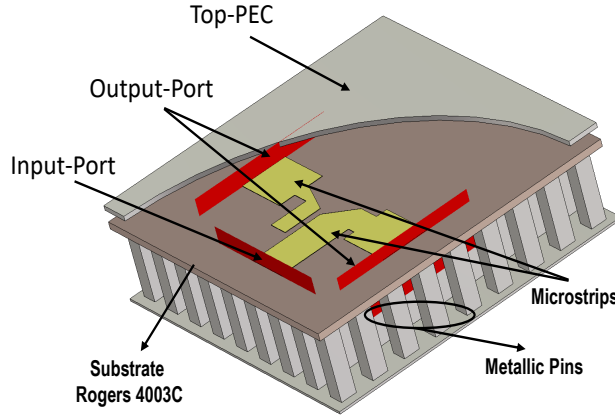
Figure 3.11: The 3-D configuration of unequal power divider based on IMGW. Source: [Paper 3].

Since the higher power ratio of the unequal power divider is required in order to have accurate Taylor distribution, this high far-out sidelobe issue will be solved in future. This unequal power divider and the low sidelobe array antenna is suitable for high quality back-hauling satisfied with ETSI or FCC standard, beam steering antenna and radar applications.
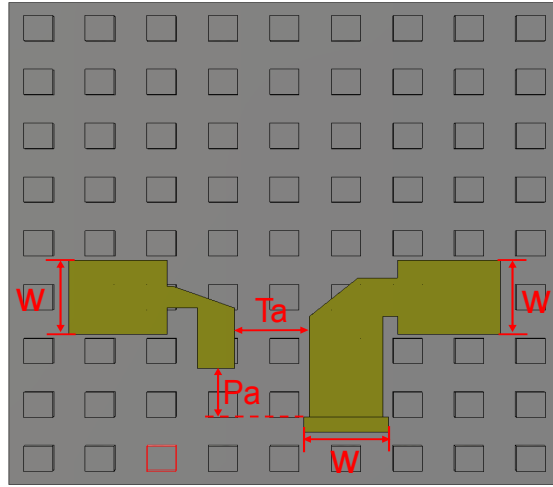
Figure 3.12: Top view of the proposed unequal power divider. The top metallic plate and the substrate have been hidden so that the geometrical dimensions of the power divider are clear to see. Source: [Paper 3].
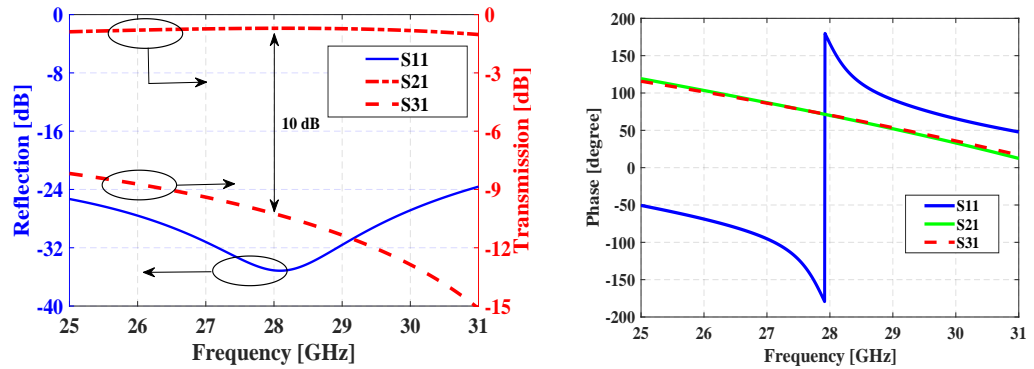
Figure 3.13: The simulated power amplitude and the simulated phase of the unequal power divider. (a) Amplitude. (b) Phase. Source: [Paper 3].

In this chapter, a theoretical analysis of the IMGW technology in mmWs has been presented. This promising geometry with low dielectric loss is able to overcome the known constraints of PCB based conventional transmission lines, hollow waveguide and ridge waveguide.The special interests on developing IMGW not only focus on array antenna, but also integration of passive and active components with MMIC in the future. Still, the assembly tolerances of bed nails and PCB is bit challenging for IMGW in mmWs. This mechanical issue should be investigated more in details in future.
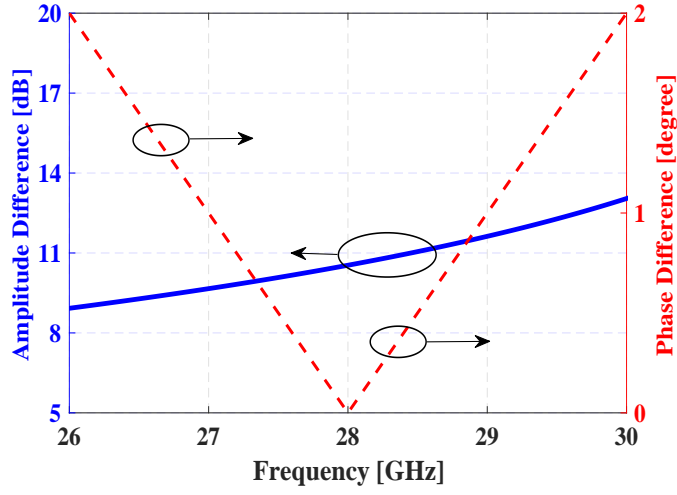
Figure 3.14: The simulated output power ratio and the phase ratio of the unequal power divider. Source: [Paper 3].

(a)   (b)
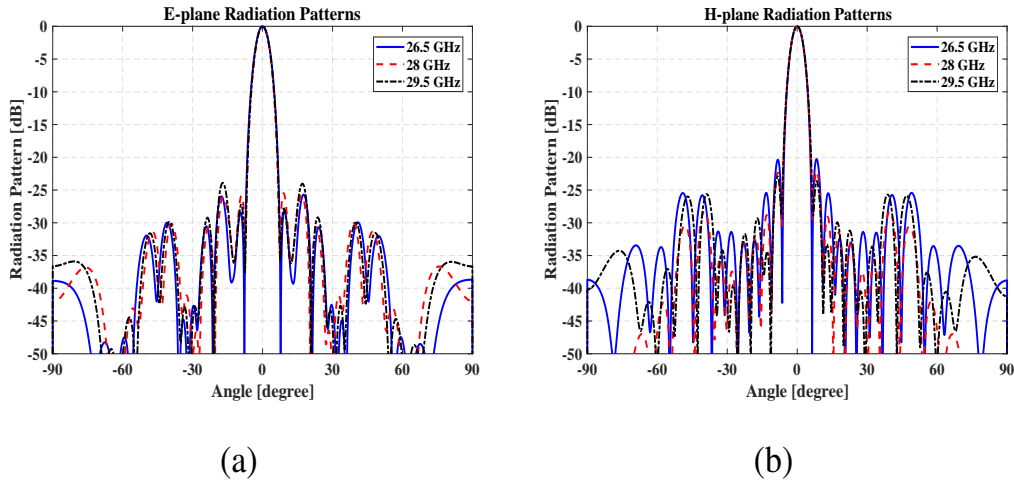
Figure 3.15: The simulated radiation patterns of the proposed array antenna in both E-plane and H-plane. Source: [Paper 3].

Chapter 4

Slot Array Antenna based on GGW in the W-Band

In Chapter 2, the limitation of the hollow waveguide for planar array applications has been already discussed. The slotted waveguide antennas are usually the best choice for high-gain high-efficiency applications in the aspect of performance. Usually, the geometrical structures of slotted waveguide antennas are very complicated so that their manufacture are very difficult and expensive, especially in mmWs [45], [49] and [50]. In reality, those complicated structures of waveguide slot array antennas are designed using several different layers and then assembly them together. The simplest method for assembling the multilayer geometries is the utilization of screws [50]. In Figure 4.1, one series-fed array antenna and another full-corporate-fed slot array antenna are assembled using a large number of screws so that the electrical contact

(a) (b)
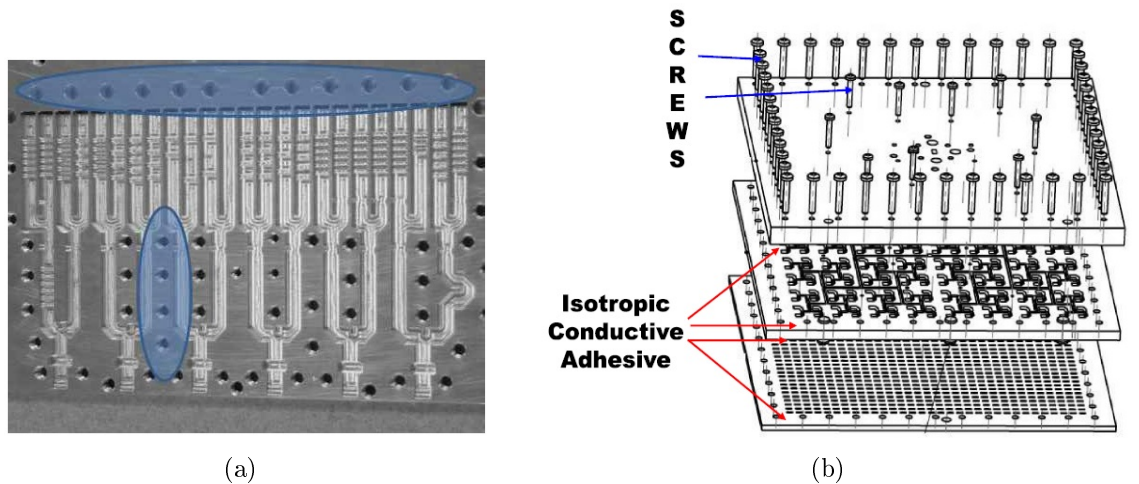
Figure 4.1: (a) The configuration of assembly method with many screws for a series-fed array antenna. (b) The configuration of assembly method with many screws for a full corporate-fed array antenna. Source: [50].

between any two plates is good enough. Nevertheless, so many screws also pose a big problem for mmWs antennas since there is no space for such many screws. Thereby, screwing is not always successful to assure good electrical contact, especially for a big array antenna in mmWs. On the other hand, vacuum welding is usually applied to join several plates together by heat or pressure. Traditional way of welding is utilization of fire as a heat source. Nevertheless, this process is not accurate and out of date. In order to accurately control the welding process, laser, plasma or electron beam are utilized as heat source in the modern welding. Because of the advantages of high-precision, efficiency, high-speed and low-distortion, the laser welding has been the most advanced and the popular welding method. However, the cost of this manufacture process is very expensive and thereby it is not suitable for mass production.

Another solution for installing multi-plates is the diffusion bonding [45]. Diffusion bonding technology is also a joining process. Diffusion bonding offers many advantages, mainly the strength of the bonding line, which is equal to the base metals. The microstructure at the bonded region is exactly the same as the parent metals. On the other hand, this joining process requires several strictly controlled condition: clean and smooth contacting surfaces which are free from oxides, high temperature condition(around 1000°C with precise thermal control) to promote diffusion process. In diffusion bonding, the bond strength is achieved by pressure, temperature, time of contact, and cleanness of the surfaces. Diffusion bonding is an attractive manufacturing option for joining dissimilar metals and for making the component with critical electrical continuity requirements. However, this manufacture process is affected by many factors–pressure, temperature, time of contact, and cleanness of the surfaces. Thereby, it is very difficult and time-consuming to accurately control the diffusion bonding process and the deformed geometries are very sensitive in mmWs.

The recently introduced concept of GGW [51] is a new type of wave guiding structure to overcome this manufacture problem in mmWs. As shown in Figure 4.2, the GGW is a modified parallel-plate waveguide in which one plate is smooth while the
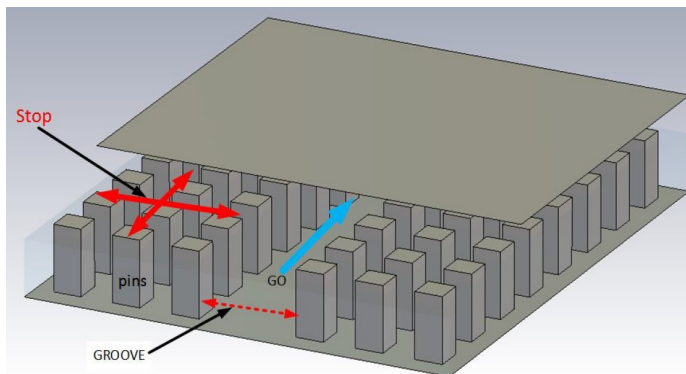
Figure 4.2: 3-D Configuration of a GGW.

other is a textured surface. In the GGW, the electromagnetic wave is forced to propagate along the desired path. A TE mode can propagate along grooves embedded within a periodic metallic pins [52]. No substrate material is needed in this structure, and the dielectric loss is thereby totally avoided. And the most advantage for GGW is that there is no requirement of electrical contact between the metallic plates upper and below. This huge advantage avoids the expensive laser welding and diffusion bonding manufacturing.

4.1 Slot Array Antenna by GGW in W-band

In [paper 4], a slot array antenna based on GGW in W-band is reported to validate its powerful strength over hollow waveguide. Figure 4.3 depicts the whole configuration of the proposed array antenna. As is depicted in the figure, the array antenna based on GGW consists of three layers — the bottom distribution layer, the backed-cavity layer and top radiation slot layer. In order to achieve low sidelobe characteristics, we have utilized a diagonal plane of uniformly excited square array arrangement. The
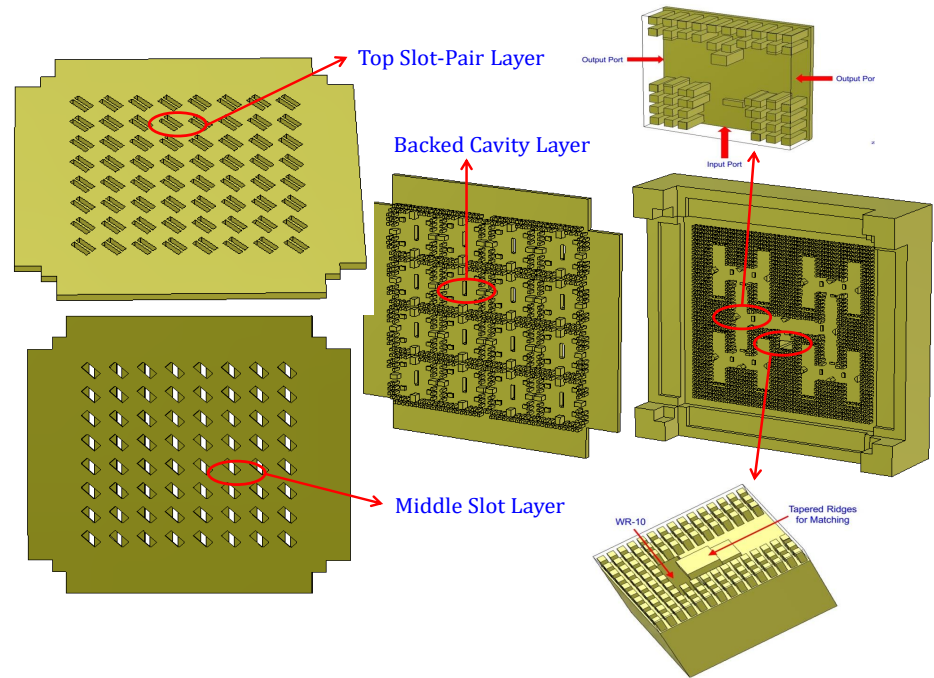
Figure 4.3: Configuration of the proposed corporate-feed slot array antenna based on GGW. Source: [Paper 4].

diagonal plane has equivalently tapered excitation, and the first relative sidelobe level in the diagonal plane is -26 dB, whereas that in the plane parallel to the side is -13.2 dB. By using the diagonal plane, low sidelobe characteristics without degradation of aperture efficiency can be realized in the diagonal plane which is the horizontal plane in most cases. Given the rising of the cross-polarization level caused by 45° degree rotation, a narrow-slot pair configuration on the top is designed to suppress the cross-polarization [53]. The proposed antenna has been fabricated by computerized numerical control(CNC) milling machine.

The proposed 2×2 sub-array is illustrated in Figure 4.4 so that the detailed geometry can be clearly illustrated. Top radiation part consists of three parts — exciting slot, 45° radiation horn and a narrow-slot pair on the top. The designed sub-array has 6×6 mm^2 dimensions. The sub-array is optimized in the infinite array environment by using CST Microwave Studio where the mutual coupling between sub-arrays are automatically included. The simulated reflection coefficient of the sub-array is illustrated in Figure 4.5. The sub-array bandwidth is 29% (71—95 GHz) with the VSWR better than 1.7. The directivity versus frequency of an 32×32 array with the same aperture size is shown in Figure 4.6. The blue line in the graph shows the maximum available directivity between 100% and 80% aperture efficiency. The designed air gap is 0.05 mm so that the good electrical contact are not allowed between different layers.

The configuration of the T-junction based on GGW is illustrated in Figure 4.7.
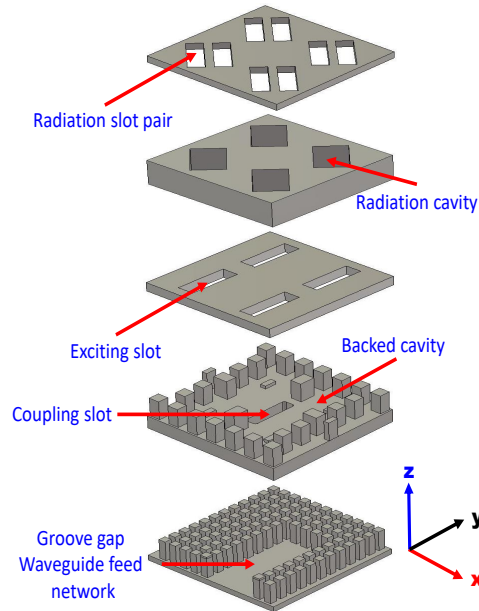
Figure 4.4: Model for the analysis of the 2×2-element sub-array. Source: [Paper 4].
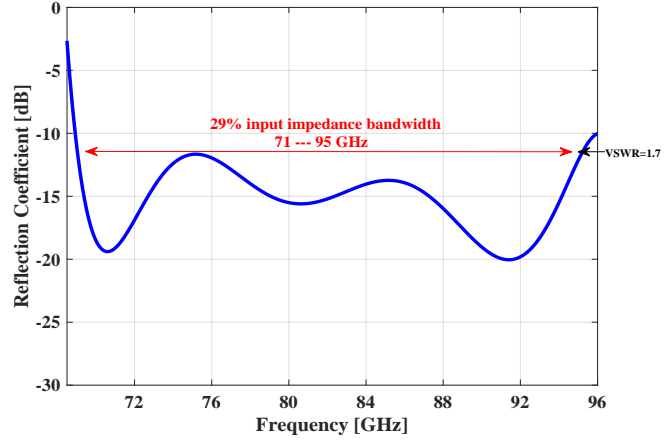
Figure 4.5: The reflection coefficient of the sub-array. Source: [Paper 4].
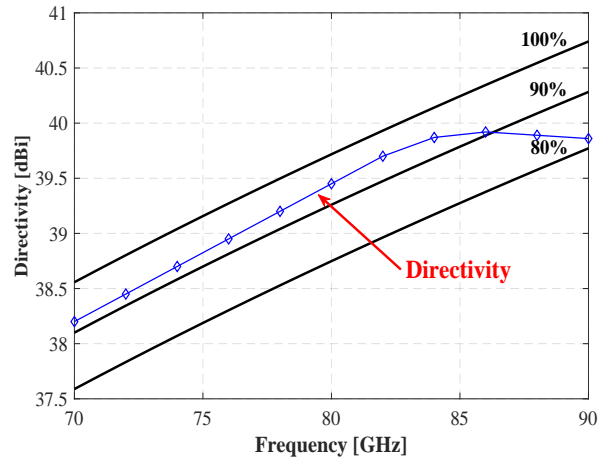
Figure 4.6: The simulated directivity of the 32×32 slot array according to the periodic boundary condition. Source: [Paper 4].

The proposed topology provides power division with symmetrical amplitude distribution. As shown in Figure 4.7, this power divider is a GGW T-junction with tuning pin in the input port and split the incoming power from input port to the output ones. The height of tuning pin is lower than the normal metallic pins and has been utilized as a tuning parameter. In order to satisfy the matching requirements over the desired frequency band, the position and height of tuning pin and also the width of input groove are optimized. The final simulated results for the design are presented in Figure 4.8. As can be seen, the reflection coefficient of the entire T-junction power
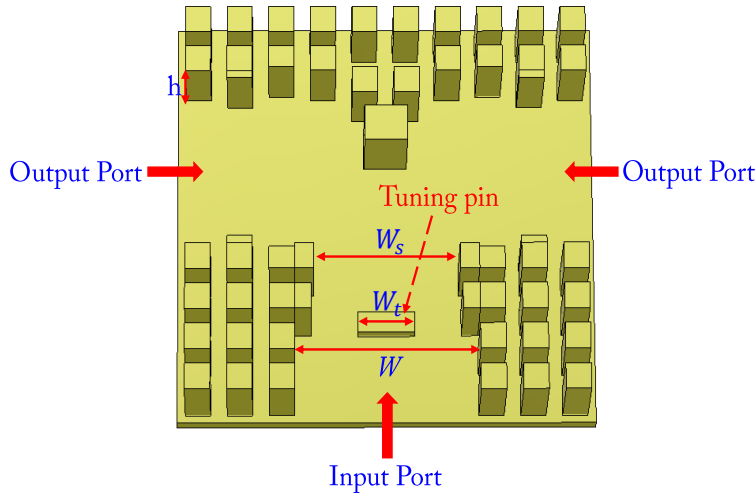
Figure 4.7: The configuration of T-junction power divider based on GGW. The top metallic plate is hidden to clearly depict the geometry of the entire power divider. $h = 1.1mm$, $W = 2.5mm$, $W_t = 1.2mm$ and $W_s = 1.8mm$.
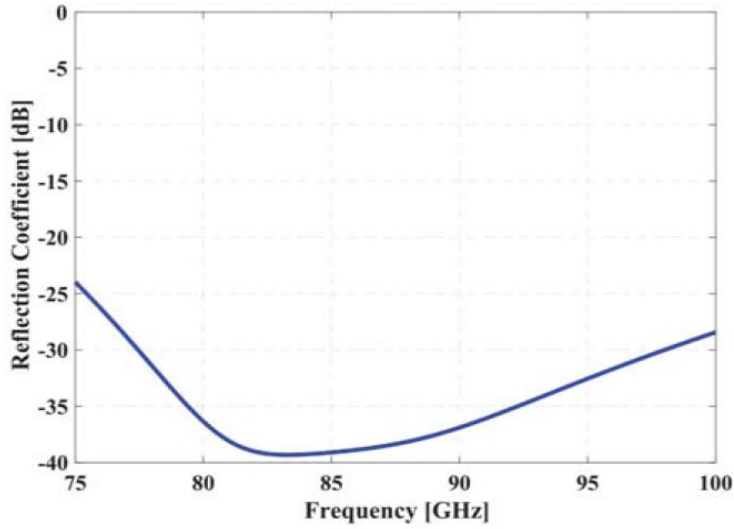
Figure 4.8: The simulated S-parameters of the T-junction power divider shown in Figure 4.7.

divider is below -25 dB over the simulated bandwidth from 75-100 GHz.

In reality, GGW structure should have a transition from a standard rectangular waveguide (WR-10) in order to excite GGW structure and to perform measurements. The transition transforms electromagnetic fields from the rectangular waveguide mode to the GGW mode. The geometries of the proposed vertical transitions are shown in Figure 4.9. The motivation for such a vertical transition is to excite
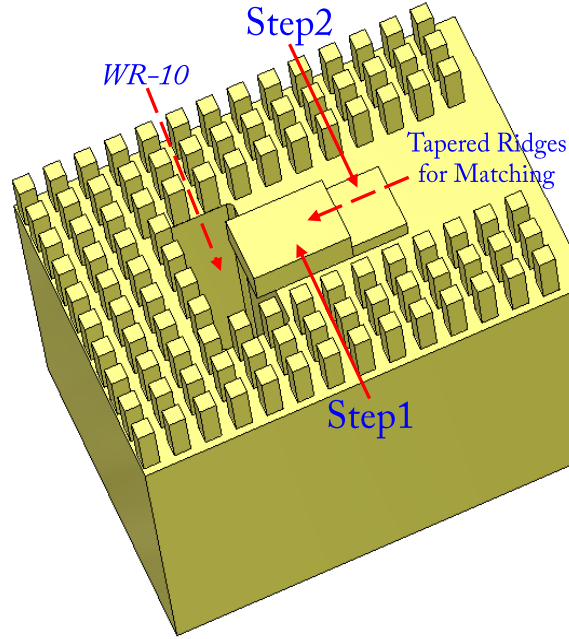
Figure 4.9: Vertical transition from WR-10 to GGW. The top metallic plate is hidden to clearly depict the geometry of the entire transition geometry.

the slot array antenna later on where it is convenient to excite the antenna from the back. The simulated result shows a -20 dB return loss is achieved between 70-100 GHz as shown in Figure 4.10.
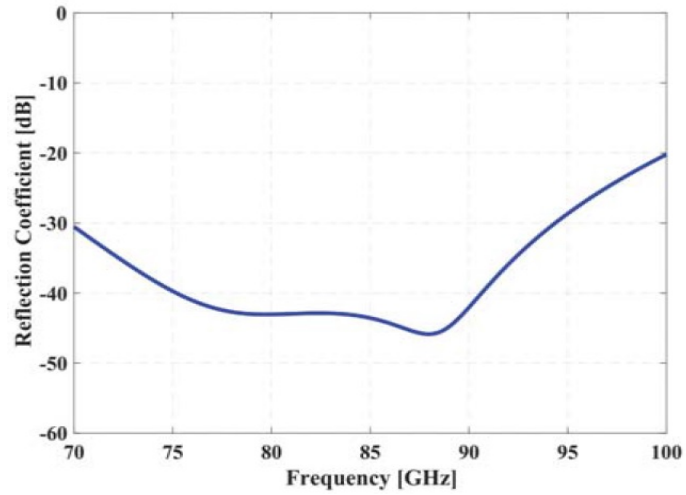
Figure 4.10: Simulated reflection coefficient of the geometry of vertical transition.
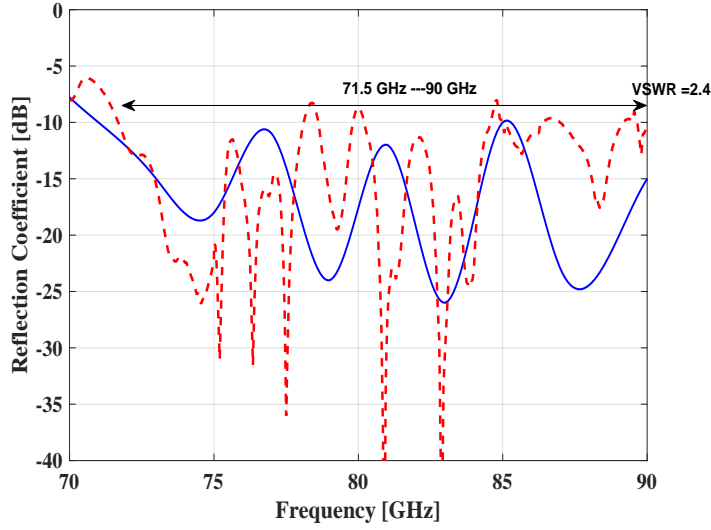
Figure 4.11: The simulated and the measured reflection coefficients of the proposed 8×8 slot array antenna. The blue dash line is the simulated reflection coefficient, and the red dashed line is the measured one. Source: [Paper 4].

(a)   (b)
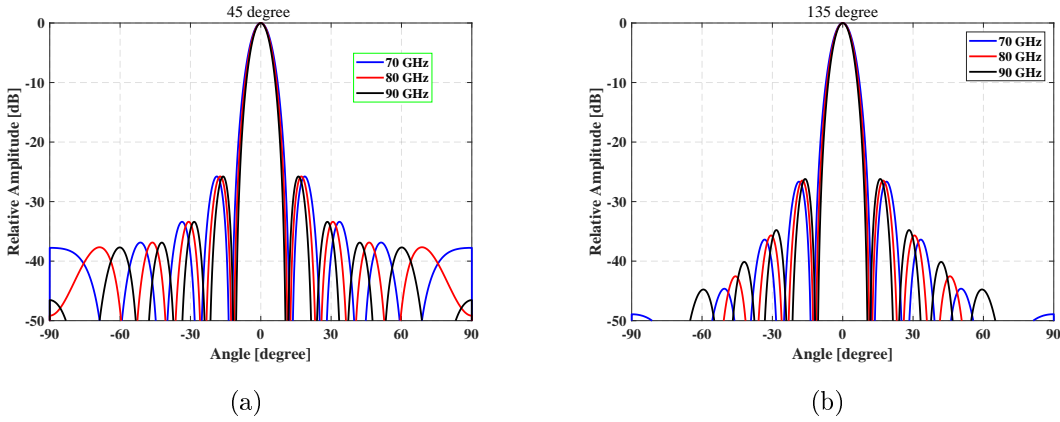
Figure 4.12: Simulated radiation patterns of antenna array at (a) Horizontal planes and (b) Vertical planes at frequencies 70, 80, and 90 GHz. Source: [Paper 4].

The reflection coefficient of the antenna array was measured by an Agilent PNA N5227A and W-band millimeter-wave extender module. The antenna has been fed through a standard WR-10 waveguide. Figure 4.12 shows the simulated and measured reflection coefficients for the antenna. As can be seen, the fabricated antenna has an impedance bandwidth (VSWR ≤ 2.4) of 23% covering 71.5 to 90 GHz. Generally, the measured results are in quite good agreement with the simulated ones. However, there are some differences between them due to manufacturing and assem-
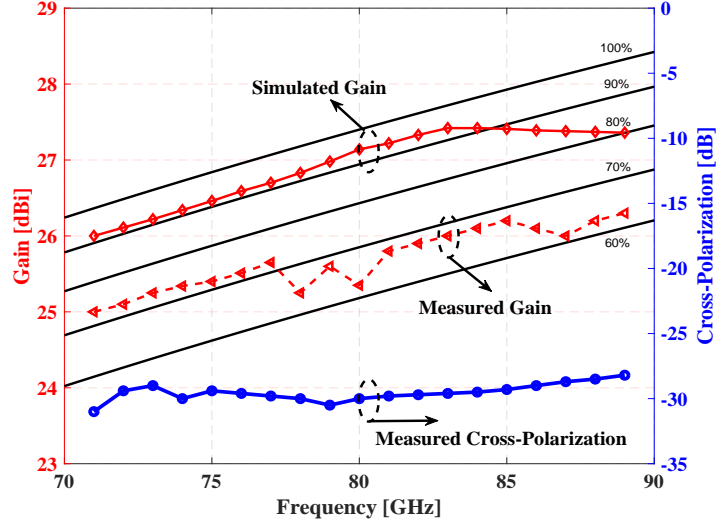
Figure 4.13: The simulated and measured gains of the proposed array antenna. The measured one shows the antenna efficiency is higher than 60%. The measured cross-polarization is better than -27 dB, which fulfills the ETSI standard. Source: [Paper 4].

bling tolerances. The simulated far-field radiation patterns of proposed antenna at 70, 80 and 90 GHz in both E- and H-planes are depicted in Figure 4.12. Low sidelobe characteristics are obtained over the bandwidth investigated here. No grating lobe is observed. The simulated first sidelobe levels are less than -26 dB. The measured frequency characteristics of the gain and the cross polarization are shown in Figure 4.13. The gain and the cross polarization are measured by V- and W-band far-field measurement systems for 70—75 GHz and 75—90 GHz, respectively. In the 71—89 GHz band, the gain variation is 25—26.2 dBi. The bandwidth for a gain of more than 25 dBi and the antenna efficiency of more than 60% is observed for the proposed antenna.. The cross polarization is suppressed below -27 dB over the full bandwidth.

In this chapter, the fabrication challenges of traditional hollow waveguide in mmWs has been analyzed first. It is understandable that GGW has advantages to overcome them in mmWs. Then, the design work of a slot array antenna based on GGW is summarized to verify its competitive strength over the traditional technologies. However, some issues about the design should be also noticed. First, in higher frequency band (over 75 GHz) the dimensions of metallic pins should be carefully selected so that they can be fabricated in low cost ways, especially CNC milling technology and molding, and have a proper stopband, the low loss property and even the low coupling effect between two neighbored waveguide structures. Secondly, the proposed antenna is assembled by only four screws in the four corners of the antenna layers, which may cause the misalignment between the two layers. Usually, the mis-

alignment makes the reflection coefficient of the entire array antenna worse. In [Paper 5], an investigation of the effect of misalignment on performance has been done. The results of [Paper 4] show that the reflection coefficient of the millimeter wave array antennas still work ordinarily in operating frequency band within 0.05 mm misalignment. In addition, the surface roughness inside the waveguide also affects the loss of the GGW. For applications in industry, silver- or copper-plating is usually necessary.

Chapter 5

The Applications of RGW in mmWs

As is well-known, the bandwidth of the rectangular waveguide is enough for many system applications. TE_{10} mode is usually the dominant mode in the rectangular waveguide and it has cutoff wavelength of about twice of width of hollow waveguide. However, sometimes it is not suitable for larger frequency band applications. A traditional ridged waveguide is built by putting a longitudinal metallic block inside of a hollow waveguide, as depicted in Figure 5.1. Generally, the ridge act as a uniform distributed loadings, which tend to lower the phase velocity and reduce the characteristic impedance. Moreover, the ridge will lower the cutoff frequency of the dominant mode and raise the cutoff frequency of the next higher order modes. Therefore, it increases the bandwidth compared with a normal hollow waveguide. As a result, the geometrical width of a ridge waveguide is usually smaller than a hollow waveguide for exciting an electromagnetic mode with same cutoff frequency. This feature is needed for low sidelobe array antennas because the spacing between slots is only half λ of
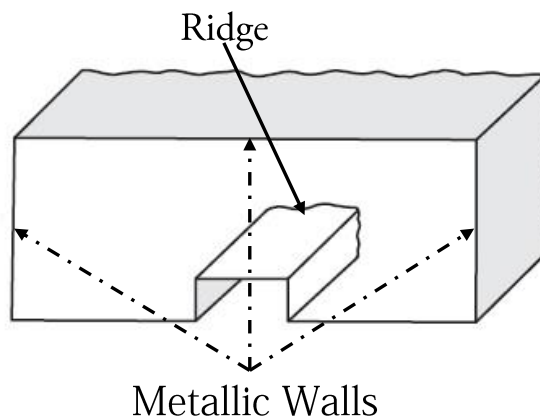
Figure 5.1: 3-D configuration of a ridge waveguide.
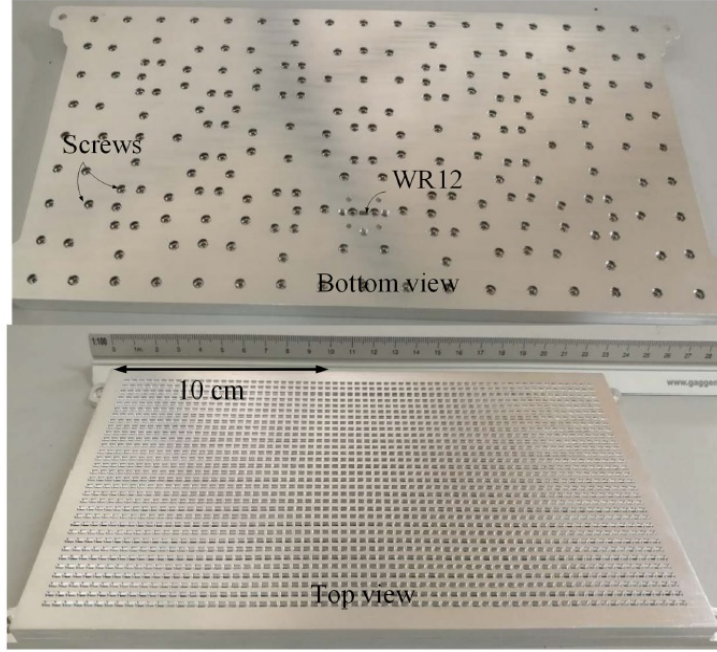
Figure 5.2: Photograph of the fabricated slot array antenna. The array antenna consists of three layers. All three layers are installed by a large number of screws. Source: [55].
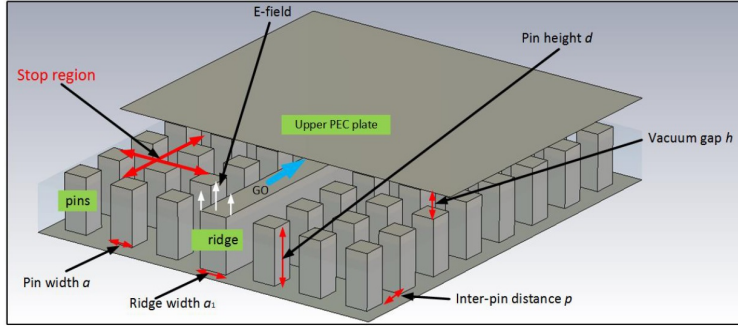
Figure 5.3: 3-D Configuration of a RGW.

operating frequency and the space for the layout of antenna feed lines is usually very limited. However, the same challenges of fabrication occurred in hollow waveguides also exist in ridge waveguides [54]. As shown in Figure 5.2, a slot array antenna with ridge waveguide distribution network in E-band has been installed by screws to install all three layers.

As an improvement of ridge waveguide in mmWs, the RGW is a new type of wave guiding structure to simplify the manufacturing problem in mmWs. As shown in Figure 5.3, the waveguide is generated in a narrow gap between parallel metal

plates. One of the plates is textured by metallic pins that prevents global parallel plate modes from propagating. The texture structure also includes single metallic ridge forming the transmission line or waveguide. The RGW does not need any metallic connection between the two plates. Besides the advantage of easy fabrication, the RGW is more flexible to increase the width of the ridge for reducing the conductor loss. Moreover, radiation loss is reduced to the minimum since the RGW is inherently packaged. Thereby, RGW is also easy to integrate with active component. In this chapter, a slot array antenna with single-layered distribution network based on RGW in [Paper 5] is summarized. Then, another slot array antenna with double-layer full-corporate feed network in the D-band in [paper 6] is described briefly. Those slot array antennas show that the RGW is a good candidate for array antennas, filters and packaging in not only mmWs, but also sub-millimeter waves frequency bands.

5.1 Single-Layered Slot Array based on RGW in the V-Band

Recently, double-Layered full-corporate fed slot array antennas in mmWs are very popular [23] [27] [29] [45] and [53]. As illustrated in Figure 5.4, this type of array antennas consist of three layers: distribution feed network layer, backed cavity layer, and radiation slots layer. One function of the backed caivity is to provide enough
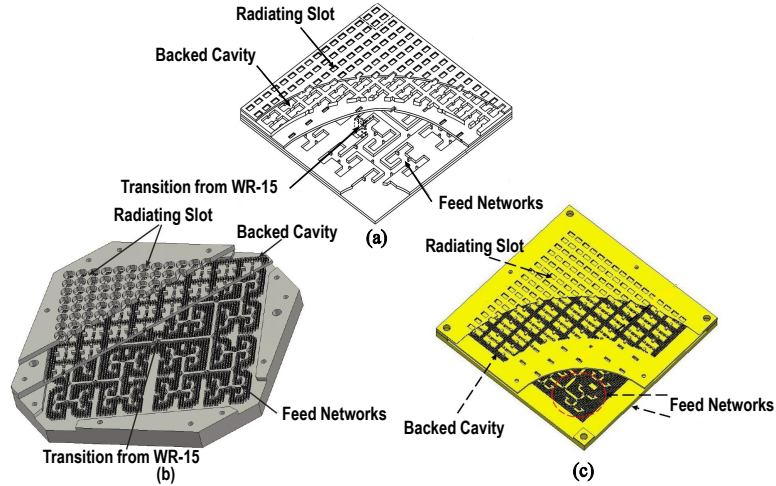
Figure 5.4: (a) depicts a cavity-backed slot array antenna fed by hollow waveguide. (b) shows a cavity-backed slot array antenna fed by RGW and a similar antenna fed by inverted microstrip gap waveguide stated is illustrated in (c). These three full corporate-feed antennas consist of three layers — distribution feed networks, backed cavity and radiation slots and their operating frequency all in the 60-GHz band. Source: [Paper 5].

space for the distribution network. Another intention of the backed cavity is to improve the bandwidth of the array antenna.

In [Paper 5], we introduced a new geometry of slot array antenna in mmWs. This array antenna consists of only one layer of corporate-feed distribution network and one layer of the radiation slots. As illustrated in Figure 5.5, the array antenna avoids utilization of the backed-cavities by a new layout of the corporate-feed distribution network in RGW. In this section, the analysis of the radiation slot layer is first presented, and then the design and the performance of distribution network is summarized. As depicted in Figure 5.5, the shape of the radiation slot in this array antenna is designed as a shape of butterfly, which is actually a double-ridged slot with circularly curved corners and smoothly profiled ridges. The double ridges lower the cutoff frequency of the dominant mode and at the same time raise the cutoff frequency of the next higher order modes in the radiation slot. Therefore, it increases the bandwidth of the array antenna compared with that by using a normal rectangular slot. Secondly, for exciting electromagnetic wave, the double-ridged waveguide usually has the smallest shape compared with the rectangular slot. This is the main consideration of using the butterfly shape slot because if a rectangular slot is used the half-wavelength rectangular slot would extend to the neighboring feed lines. To excite the electromagnetic wave in the slot, the magnetic-field created
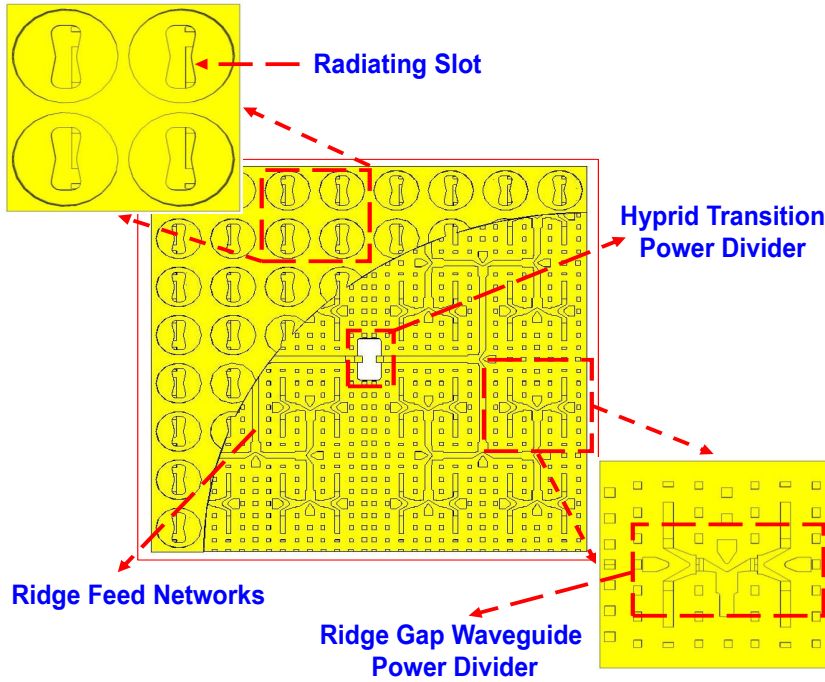
Figure 5.5: Top view of proposed single-layered corporate-feed 8×8 slot array antenna. Source: [Paper 5].
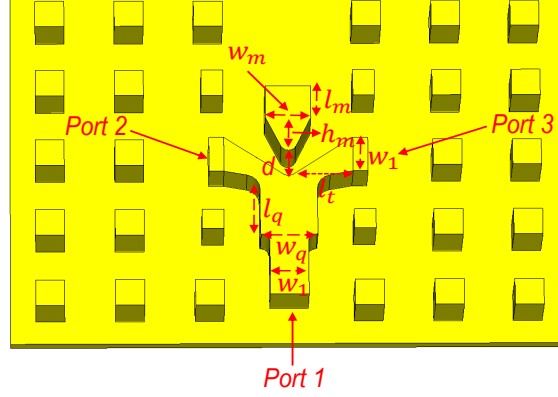
Figure 5.6: 3-D configuration of the T-junction power divider based on RGW. The upper metallic plate is hidden. $w_1 = 0.54mm$, $w_q = 0.8mm$, $l_q = 0.72mm$, $l_t = 0.92mm$, $d = 0.4mm$, $w_m = 0.72mm$ and $l_m = 0.6mm$. Source: [Paper 5].

by the ridge line of the feed layer should rotate along the vertical direction of the double-ridged slot. Then, the electromagnetic wave can radiate with the same phase and polarization from the slot. This method is actually a magnetic coupling radiation, which is different from excitation method stated in [29] [35],and [56]. It avoids the utilization of the conventional bend ridge line and makes the feed network very compact so that the layout of the feed network is possible to fit in such limited space as in the single-layered corporate-feed network case.

For achieving good radiation patterns, the spacing between slots is selected as 4.2 mm, which is equal to $0.87\lambda_0$. Having considered the layout of the distribution network, four rows of metallic pins are required for the dimension of 4.2 mm, and
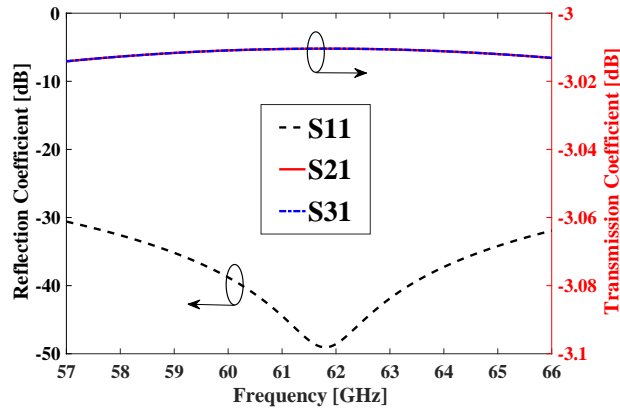
Figure 5.7: Simulated reflection coefficient of the T-junction power divider shown in Figure 5.6. Source: [Paper 5].
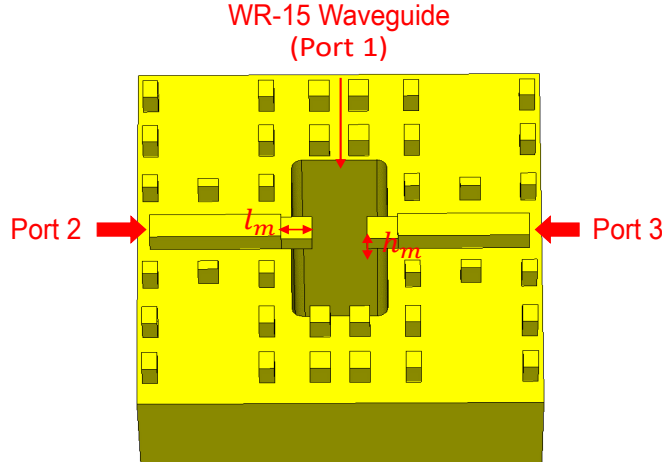
Figure 5.8: 3-D configuration of the hybrid power divider from WR-15 to RGW. The upper metallic plate is hidden. $h_m = 0.45mm$ and $l_m = 0.75mm$. Source: [Paper 5].

the corresponding periodicity of metallic pins is 1.05 mm. Then, for layout spaces of the ridge lines and their easy fabrication, the pin's width is selected as 0.4 mm. The corporate-feed network utilizes T-junction power dividers to feed all slots in the whole array antenna. The configuration of the T-junction based on RGW power divider used in this work is depicted in Figure 5.6. The corresponding simulated reflection coefficient is shown in Figure 5.7, which is below -30 dB from 57 to 66 GHz. The whole array antenna in this work is excited through a standard V-band rectangular waveguide (WR-15) at the bottom of whole structure. In this work we prefer a hybrid power divider similar as that described in [57]. The hybrid structure
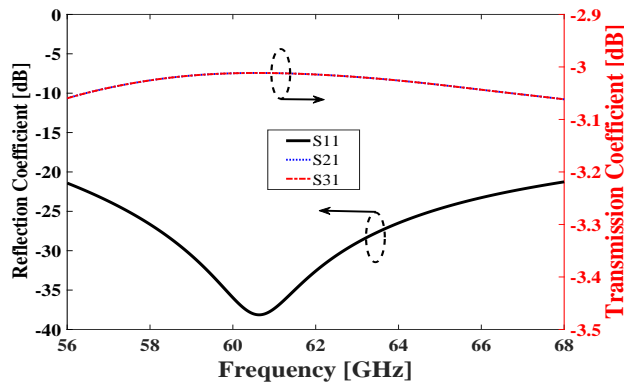
Figure 5.9: Simulated reflection coefficient of the hybrid power divider from WR-15 to RGW shown in Figure 5.7. Source: [Paper 5].
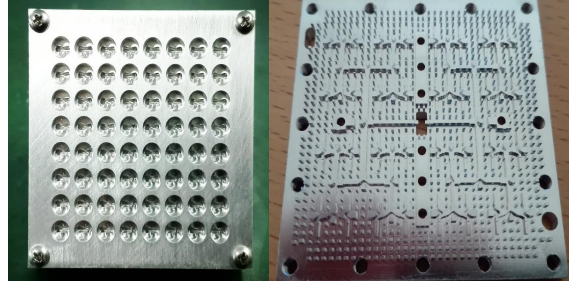
Figure 5.10: Configuration of the 8×8 slot array and photos of the fabricated antenna. Source: [Paper 5].

is illustrated in Figure 5.8. The simulated S-parameters of the structure are shown in Figure 5.9. Its reflection coefficient S_{11} in the whole band 56 – 68 GHz is below -20 dB. In addition, we should point out that the phases of the output ports have 180 degree difference. The two half parts of the distribution networks are mirrored out-of-phase from hybrid transition part.

The fabricated 8×8 slot array antenna is illustrated in Figure 5.10. The entire structure is simulated in CST Microwave Studio. The simulated reflection coefficient of the complete antenna is below -15 dB from 57 to 66 GHz, as shown in Figure 5.11. However, the measured reflection coefficient is a bit higher than simulated one because the assembly tolerance of the proposed antenna and the roughness of ridge surface. The simulated and the measured far-field radiation patterns of proposed
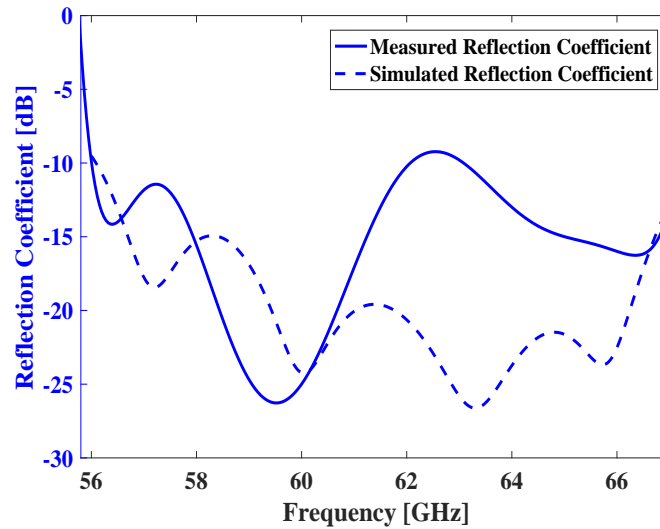
Figure 5.11: The simulated and the measured reflection coefficients of the proposed array antenna. Source: [Paper 5].
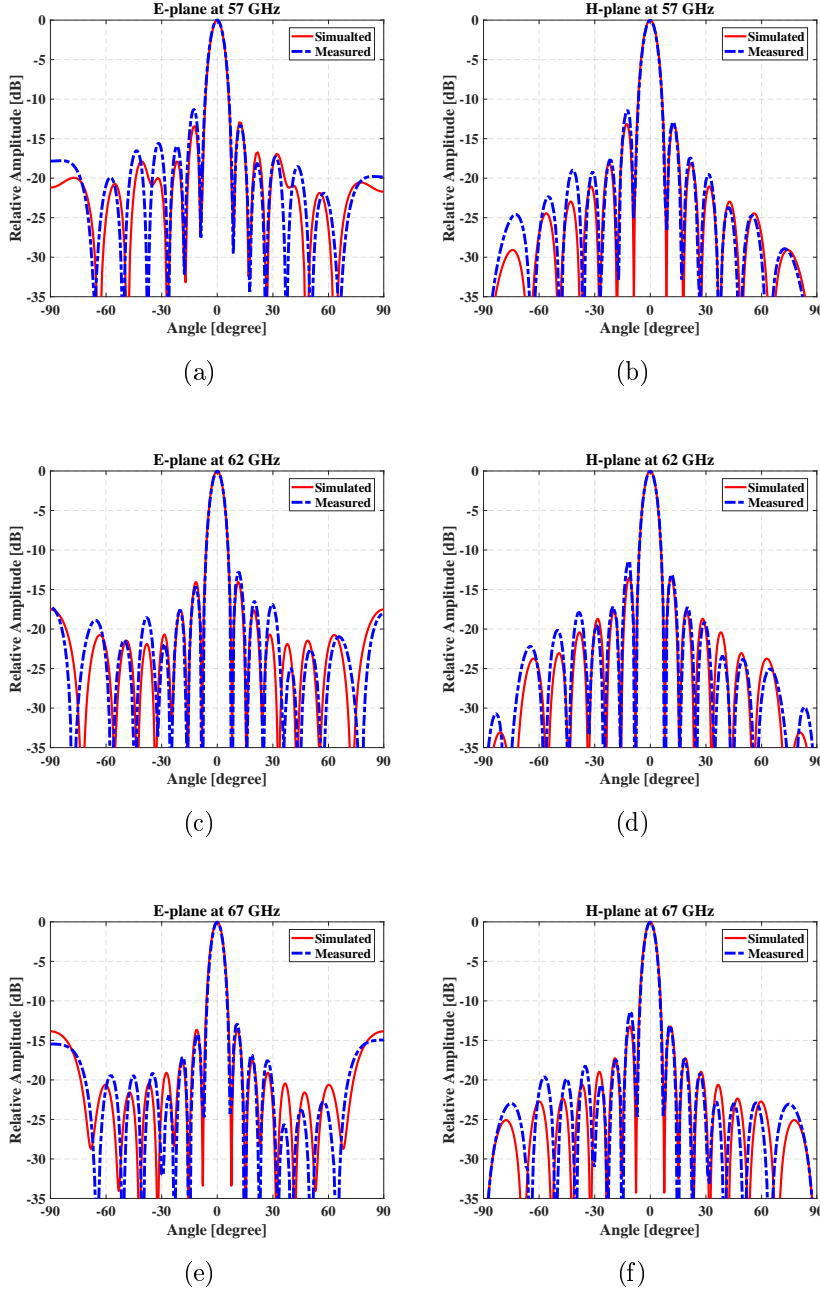
Figure 5.12: The simulated and the measured radiation patterns of proposed array antenna on both E-plane and H-plane at 57 GHz, 62 GHz and 67 GHz. Source: [Paper 5].

antenna at 57, 62 and 67 GHz in both E- and H-planes are depicted in Figure 5.12. The measured radiation patterns show a good agreement with the simulated results. The measured and the simulated antenna gains are shown in Figure 5.13. It can be observed that the realized gain varies from 25.8 to 27 dBi over 57 to 66 GHz, whereas the antenna efficiency is more than 70%, a very good performance.
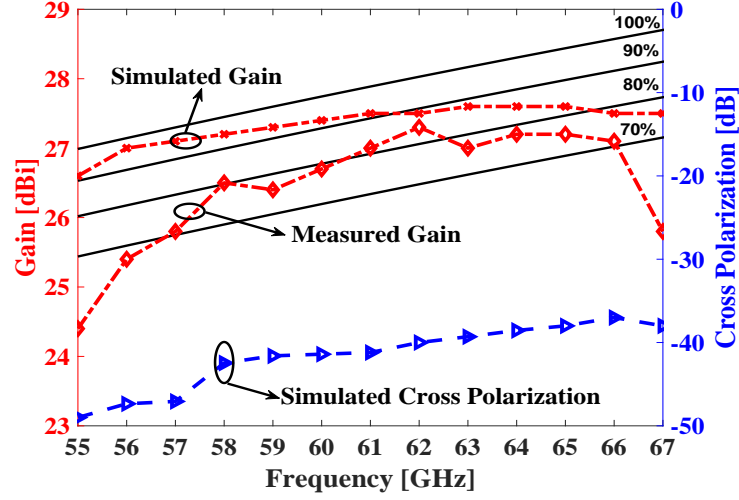
Figure 5.13: Red lines: simulated and measured gains of the proposed array antenna. Blue line: simulated cross-polarized value. Source: [Paper 5].

5.2 High-Gain High-Efficiency Slot Array Antenna based on RGW at 140 GHz

Microwave backhaul technology plays a significant role in providing reliable mobile network performance. Beyond 100-GHz, spectrum has been allocated for fixed service systems mainly focusing on W-band (75-110 GHz) and D-band (110-170 GHz). As described in the previous chapters, microstrip, SIW and LTCC technologies are related with the substrate, and their high dielectric losses are insufferable above 100 GHz. Those transmission lines with substrate are not convenient for high-gain high-efficiency array antennas beyond 100 GHz. On the other hand, the traditional hollow waveguide and ridge waveguide suffer from the manufacturing problem and cost since the geometrical dimensions of waveguide structures above 100 GHz are relatively small. For high-gain high-efficiency array antenna design, the gap waveguide is probably the best choice. However, the challenges of gap waveguide in frequency bands above 100 GHz should also be considered. Since the gap waveguide also solved the problem of electrical contact, the manufacture method is then the key issue for

above-100 GHz frequency band. If the geometrical dimensions of the metallic pins are smaller than 0.3 mm, it is very difficult to fabricate it by CNC milling, EDM or molding techniques. The other manufacture technologies, dry etching, wet etching and lithography for integrated circuits are probably the choices for gap waveguide structure fabrication. Nevertheless, the dry etching and lithography technologies are extremely expensive, and the accuracy of wet etching is not acceptable for fabrication of gap waveguide in above-100GHz frequency band. All in all, how to select feasible pins in above-100 GHz frequency bands with a low cost manufacture technology is a big issue for high-gain high-efficiency array antenna. In [Paper 6], a successful example for high-gain high-efficiency array antenna based on RGW at 140 GHz is presented. The prototype of the proposed array antenna is still fabricated by CNC milling technology so that the mass production is left to be solved in future.

As seen in Figure 5.14, the frequency band 135-155 GHz has the lowest air attenuation over the whole D-band. It is very advantageous to utilize this frequency band for high data rate wireless links. Due to several limitations in commercially available D-band electronics such as output power, local oscillator leakage and packaging losses, the high-gain and high-efficiency antenna plays a very important role for the point-to-point wireless links. A high-gain high-efficiency slot array antenna is probably very suitable for such a wireless system. The proposed array antenna consists of 32×32 radiation slots, backed cavities and full-corporate distribution network based on RGW. As shown in Figure 5.15, the entire array antenna consists of three layers – the radiation slot layer, backed-cavity layer and distribution network layer based on RGW.
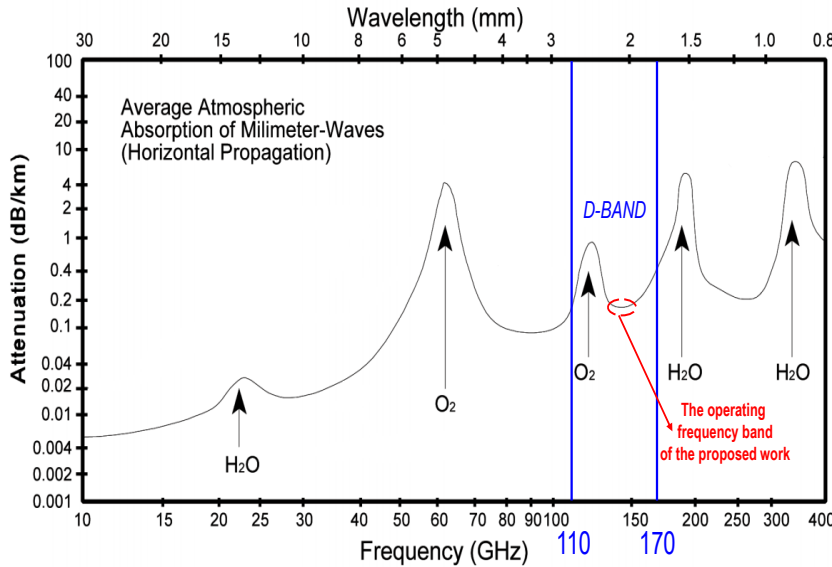
Figure 5.14: Average atmospheric absorption of millimeter-waves at sea level. Source: [Paper 6].
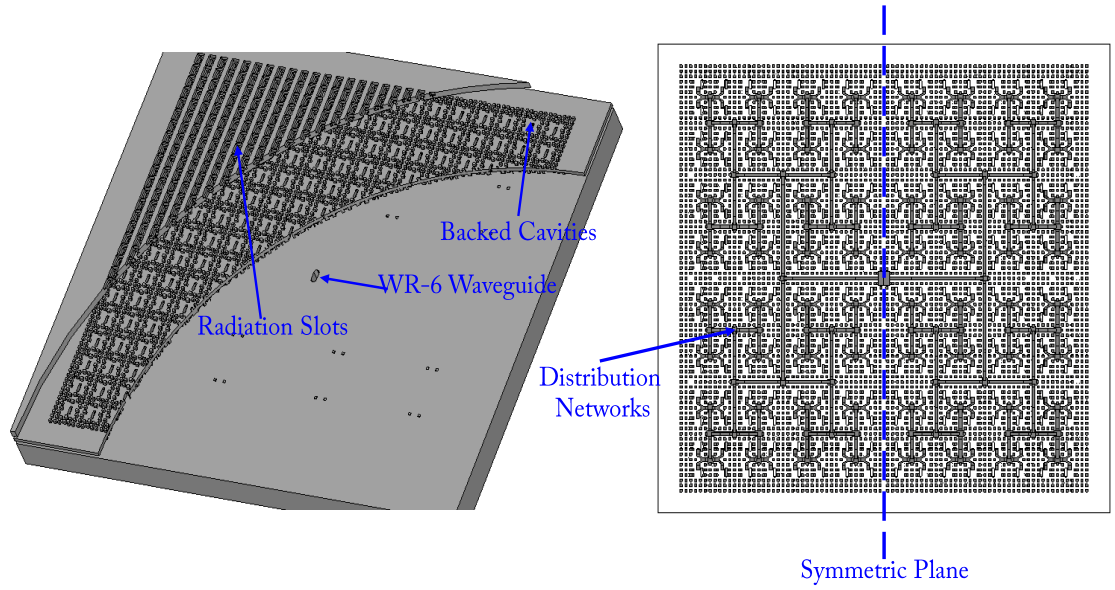
Figure 5.15: The proposed 32×32 slot array antenna and its full corporate-feed distribution networks. Source: [Paper 6].

The top of the entire array antenna is the radiation layer, which contains radiation slots with rectangular flare. The function of the flared slot is to improve the bandwidth of the sub-array. Below the slot layer, a gap waveguide cavity layer is placed. The electromagnetic coupling to the cavity is achieved through a coupling
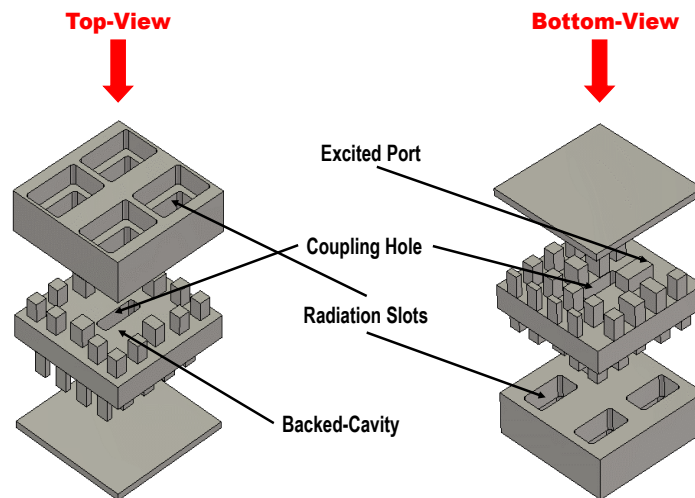
Figure 5.16: Distributed view of the proposed 2×2 cavity-backed slot sub-array. Source: [Paper 6].
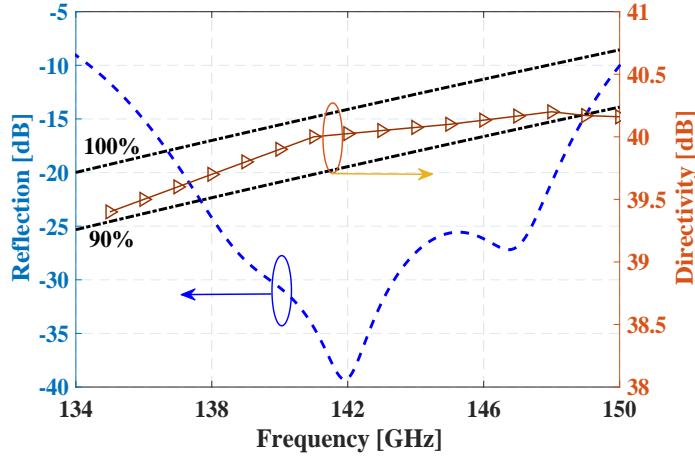
Figure 5.17: Simulated directivity and reflection coefficient of the 2×2 sub-array. Source: [Paper 6].

slot, which is excited via a RGW feeding line on the bottom layer. The distribution network is placed on the back side of the cavity layer. The major reason for the design is to avoid the misalignment error that occurs with assembly if the backed cavity and the feed layers are separated in two different layers. Thereby, the bottom waveguide layer is a smooth metallic plate. All three layers are separated by a small gap, no electrical contact required between layers.
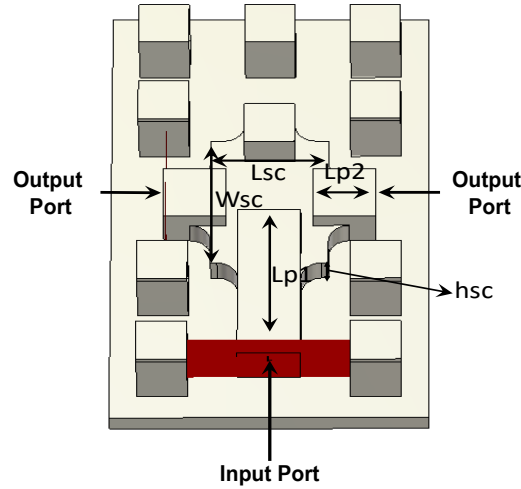
Figure 5.18: Geometry of the discontinuous T-junction power divider based on RGW in this work. The upper metallic plate is hidden. $L_{p1} = 1.35mm$, $L_{p2} = 0.45mm$, $L_{sc} = 0.84mm$, $W_{sc} = 1.16mm$ and $h_{sc} = 0.27mm$, Source: [Paper 6].
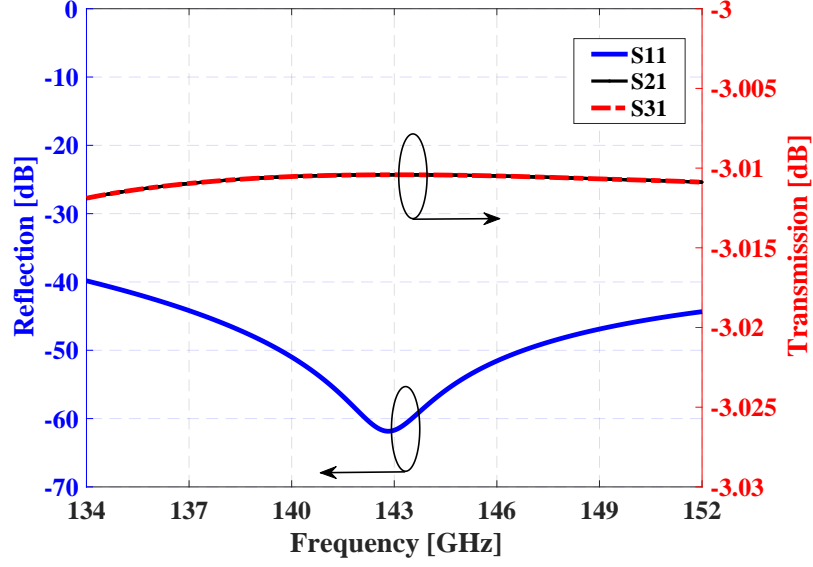
Figure 5.19: Simulated reflection coefficient and transmission coefficient of the power divider in Figure 5.18. Source: [Paper 6].

The geometry of sub-array of the proposed array antenna is shown in Figure 5.16. The element spacing is selected as 1.8 mm, to $0.81\lambda_0$. As illustrated in Figure 5.16, the configuration of a 2×2-element sub-array is first designed using periodic boundary condition in CST Microwave Studio. In Figure 5.17, the blue line shows the reflection coefficient, and an 11.5% impedance bandwidth (over 134-150 GHz) with the input reflection coefficient below -10 dB is achieved. The yellow line with triangle marks depicts the simulated directivity of the 32×32 slot array in infinite array environment. The simulated antenna efficiency is higher than 90% from 135 to 148 GHz.

In the above-100GHz frequency band, the periodic length is so small that the T-junction power divider with continuous bend ridge is impossible to fit in. For this reason, we have developed a stepped T-junction power divider, as depicted in Figure 5.18. The corresponding simulated reflection coefficient is shown in Figure 5.19, which is below -40 dB from 134 to 152 GHz. This simulated performance is much better than the previous designs. The whole array antenna in this paper is excited through a standard D-band rectangular waveguide (WR-6) at the bottom of the whole structure. Then, a hybrid power divider is designed, and its geometry is illustrated in Figure 5.20. The simulated S-parameters of the structure both in amplitude and phase are shown in Figure 5.21. The reflection coefficient is below -27 dB in the whole band 134-150 GHz. In addition, such a hybrid structure is essentially a differential feeding geometry so that the phases of the output ports have 180 degree
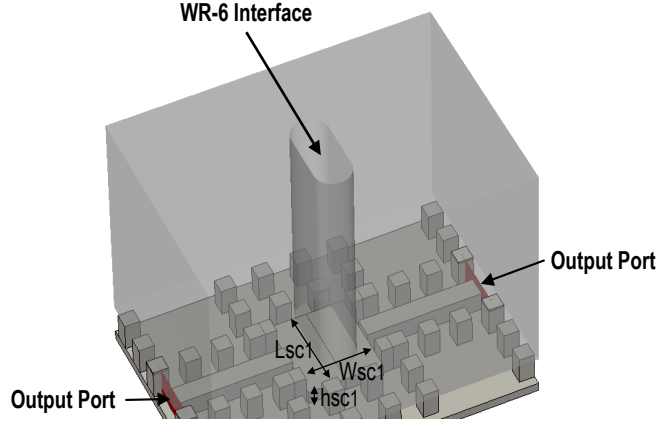
Figure 5.20: Geometrical illustration for hybrid transition from WR-6 to RGW. $L_{sc1} = 2.05mm$, $W_{sc1} = 1.77mm$ and $h_{sc1} = 0.3mm$. Source: [Paper 6].

(a)   (b)
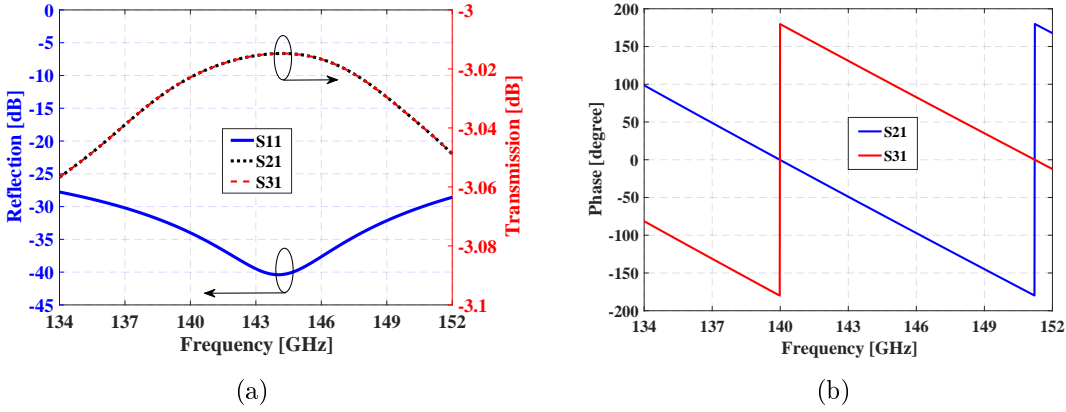
Figure 5.21: Simulated S-parameter results of designed hybrid transition from WR-6 to RGW. (a) Amplitude. (b) Phase. Source: [Paper 6].

difference, as shown in Figure 5.21(b). In order to compensate the difference of the output phases, the two half parts of the distribution network are in a mirror geometry. The entire structure is simulated in CST Microwave Studio, and the simulated reflection coefficient of the completed antenna is below -10 dB from 135 to 150 GHz, as shown in Figure 5.22. Nevertheless, the measured one is a bit higher than the simulated one. The misalignment of three antenna layers from assembling is always a problem for such a high frequency band. In addition, the extra ohmic losses caused by ridge surface roughness from CNC milling fabrication should be also considered for the difference between the simulation and the measurement. The radiation patterns and the gain were measured by a near-field measurement setup in an anechoic chamber. The simulated and the measured radiation patterns of the fabricated an-
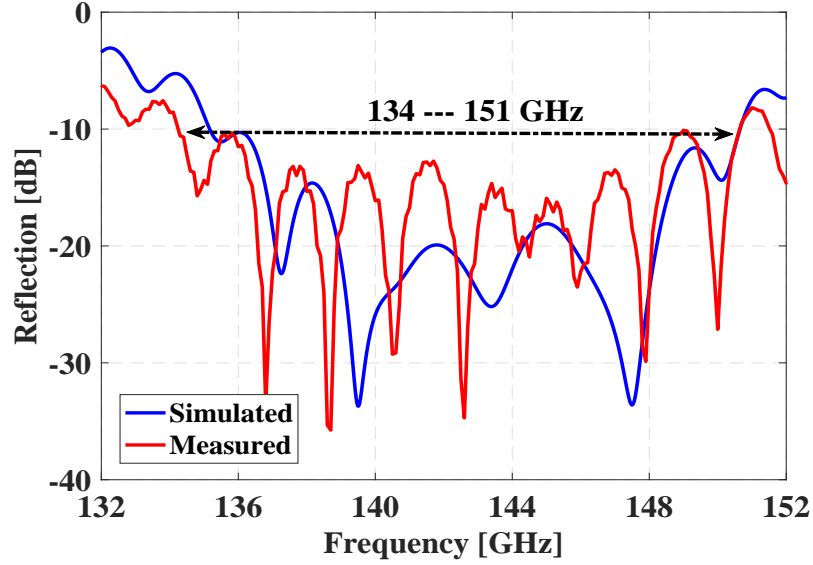
Figure 5.22: The simulated and the measured reflection coefficients of the proposed array antenna. Source: [Paper 6].

tenna at 135, 140, 145 and 150 GHz in both E- and H-planes are depicted in Figure 5.23 and Figure 5.24. The measured radiation patterns have reasonable agreements with the simulated ones while the measured side lobes are a little bit higher than simulated ones. Nevertheless, the measured radiation patterns are symmetrical, and their first side lobes both in E- and H-planes are lower than -13 dB. The measured gain is higher than 37 dBi with the measured antenna efficiency higher than 50% from 136 to 150 GHz, as depicted in Figure 5.25. There are is a difference of about 1.6 dB between the measured and the simulated gains in the whole frequency band. The roughness of the metallic surface is a reason for increasing the conductor loss in this frequency band.

In this chapter, we have described the background of the transmission line–RGW. This structure inherits the advantages of traditional ridge waveguide. Moreover, it does not require the electrical contact and therefore overcomes the manufacturing problem in mmWs. After correct selections of metallic pins, RGW becomes a good choice in the above-100 GHz frequency band. Compared with another non-substrate geometry, such as GGW, RGW is more compact for high-gain and high-efficiency slot array antennas. However, several challenges in the design based on RGW should also be taken into consideration. Firstly, the conductor loss of RGW is a little higher than groove gap waveguide. Thereby, the loss budget should be very carefully calculated when a large array antenna is designed. Secondly, the RGW structure is more complicated than groove gap waveguide lines because of the geometries of the
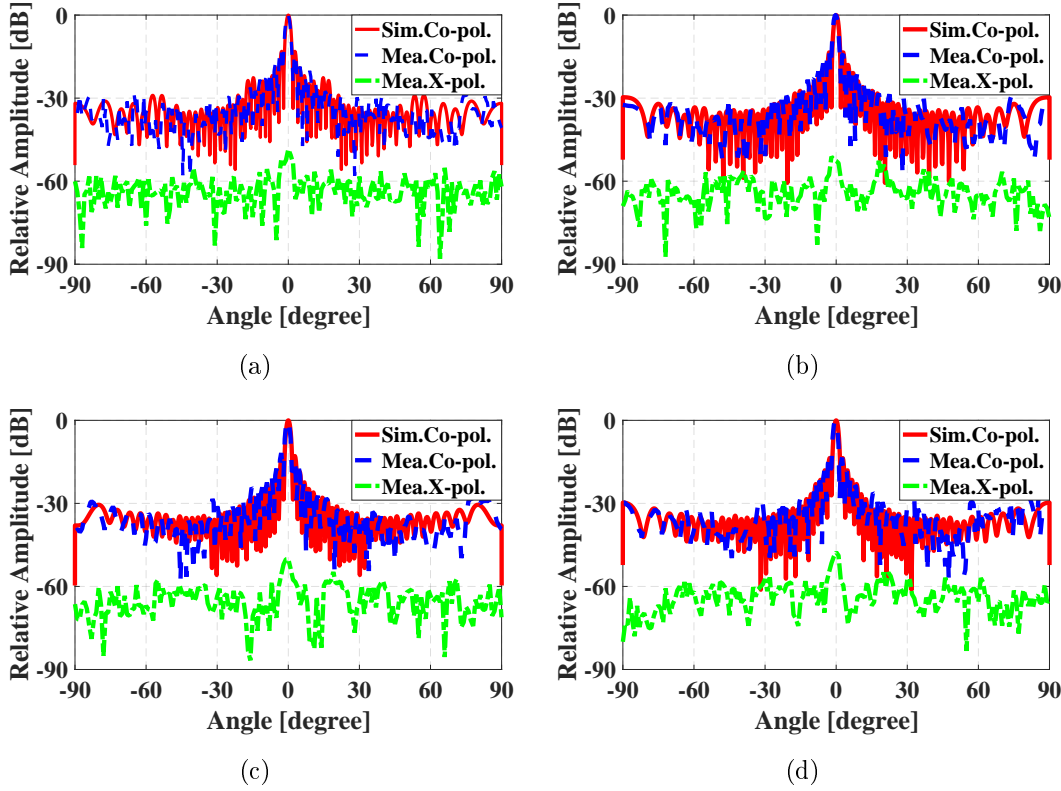
Figure 5.23: The simulated and the measured radiation patterns of proposed array antenna on E-plane at (a) 135 GHz, (b) 140 GHz, (c) 145 GHz and (d) 150 GHz. Source: [Paper 6].

ridge, which brings more variables in the design for optimization in a positive side but more difficult for manufacturing in a negative side. In addition, the coupling effect between two neighboring RGW feed lines is usually stronger than that caused by groove gap waveguides. Then, search for the minimal coupling effect between two neighboring RGW feed lines is an issue before the design of a big array antenna. The space between the ridge line and metallic pins in RGW should be optimized by taking into account the manufacturing possibilities such as CNC or molding.
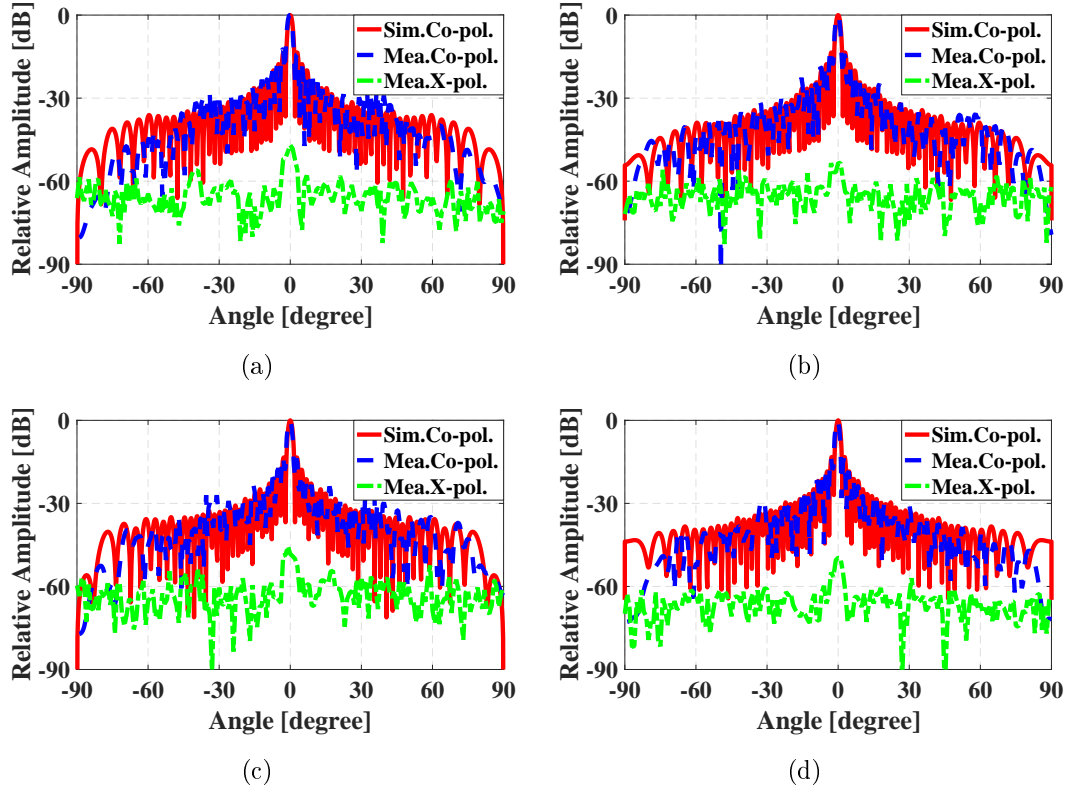
Figure 5.24: The simulated and the measured radiation patterns of proposed array antenna on H-plane at (a) 135 GHz, (b) 140 GHz, (c) 145 GHz and (d) 150 GHz. Source: [Paper 6].
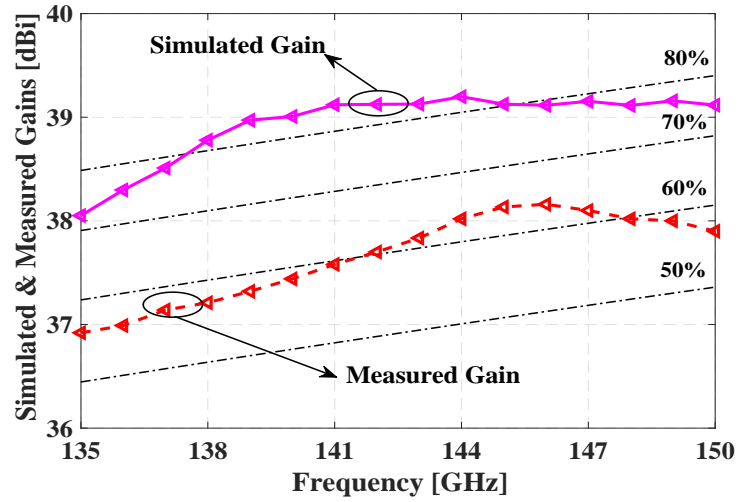
Figure 5.25: Simulated and measured gains of the proposed array antenna. Source: [Paper 6].

Chapter 6

Summary and Conclusion

As a newly invented waveguide geometry, gap waveguide technology is able to overcome some of the limitations of the traditional transmission lines(microstrip, coplanar waveguide and rectangular hollow waveguide). Specially, the gap waveguide technology shows very strong competitive strength for Ka- to D-band applications, with the features of low loss and flexible fabrication and assembly. This thesis presents several types of the slot array antennas fed by IMGW, RGW and GGW. Moreover, the realization of gap waveguide structures is explored by using several different fabrication methods, such as die-sink EDM and CNC micro-machining. The first part of this thesis comprises an introduction of gap waveguide theory, the slot array antenna designed by gap waveguide geometry from V-band to D-band. From the measurement results, the gap waveguide structures show big advantages over the traditional hollow waveguide and microstrip line. The second part of the thesis consists of selected published and submitted research papers by the author.

Chapter 7

Contributions of the Thesis and Future Directions

In the aforementioned chapters, three geometries of gap waveguide technologies and their applications for mmWs high-gain array antenna have been introduced. The gap waveguide has been proposed as a promising technology to overcome the problems that traditional planar transmission lines and hollow waveguides usually face above 25 GHz. The target of this thesis is to describe recent developments of gap waveguide technology on aspects concerning: slot array array antennas design, taking into consideration the issues such as manufactruing tolerance and cost perspective.

The first part of the thesis has been comprised an overview about the theory of gap waveguide, the advantages over the traditional transmission lines and hollow waveguides and several types of high-gain array antennas. The second part of the thesis consists of the research outcomes by the author, and the followed section mainly summarizes the appended articles.

Paper 1: Analytical Solutions to Characteristic Impedance and Losses of Inverted Microstrip Gap Waveguide Based on Variational Method

This paper presents an analytical analysis of newly IMGW. By applying the classical variational method the characteristic impedance, dielectric loss, and conductor loss of the IMGW are obtained. Among the all losses in mmWs, the dielectric loss is the dominant one in traditional microstrip and covered microstrip. We have theoretically evaluated that the unavoidable dielectric loss is characterized by three factors: the electromagnetic field distributions in both the air gap and the substrate, the loss tangent value and the thickness of the substrate. Therefore, a general guideline of how to reduce the dielectric loss is obtained: using thin substrate, using low loss substrate and optimizing the field distribution in the IMGW. The calculated

characteristic impedance and losses of IMGW with the present analytical method have been verified by commercial software CST. Furthermore, we have theoretically proved that the total loss of electromagnetic energy in the IMGW is much lower than that of covered microstrip line in mmWs.

My contribution- I analyzed the theory, simulations, and wrote the paper.

Paper 2: Design and Fabrication of a High Gain 60-GHz Cavity-backed Slot Antenna Array fed by Inverted Microstrip Gap Waveguide

This article deals with the design of a 16×16 slot array antenna fed by IMGW. The whole structure designed in this work consists of radiating slots, a groove gap cavity layer, a distribution feeding network and a transition from standard WR-15 waveguide to the IMGW. Firstly, a 2×2 cavity-backed slot sub-array is designed with periodic boundary condition to achieve good performances of radiation pattern and directivity. Then a complete IMGW feeding network with a transition from WR-15 rectangular waveguide to the IMGW has been realized to excite the radiating slots. The complete antenna array is designed at 60-GHz frequency band and fabricated using EDM technology. The measurements show that the antenna has a 16.95% bandwidth covering 54-64 GHz frequency range. The measured gain of the antenna is more than 28 dBi with the efficiency higher than 40% covering 54-64 GHz frequency range.

My contribution- I designed, simulated, performed the measurements, and wrote the paper.

Paper 3: Low sidelobe Slot Array Antenna based on Inverted Microstrip Gap Waveguide at 28 GHz

This paper presents a novel design of a low sidelobe array antenna at 28 GHz. The proposed array antenna is fed by a classic full-corporate double-layer distribution network based on the IMGW. In order to achieve low sidelobe property, a classic Taylor synthesis method is adopted in this work. In the distribution network, a couple of unequal power dividers with identical output phases are applied for the low sibelobe in this work. The fundamental radiator is 2×2 slot sub-array, and the entire array antenna is constructed by 8×8 of such kind sub-arrays. The simulated radiation patterns show that the first sidelobe levels, front-back ratio in both E-plane and H-plane from 26.5 GHz to 29.5 GHz are very well improved compared with traditional ones with the equal amplitude and phase distribution networks. The input impedance

bandwidth is about 12% with the reflection coefficient below -10 dB, and the gain is more than 29 dBi from 26.5 GHz to 29.5 GHz.

My contribution- I designed, simulated, performed the measurements, and wrote the paper.

Paper 4: Design of Wideband Slot Array Antenna by Groove Gap Waveguide in Millimeter Waves

This paper systematically presents a new design of a high-efficiency corporate-fed slot array antenna based on GGW in the W-band. A cavity-backed slot sub-array is firstly designed in a GGW cavity. The cavity is fed through a coupling hole from GGW distribution network at the bottom layer. The sub-array is numerically optimized in an infinite array environment. Low side lobes are obtained in both horizontal and vertical planes by diagonal placement of the radiation slot rotating by 45 degrees. Furthermore, the radiation narrow slot pair is adopted so that the good cross polarization is achieved. The fabricated antenna depicts more than 25% bandwidth with input reflection coefficient better than -8 dB and the aperture efficiency higher than 60% with around 25 dBi realized gain between 70 and 90 GHz. The measured cross polarization level is below -27 dB, which satisfies the ETSI standard.

My contribution- I designed, simulated, performed the measurements, and wrote the paper.

Paper 5: A Slot Array Antenna With Single-Layered Corporate-Feed Based on Ridge Gap Waveguide in the 60 GHz Band

This paper presents an 8×8-element slot array antenna with single-layered corporate-feed based on the RGW technology in the 60 GHz band. As is well known, a corporate-feed slot array antenna usually has backed cavities to increase the bandwidth and provides to a space for its distribution network, and therefore three layers in total: one layer for radiating slots and two layers for feed network with one layer of back cavities and the other one of power dividers. The antenna in this paper is designed by utilizing only two separate metallic layers: a corporate-feed network layer and a radiating slot layer. Compared with the conventional three layered slot array antennas, the proposed antenna avoids the utilization of the backed cavity layer so that its complexity and manufacture cost decrease. In order to solve the problem of the narrow bandwidth caused by taking away the backed cavities, we utilize double-ridged radiating slots instead of the conventional rectangular ones. A compact transition power divider from standard waveguide WR-15 to the RGW is introduced to excite the proposed array antenna. The 8×8-element slot array antenna has been

fabricated by computerized numerical control machining technique. The measured results demonstrate that the -10 dB reflection coefficient has around 17% bandwidth covering 56.5-67 GHz frequency range, and the measured gain is better than 26 dBi with more than 70% antenna efficiency over 58-66 GHz.

My contribution- I designed, simulated, performed the measurements, and wrote the paper.

Paper 6: Design and Fabrication of a 32×32-element Slot Array Antenna based on Ridge Gap Waveguide in D-Band

This paper presents a new design of slot array antenna based on RGW at 140-GHz. The proposed array antenna consists of 32×32 radiation slots, backed cavities and full-corporate distribution network based on RGW. In order to fabricate the proposed array antenna by CNC technology, the periodic pin structure has been chosen with an aspect ratio of 1.5:1. Since the layout space for the distribution networks is very limited, a novel stepped T-junction power divider is introduced in this work. The achieved reflection coefficient is much lower than that of the previous continuous T-junction power dividers which enables easy cascading of several T-junctions for building up a very large feed network. The measured results demonstrate about 11.4% of reflection coefficient bandwidth (S_{11} < -10 dB) covering the 135-151 GHz frequency range, and the measured gain is larger than 37 dBi over the band with more than 50% antenna efficiency.

My contribution- I designed, simulated, performed the measurements, and wrote the paper.

7.1 Future research work

This thesis has presented my recent investigations on gap waveguide technology for high-gain high-efficiency array antenna. Moreover, gap waveguide shows very strong competitive features over the traditional technologies in mmWs frequency bands. Here I have some suggestions for research directions in the future:

1. Investigation of the applications of gap waveguide technology for automotive radar systems by using the low loss and packaging features.

2. Ultra-low sidelobe array antennas in mmWs, which satisfy with the ETSI or FCC Class III standard radiation patterns.

3. Passive multi-beam antenna based on Bulter Matix configuration and active beam scanning antenna with integrated TX/RX modules.

References

[1] P. Smulders, "Exploiting the 60-ghz band for local wireless multimedia access: Prospects and future directions," *IEEE Communications Magazine*, vol. 40, no. 1, pp. 140–147, 2002.

[2] L. Lin and Z. Li, "Study of transmission effects of millimeter wave through fog and haze," in *2016 IEEE Advanced Information Management, Communicates, Electronic and Automation Control Conference (IMCEC).* IEEE, 2016, pp. 1591–1596.

[3] D. Deslandes and K. Wu, "Integrated microstrip and rectangular waveguide in planar form," *IEEE Microwave and Wireless Components Letters*, vol. 11, no. 2, pp. 68–70, 2001.

[4] F. Xu and K. Wu, "Guided-wave and leakage characteristics of substrate integrated waveguide," *IEEE Transactions on Microwave Theory and Techniques*, vol. 53, no. 1, pp. 66–73, 2005.

[5] L. Wang, X. Yin, S. Li, H. Zhao, L. Liu, and M. Zhang, "Phase corrected substrate integrated waveguide h-plane horn antenna with embedded metal-via arrays," *IEEE Transactions on Antennas and Propagation*, vol. 62, no. 4, pp. 1854–1861, April 2014.

[6] T. Li and Z. N. Chen, "Control of beam direction for substrate-integrated waveguide slot array antenna using metasurface," *IEEE Transactions on Antennas and Propagation*, vol. 66, no. 6, pp. 2862–2869, June 2018.

[7] L. Wang, X. Yin, M. Esquius-Morote, H. Zhao, and J. R. Mosig, "Circularly polarized compact ltsa array in siw technology," *IEEE Transactions on Antennas and Propagation*, vol. 65, no. 6, pp. 3247–3252, June 2017.

[8] T. Li and Z. N. Chen, "Wideband substrate-integrated waveguide-fed endfire metasurface antenna array," *IEEE Transactions on Antennas and Propagation*, vol. 66, no. 12, pp. 7032–7040, Dec 2018.

REFERENCES

[9] D. Guan, C. Ding, Z. Qian, Y. Zhang, Y. Jay Guo, and K. Gong, "Broadband high-gain siw cavity-backed circular-polarized array antenna," *IEEE Transactions on Antennas and Propagation*, vol. 64, no. 4, pp. 1493–1497, April 2016.

[10] S. E. Hosseininejad and N. Komjani, "Optimum design of traveling-wave siw slot array antennas," *IEEE Transactions on Antennas and Propagation*, vol. 61, no. 4, pp. 1971–1975, April 2013.

[11] Z. Hao, Q. Yuan, B. Li, and G. Q. Luo, "Wideband *w*-band substrate-integrated waveguide magnetoelectric (me) dipole array antenna," *IEEE Transactions on Antennas and Propagation*, vol. 66, no. 6, pp. 3195–3200, June 2018.

[12] J. Xiao, Z. Qi, X. Li, and H. Zhu, "Broadband and high-gain siw-fed slot array for millimeter-wave applications," *IEEE Transactions on Antennas and Propagation*, vol. 67, no. 5, pp. 3484–3489, May 2019.

[13] M. Bozzi, A. Georgiadis, and K. Wu, "Review of substrate-integrated waveguide circuits and antennas," *IET Microwaves, Antennas Propagation*, vol. 5, no. 8, pp. 909–920, June 2011.

[14] M. Bozzi, L. Perregrini, and K. Wu, "Modeling of conductor, dielectric, and radiation losses in substrate integrated waveguide by the boundary integral-resonant mode expansion method," *IEEE Transactions on Microwave Theory and Techniques*, vol. 56, no. 12, pp. 3153–3161, Dec 2008.

[15] D. Deslandes and Ke Wu, "Accurate modeling, wave mechanisms, and design considerations of a substrate integrated waveguide," *IEEE Transactions on Microwave Theory and Techniques*, vol. 54, no. 6, pp. 2516–2526, June 2006.

[16] P.-S. Kildal, E. Alfonso, A. Valero-Nogueira, and E. Rajo-Iglesias, "Local metamaterial-based waveguides in gaps between parallel metal plates," *IEEE Antennas and Wireless Propagation Letters*, vol. 8, pp. 84–87, 2009.

[17] P.-S. Kildal, "Artificially soft and hard surfaces in electromagnetics," *IEEE Transactions on Antennas and Propagation*, vol. 38, no. 10, pp. 1537–1544, 1990.

[18] J. Liu, J. Yang, and A. U. Zaman, "Analytical solutions to characteristic impedance and losses of inverted microstrip gap waveguide based on variational method," *IEEE Transactions on Antennas and Propagation*, vol. 66, no. 12, pp. 7049–7057, Dec 2018.

[19] H. Raza, J. Yang, P. Kildal, and E. Alfonso Alos, "Microstrip-ridge gap waveguide-study of losses, bends, and transition to wr-15," *IEEE Transactions on Microwave Theory and Techniques*, vol. 62, no. 9, pp. 1943–1952, Sep. 2014.

[20] M. Ferrando-Rocher, J. I. Herranz-Herruzo, A. Valero-Nogueira, and B. Bernardo-Clemente, "Performance assessment of gap-waveguide array antennas: Cnc milling versus three-dimensional printing," *IEEE Antennas and Wireless Propagation Letters*, vol. 17, no. 11, pp. 2056–2060, Nov 2018.

[21] A. Vosoogh, M. S. Sorkherizi, V. Vassilev, A. U. Zaman, Z. S. He, J. Yang, A. A. Kishk, and H. Zirath, "Compact integrated full-duplex gap waveguide-based radio front end for multi-gbit/s point-to-point backhaul links at e-band," *IEEE Transactions on Microwave Theory and Techniques*, pp. 1–15, 2019.

[22] A. Vosoogh, A. Uz Zaman, V. Vassilev, and J. Yang, "Zero-gap waveguide: A parallel plate waveguide with flexible mechanical assembly for mm-wave antenna applications," *IEEE Transactions on Components, Packaging and Manufacturing Technology*, vol. 8, no. 12, pp. 2052–2059, Dec 2018.

[23] A. Farahbakhsh, D. Zarifi, and A. U. Zaman, "60-ghz groove gap waveguide based wideband h -plane power dividers and transitions: For use in high-gain slot array antenna," *IEEE Transactions on Microwave Theory and Techniques*, vol. 65, no. 11, pp. 4111–4121, Nov 2017.

[24] A. Vosoogh, M. S. Sorkherizi, A. U. Zaman, J. Yang, and A. A. Kishk, "An integrated ka-band diplexer-antenna array module based on gap waveguide technology with simple mechanical assembly and no electrical contact requirements," *IEEE Transactions on Microwave Theory and Techniques*, vol. 66, no. 2, pp. 962–972, Feb 2018.

[25] A. Vosoogh, A. Haddadi, A. U. Zaman, J. Yang, H. Zirath, and A. A. Kishk, "w-band low-profile monopulse slot array antenna based on gap waveguide corporate-feed network," *IEEE Transactions on Antennas and Propagation*, vol. 66, no. 12, pp. 6997–7009, Dec 2018.

[26] M. Al Sharkawy and A. A. Kishk, "Long slots array antenna based on ridge gap waveguide technology," *IEEE Transactions on Antennas and Propagation*, vol. 62, no. 10, pp. 5399–5403, Oct 2014.

[27] B. Cao, H. Wang, Y. Huang, and J. Zheng, "High-gain l-probe excited substrate integrated cavity antenna array with ltcc-based gap waveguide feeding network for w-band application," *IEEE Transactions on Antennas and Propagation*, vol. 63, no. 12, pp. 5465–5474, Dec 2015.

[28] A. Dadgarpour, M. S. Sorkherizi, T. A. Denidni, and A. A. Kishk, "Passive beam switching and dual-beam radiation slot antenna loaded with enz medium and excited through ridge gap waveguide at millimeter-waves," *IEEE Transactions on Antennas and Propagation*, vol. 65, no. 1, pp. 92–102, Jan 2017.

REFERENCES

[29] D. Zarifi, A. Farahbakhsh, and A. U. Zaman, "A gap waveguide-fed wideband patch antenna array for 60-ghz applications," *IEEE Transactions on Antennas and Propagation*, vol. 65, no. 9, pp. 4875–4879, Sep. 2017.

[30] M. Sharifi Sorkherizi, A. Dadgarpour, and A. A. Kishk, "Planar high-efficiency antenna array using new printed ridge gap waveguide technology," *IEEE Transactions on Antennas and Propagation*, vol. 65, no. 7, pp. 3772–3776, July 2017.

[31] P. Sadri-Moshkenani, J. Rashed-Mohassel, and M. Shahabadi, "Microstrip antenna array fed by a low-loss gap-waveguide feed network," *IEEE Transactions on Antennas and Propagation*, vol. 66, no. 8, pp. 4359–4363, Aug 2018.

[32] A. Dadgarpour, M. Sharifi Sorkherizi, and A. A. Kishk, "Wideband low-loss magnetoelectric dipole antenna for 5g wireless network with gain enhancement using meta lens and gap waveguide technology feeding," *IEEE Transactions on Antennas and Propagation*, vol. 64, no. 12, pp. 5094–5101, Dec 2016.

[33] Y. Shi, W. Feng, H. Wang, W. Che, Q. Xue, J. Wang, J. Zhang, X. Qian, M. Zhou, and B. Cao, "Novel w -band ltcc transition from microstrip line to ridge gap waveguide and its application in 77/79 ghz antenna array," *IEEE Transactions on Antennas and Propagation*, vol. 67, no. 2, pp. 915–924, Feb 2019.

[34] E. Rajo-Iglesias, P. Kildal, A. U. Zaman, and A. Kishk, "Bed of springs for packaging of microstrip circuits in the microwave frequency range," *IEEE Transactions on Components, Packaging and Manufacturing Technology*, vol. 2, no. 10, pp. 1623–1628, Oct 2012.

[35] A. U. Zaman, M. Alexanderson, T. Vukusic, and P.-S. Kildal, "Gap waveguide pmc packaging for improved isolation of circuit components in high-frequency microwave modules," *IEEE Transactions on Components, Packaging and Manufacturing Technology*, vol. 4, no. 1, pp. 16–25, 2014.

[36] U. Nandi, A. U. Zaman, A. Vosoogh, and J. Yang, "Novel millimeter wave transition from microstrip line to groove gap waveguide for mmic packaging and antenna integration," *IEEE Microwave and Wireless Components Letters*, vol. 27, no. 8, pp. 691–693, Aug 2017.

[37] M. Sharifi Sorkherizi and A. A. Kishk, "Self-packaged, low-loss, planar bandpass filters for millimeter-wave application based on printed gap waveguide technology," *IEEE Transactions on Components, Packaging and Manufacturing Technology*, vol. 7, no. 9, pp. 1419–1431, Sep. 2017.

[38] A. U. Zaman, P. Kildal, and A. A. Kishk, "Narrow-band microwave filter using high-q groove gap waveguide resonators with manufacturing flexibility and no

sidewalls," *IEEE Transactions on Components, Packaging and Manufacturing Technology*, vol. 2, no. 11, pp. 1882–1889, 2012.

[39] M. S. Sorkherizi, A. Khaleghi, and P. Kildal, "Direct-coupled cavity filter in ridge gap waveguide," *IEEE Transactions on Components, Packaging and Manufacturing Technology*, vol. 4, no. 3, pp. 490–495, March 2014.

[40] A. A. Brazalez, A. U. Zaman, and P. Kildal, "Improved microstrip filters using pmc packaging by lid of nails," *IEEE Transactions on Components, Packaging and Manufacturing Technology*, vol. 2, no. 7, pp. 1075–1084, July 2012.

[41] B. Ahmadi and A. Banai, "Direct coupled resonator filters realized by gap waveguide technology," *IEEE Transactions on Microwave Theory and Techniques*, vol. 63, no. 10, pp. 3445–3452, Oct 2015.

[42] J. Wu, Y. J. Cheng, and Y. Fan, "A wideband high-gain high-efficiency hybrid integrated plate array antenna for v-band inter-satellite links," *IEEE Transactions on Antennas and Propagation*, vol. 63, no. 4, pp. 1225–1233, 2015.

[43] J. Xu, Z. N. Chen, X. Qing, and W. Hong, "Bandwidth enhancement for a 60 ghz substrate integrated waveguide fed cavity array antenna on ltcc," *IEEE Transactions on Antennas and Propagation*, vol. 59, no. 3, pp. 826–832, March 2011.

[44] Y. Li and K.-M. Luk, "60-ghz substrate integrated waveguide fed cavity-backed aperture-coupled microstrip patch antenna arrays," *IEEE Transactions on Antennas and Propagation*, vol. 63, no. 3, pp. 1075–1085, 2015.

[45] Y. Miura, J. Hirokawa, M. Ando, Y. Shibuya, and G. Yoshida, "Double-layer full-corporate-feed hollow-waveguide slot array antenna in the 60-ghz band," *IEEE Transactions on Antennas and Propagation*, vol. 59, no. 8, pp. 2844–2851, 2011.

[46] A. A. Brazalez, E. Rajo-Iglesias, J. L. Vazquez-Roy, A. Vosoogh, and P.-S. Kildal, "Design and validation of microstrip gap waveguides and their transitions to rectangular waveguide, for millimeter-wave applications," *IEEE Transactions on Microwave Theory and Techniques*, vol. 63, no. 12, pp. 4035–4050, 2015.

[47] P. N. S. Kutiyal, A. Kedar, M. Garg, K. S. Beenamole, S. O. Kundukulam, and U. K. Revankar, "Planar microstrip antenna array for radar system with surveillance applications," in *The Second European Conference on Antennas and Propagation, EuCAP 2007*, Nov 2007, pp. 1–4.

[48] A. G. Toshev, "Analysis, design and measurement of a low sidelobe level lightweight array antenna for surveillance radar applications," in *18-th INTERNATIONAL CONFERENCE ON MICROWAVES, RADAR AND WIRELESS COMMUNICATIONS*, June 2010, pp. 1–4.

References

[49] K. Tekkouk, J. Hirokawa, R. Sauleau, M. Ettorre, M. Sano, and M. Ando, "Dual-layer ridged waveguide slot array fed by a butler matrix with sidelobe control in the 60-ghz band," *IEEE Transactions on Antennas and Propagation*, vol. 63, no. 9, pp. 3857–3867, Sep. 2015.

[50] P. Liu, J. Liu, W. Hu, and X. Chen, "Hollow waveguide 32×32-slot array antenna covering 71-86 ghz band by the technology of a polyetherimide fabrication," *IEEE Antennas and Wireless Propagation Letters*, vol. 17, no. 9, pp. 1635–1638, Sep. 2018.

[51] A. Berenguer, V. Fusco, D. E. Zelenchuk, D. Sanchez-Escuderos, M. Baquero-Escudero, and V. E. Boria-Esbert, "Propagation characteristics of groove gap waveguide below and above cutoff," *IEEE Transactions on Microwave Theory and Techniques*, vol. 64, no. 1, pp. 27–36, Jan 2016.

[52] H. Raza, J. Yang, P. Kildal, and E. Alfonso, "Resemblance between gap waveguides and hollow waveguides," *IET Microwaves, Antennas Propagation*, vol. 7, no. 15, pp. 1221–1227, December 2013.

[53] T. Tomura, J. Hirokawa, T. Hirano, and M. Ando, "A 45°linearly polarized hollow-waveguide 16×16-slot array antenna covering 71-86 ghz band," *IEEE Transactions on Antennas and Propagation*, vol. 62, no. 10, pp. 5061–5067, Oct 2014.

[54] S. Hopfer, "The design of ridged waveguides," *IRE Transactions on Microwave Theory and Techniques*, vol. 3, no. 5, pp. 20–29, October 1955.

[55] L. Qin, Y. Lu, Q. You, Y. Wang, J. Huang, and P. Gardner, "Millimeter-wave slotted waveguide array with unequal beamwidths and low sidelobe levels for vehicle radars and communications," *IEEE Transactions on Vehicular Technology*, vol. 67, no. 11, pp. 10 574–10 582, Nov 2018.

[56] A. Vosoogh, A. A. Brazalez, and P.-S. Kildal, "A v-band inverted microstrip gap waveguide end-coupled bandpass filter," *IEEE Microwave and Wireless Components Letters*, vol. 26, no. 4, pp. 261–263, 2016.

[57] A. Vosoogh, P.-S. Kildal, and V. Vassilev, "Wideband and high-gain corporate-fed gap waveguide slot array antenna with etsi class ii radiation pattern in *v*-band," *IEEE Transactions on Antennas and Propagation*, vol. 65, no. 4, pp. 1823–1831, 2017.

[58] E. F. Nichols and J. D. Tear, "Short electric waves," *Phys. Rev.*, vol. 21, pp. 587–610, Jun 1923. [Online]. Available: https://link.aps.org/doi/10.1103/PhysRev.21.587

Part II

Included Papers

Paper 1

Analytical Solutions towards Inverted Microstrip
Gap Waveguide for characteristic Impedance and
Losses based on variational Method

Jinlin Liu, Jian Yang and Ashraf Uz Zaman

The layout of this paper has been revised in order to comply with the rest of
the thesis.

Analytical Solutions towards Inverted Microstrip Gap Waveguide for characteristic Impedance and Losses based on variational Method

Jinlin Liu, Jian Yang and Ashraf Uz Zaman

Abstract

This paper initially introduces analytical solutions to newly invented inverted microstrip gap waveguide (IMGW). Applying classical variational method the characteristic impedance, dielectric loss and conductor loss of the IMGW are obtained. The calculated characteristic impedance with present method has been verified by commercial software CST. Furthermore, we have theoretically proved that the total loss of electromagnetic energy in the IMGW is much lower than that of covered microstrip line in millimeter waves (mmWs). Thereby, the IMGW has big advantages over microstrip lines for high-gain, high-efficiency array antenna in mmWs.

1 Introduction

Moving upwards in the spectrum for developing future wireless systems involves significant challenges from the hardware aspect [1]. Millimeter waves (mmWs) hardware modules need to be feasible in easy fabrication, high integration and low cost. Traditional hollow rectangular waveguide is normally manufactured in two parts and joined together. The two metallic structures usually suffer from the problem of poor electrical contacts. Another conventional transmission line, microstrip line, suffers from increased dielectric losses at high frequencies and spurious resonance when it is encapsulated or packaged. A covered microstrip line can overcome some of these disadvantages, but still presents high losses in the dielectrics in mmWs. Other solutions like substrate integrated waveguide (SIW) [2] exhibit the same unwanted losses in the dielectrics as frequency increases [3]. As a contrast, recently introduced gap waveguide technology [4]-[7] has low losses and low cost for manufacture. According to the theory of soft- and hard-surfaces [8], perfect electric conductor (PEC) and perfect magnetic conductor (PMC) parallel plates are able to create a frequency stopband where no waves can propagate through when the distance between the two plates is smaller than a quarter wavelength. As is well known, PMC does not exist in nature so we have to apply metallic textured pins surface for realizing an approximate PMC boundary condition.

There are four different realizations of gap waveguides — ridge gap waveguide,
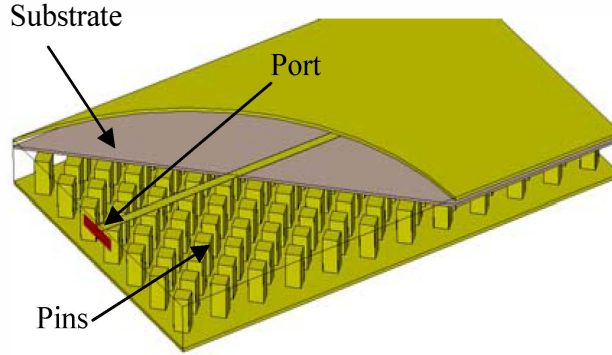
Figure 1: 3-Dimensional geometry for IMGW.

groove gap waveguide, inverted microstrip gap waveguide (IMGW) [6] and microstrip-ridge gap waveguide [9]. In the recent years some promising achievements on gap waveguide technology in the fields of passive element circuits [10]-[12], packaging technology [13] and high gain antennas [14]-[17] have been reported. Among the four realized structures the IMGW has certain advantages over the other three because its pin plate has uniform pattern that can be easily manufactured. Fig. 1 illustrates a general IMGW which is based on the utilization of a thin substrate over a periodic metallic pins pattern. This periodic pins layer constitutes an approximate PMC surface [8], which together with the PEC plate suppresses all propagations. Thereby, a local quasi-TEM mode is able to propagate only along the microstrip.

So far solving electromagnetic problems of the IMGW merely depends on the commercial CAD tools. Therefore, there are uncertainties with only commercial numerical solvers. First of all, it is difficult and not 100% sure how to set up waveguide port in CAD models to evaluate the characteristic impedance so that an analytical solution is needed to verify the numerical port definition. Secondly, we would like to have easy calculated formulas and figures for dielectric loss and conductor loss of the IMGW in order to make a good design of high-gain antennas by using IMGW, which requires analytical solutions of the IMGW. Towards such kinds of themes of microstrip lines there have been already an extensive amount of work done in the past decades — equivalent circuits model [18], theory of conformal mapping [19]-[21], perturbation method [22], variational method [23]-[25], spectral-domain method [26]-[28] and potential theory [29]-[30]. For a shielded microstrip line with outer conductor it is convenient to establish a variational method and solve the corresponding Green's function in a closed form [25]. Nevertheless, it is not possible to obtain the Green's function in closed form for the case of a parallel-plate transmission line with multilayered dielectrics. In [24] a variational method analysis for microstrip lines was carried out in spectral domain to determine the Green's function in a simple way. In this paper we apply a variational method for IMGW to solve the mentioned problems.

The same strategy is also applied to a covered microstrip line so that the comparison of their losses is made in this work.

The organization of this paper is as fellows. Firstly the Fourier transform is applied to both IMGW and covered microstrip line and the differential equation is solved by Green's function in spectral domain. The theoretical analysis on characteristic impedance, dielectric loss and conductor loss are discussed based on the analysis. Then, the corresponding simulated results in CST Microwave Studio are discussed and compared with the analytical solutions. Finally, conclusions and limitations of this method are described.

2 Fundamental Theory

2.1 Solutions by spectral Domain Method

According to [31], the TEM mode in a transmission line can be described by a model of electrostatic fields as the dominant mode, even when a nonuniform medium is applied in the structure. This kind of approximation has been proved to be reasonable when the cross-sectional dimensions of a transmission line are smaller than the propagated wavelength. Therefore, TEM mode problems may be treated by electrostatic theory, namely solving Poisson equation or Laplace equation. The basic idea in the present work is illustrated in Fig. 2. For directly solving Poisson equation to the parallel plates IMGW it is very difficult while the boundary conditions along the x axis are not specified (upper and bottom plates and the substrate are infinite along x axis), as depicted in Fig. 3. Therefore, the utilization of Fourier transform to go to spectrum domain will make the solution much easier. The general cross-sectional prototype of the IMGW is illustrated in Fig. 3. Assuming the width of the strip $w << \lambda$ and the height $b < \lambda/4$, where λ is the wavelength at an operation frequency so that electrostatic condition can be approximately fulfilled. The corresponding electric
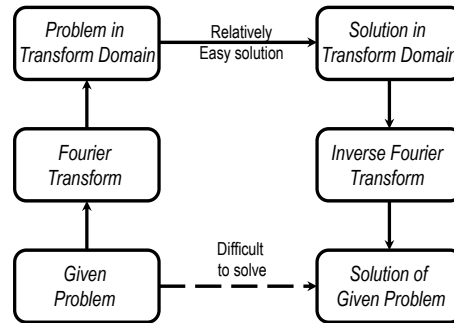
Figure 2: Typical block diagram in Fourier transform method.
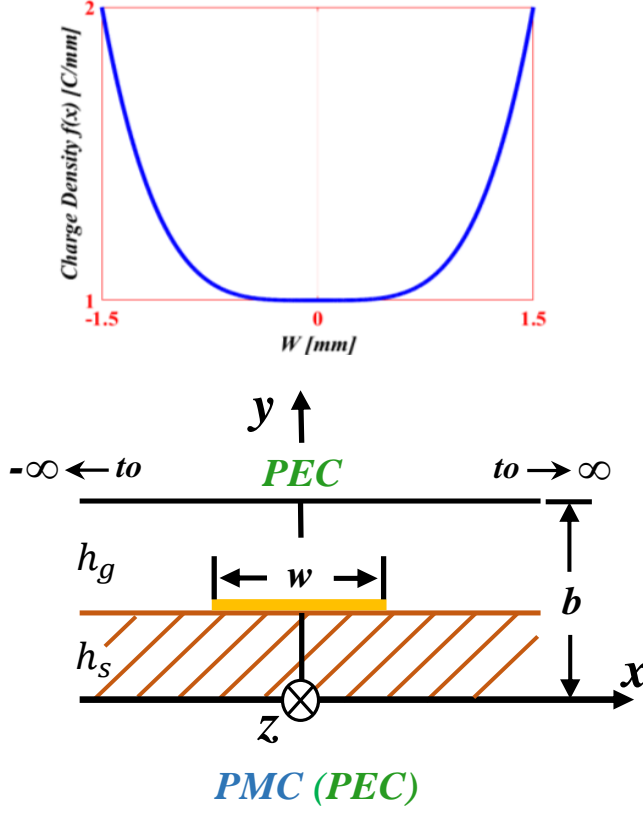
Figure 3: The upper figure illustrates the charge density $f(x)$ versus the width w of the microstrip. The figure below the upper one depicts the ideal cross-sectional view of an IMGW or a covered microstrip gap waveguide to be analyzed in this work. For the IMGW case the metallic pin structure is treated as PMC boundary condition. For the covered microstrip line the bottom boundary condition is PEC.

potential distribution $\psi(x,y)$ is related to the charge density $\rho(x,y)$ by Poisson's equation

$$\nabla^2\psi(x,y) = \frac{\partial^2\psi(x,y)}{\partial x^2} + \frac{\partial^2\psi(x,y)}{\partial y^2} = -\frac{\rho(x,y)}{\varepsilon} \qquad (1)$$

where ε is the permittivity. In reality, the thickness of microstrip we have is much smaller than the width w so that the microstrip is considered as infinite thin and $\rho(x,y)$ can be described by

$$\rho(x,y) = f(x)\delta(y-h_s), \qquad (2)$$

where $\delta(y-h_s)$ is Dirac's function and $f(x)$ the charge density distribution on the microstrip. According to Thomson's theorem, the charges distribute themselves on

the conducting structures so that the electric energy is minimized. An approximation of the charge density was given by [25]

$$f(x) = 1 + \left|\frac{2x}{w}\right|^3, \qquad |x| \le \frac{w}{2} \tag{3}$$

as shown in the Fig. 3. The Green's function G is regarded as the potential due to a unit charge in an infinitely small volume at (x', y'). Therefore, it is the solution to the equation of

$$\nabla^2 G(x - x', y - y') = -\frac{1}{\varepsilon}\delta(x - x')\delta(y - y') \tag{4}$$

where $\delta(x - x')\delta(y - y')$ is Dirac's function which expresses a unit charge at (x', y'). Once Green's function G is obtained, the electric potential $\psi(x, y)$ due to charge distribution $\rho(x', y')$ is given by the superposition principle which can be expressed as:

$$\psi(x, y) = \int_l G(x - x', y - y')\rho(x', y')dl' \tag{5}$$

where the integral is defined over the conductor contour l in 2-D structure. Now we apply Fourier transform to convert the 2-D problem to spatial 1-D problem in spectrum,

$$\widetilde{\psi}(k, y) = \int_{-\infty}^{\infty} \psi(x, y)e^{-jkx}dx \tag{6}$$

According to the differential property of Fourier-Transform, namely, $\frac{\partial^2 \psi(x,y)}{\partial x^2} \Leftrightarrow (jk)^2\widetilde{\psi}(k, y)$, (1) can be written as:

$$-k^2\widetilde{\psi}(k, y) + \frac{\partial^2 \widetilde{\psi}(k, y)}{\partial y^2} = 0 \qquad (y \ne h_s). \tag{7}$$

In spectral domain the solution of the potential distribution can be expressed from (5) and (6) as:

$$\widetilde{\psi}(k, y) = \widetilde{f}(k)\widetilde{G}(k, y - h_s), \tag{8}$$

where $\widetilde{f}(k)$ and $\widetilde{G}(k, y - h_s)$ are the charge density and the Green's function in spectrum domain. The corresponding expressions are as follows:

$$\widetilde{f}(k) = \int_{-\infty}^{\infty} f(x')e^{-jkx'}dx' = \frac{4}{k}sin\big(kw/2\big)$$

$$+ \frac{12}{k^2 w}\left[cos(kw/2) - \frac{2sin(kw/2)}{kw/2} + \frac{sin^2(kw/4)}{(kw/4)^2}\right] \tag{9}$$

$$\widetilde{G}(k, y - h_s) = \int_{-\infty}^{\infty} G(x - x', y - h_s)e^{-jk(x-x')}dx \tag{10}$$

Now we have already converted the second-order, source excited differential equation in (1) to a standard Sturm-Liouville problem, as expressed in (7). The boundary

condition for the IMGW structure (upper PEC and bottom PMC) illustrated in Fig. 3 are given as follows:

$$\frac{\partial \widetilde{\psi}_i(k,0)}{\partial y} = 0 \tag{11a}$$

$$\widetilde{\psi}_i(k,b) = 0 \tag{11b}$$

$$\varepsilon_s \frac{\partial \widetilde{\psi}_i(k,h_s^-)}{\partial y} - \varepsilon_0 \frac{\partial \widetilde{\psi}_i(k,h_s^+)}{\partial y} = \widetilde{\rho}(k,y) \tag{11c}$$

$$\widetilde{\psi}_i(k,h_s^+) = \widetilde{\psi}_i(k,h_s^-) \tag{11d}$$

where ε_s stands for the permittivity of the substrate materials, $\widetilde{\psi}_i$ the electric potential of the IMGW. We utilize boundary conditions (11) to obtain the Green's function from the equation (7). It leads to (13) and (14), where $\widetilde{G}_{i,s}(k,y)$ and $\widetilde{G}_{i,g}(k,y)$ are the Green's functions of the IMGW in the substrate and the air gap, respectively.

Similarly, the boundary condition for the covered microstrip line structure (upper PEC and bottom PEC) illustrated in Fig. 3 are given as follows:

$$\widetilde{\psi}_c(k,0) = 0 \tag{12a}$$

$$\widetilde{\psi}_c(k,b) = 0 \tag{12b}$$

$$\varepsilon_s \frac{\partial \widetilde{\psi}_c(k,h_s^-)}{\partial y} - \varepsilon_0 \frac{\partial \widetilde{\psi}_c(k,h_s^+)}{\partial y} = \widetilde{\rho}(k,y) \tag{12c}$$

$$\widetilde{\psi}_c(k,h_s^+) = \widetilde{\psi}_c(k,h_s^-) \tag{12d}$$

From (7) and (12), we obtain the Green' functions for the covered microstrip line presented in (15) and (16), where $\widetilde{G}_{c,s}(k,y)$ and $\widetilde{G}_{c,g}(k,y)$ stand for the Green's functions of the covered microstrip line in the substrate and the air gap, respectively. Then, the electric potential in (5) can be expressed by inverse Fourier transformation

---

$$\widetilde{G}_{i,s}(k,y) = \frac{sinh(kh_g)cosh(ky)}{k[\varepsilon_0 cosh(kh_s)cosh(kh_g) + \varepsilon_s sinh(kh_s)sinh(kh_g)]} \qquad 0 \le y \le h_s \tag{13}$$

$$\widetilde{G}_{i,g}(k,y) = \frac{cosh(kh_s)sinh(k(b-y))}{k[\varepsilon_0 cosh(kh_s)cosh(kh_g) + \varepsilon_s sinh(kh_s)sinh(kh_g)]} \qquad h_s \le y \le b \tag{14}$$

$$\widetilde{G}_{c,s}(k,y) = \frac{sinh(kh_g)sinh(ky)}{k[\varepsilon_0 sinh(kh_s)cosh(kh_g) + \varepsilon_s cosh(kh_s)sinh(kh_g)]} \qquad 0 \le y \le h_s \tag{15}$$

$$\widetilde{G}_{c,g}(k,y) = \frac{sinh(kh_s)sinh(k(b-y))}{k[\varepsilon_0 sinh(kh_s)cosh(kh_g) + \varepsilon_s cosh(kh_s)sinh(kh_g)]} \qquad h_s \le y \le b \tag{16}$$

as:

$$\psi(x, y) = \frac{1}{2\pi} \int_{-\infty}^{\infty} \widetilde{f}(k)\widetilde{G}(k, y)e^{jkx}dk \qquad (17)$$

2.2 Characteristic Impedance of the IMGW

The characteristic impedance is the ratio of the amplitudes of the voltage and the current of a single wave propagating along the transmission line. Obviously it plays a key role in design of distribution networks for antennas. In the TEM mode approximation the characteristic impedance Z_0 is usually evaluated by the line capacitance C [25]

$$Z_0 = \frac{1}{c\sqrt{C_0 C}} \qquad (18)$$

where c is the velocity of light in free space and C_0 is the line capacitance for the case $\varepsilon_s = \varepsilon_0$. Here, the corresponding line capacitance C is defined as:

$$C = \frac{Q}{\psi_0} = \frac{2\pi Q}{\int_{-\infty}^{\infty} \widetilde{f}(k)\widetilde{G}_i(k, 0)dk} \qquad (19)$$

where $\widetilde{G}_i(k, 0)$ is a particular case that the Green's function is evaluated at $y = h_s$,

$$\widetilde{G}(k, 0) =$$

$$\frac{sinh(kh_g)cosh(kh_s)}{k[\varepsilon_0 cosh(kh_s)cosh(kh_g) + \varepsilon_s sinh(kh_s)sinh(kh_g)]}. \qquad (20)$$

And the total charge Q is given by:

$$Q = \int_{-w/2}^{w/2} f(x)dx = \frac{5w}{4} \qquad [C] \qquad (21)$$

For the electrostatic problem, the potential on the microstrip has no variation along x. So we can find the potential ψ_0 on the strip at $(x = 0, y = h_s)$ by inverse Fourier transformation of (17) as:

$$\psi_0 = \psi(k, 0) = \frac{1}{2\pi} \int_{-\infty}^{\infty} \widetilde{f}(k)\widetilde{G}(k, 0)e^{jk \cdot 0}dk$$

$$= \frac{1}{2\pi} \int_{-\infty}^{\infty} \widetilde{f}(k)\widetilde{G}(k, 0)dk \qquad (22)$$

2.3 Attenuation

Theoretically, the loss components of a transmission line conclude dielectric loss and conductor loss. Attenuation due to the conductors is obtained by the following [25]

$$\alpha_c = \frac{R_s \int_l i_s^2 dl}{2\int_S v\varepsilon(\nabla\psi)^2 dS}, \quad [Neper/Unit~Length] \qquad (23)$$

where $R_s = \sqrt{0.5\omega\mu_0/\sigma_c}$ is the surface resistance, σ_c the conductivity of the microstrip, $i_s = v\rho(x, h_s)$ the current density on the microstrip, and $v = c\sqrt{C_0/C}$ the propagation velocity. The integral in the numerator is defined as the contour l of the microstrip and the integral in the denominator is defined over the whole cross-sectional area S. Notice that the unit of the conductor loss here is $Neper/Unit\ Length$, where 1 Neper = 8.6859 dB. The material for microstrip is usually Copper, the conductor loss is therefore determined by the line capacitance and the electromagnetic energy stored in the dielectrics. On the other hand, the dielectric loss can be calculated by [25]

$$\alpha_d = \frac{\sigma_d \int_S (\nabla\psi)^2 dS}{2\int_S v\varepsilon(\nabla\psi)^2 dS}, \quad [Neper/Unit\ Length] \tag{24}$$

where the integral is defined over the whole cross-sectional area S. The σ_d in (24) are

Figure 4: The left figure illustrates a covered microstrip line with PMC boundary condition at the bottom. In the right one the PMC boundary condition is replaced by metallic pins.
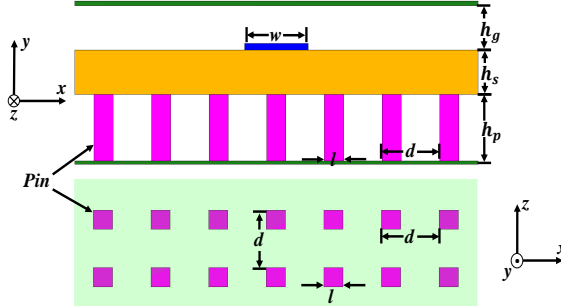
Figure 5: The illustration of detailed geometrical dimensions utilized for the following research.

presented as the conductivity of the dielectric material. The dielectric loss depends on not only the permittivity and the conductivity of the substrate, but also the potential distribution in the air gap and the substrate.

3   Theoretical and Simulated Results

In order to verify the analysis described above, numerical models were set up in CST with realization of PMC. As is shown in Fig. 4, we set up a simple straight covered

microstrip line with PMC boundary condition at the bottom. Then real metallic pins are added to realize the PMC boundary condition. The characteristic impedances of those two cases can be read from numerical ports in the CST Microwave Studio. An optimized waveguide port in [32] has been applied for the IMGW case in order to minimize the reflection coefficient. We have set up models in Ka-band, V-band and E-band. The 3-D geometrical dimensions for the corresponding structure are depicted in Fig. 5 and TABLE I. The substrate materials utilized in simulations are Rogers RO4003C with relative permittivity $\varepsilon_s = 3.55$ and loss tangent tan$\delta =$

Table 1: Geometrical Parameters of the structure in the Fig.5 in Ka-,V- and E-bands

Parameters[mm]/Frequency Bands	Ka-Band	V-Band	E-Band
d	2.4	1.1	0.8
l	1.2	0.4	0.3
h_p	1.5	1.1	0.55
h_s	0.3	0.4	0.2
h_g	0.4	0.25	0.15
w	1.2	1	0.8

0.01 at 60 GHz. RO4003C has advantages to be utilized in high-gain array antenna design [17] and microwave filter [10] because it is mechanically rigid enough and has a smaller losses value than traditional substrate FR4.

3.1   Theoretical and simulated characteristic Impedances

Figure 6: The dispersion diagram produced by the IMGW with geometrical dimensions: $d = 2.4$ mm, $l = 1.2$ mm, $h_p = 1.5$ mm, $h_s = 0.3$ mm and $h_g = 0.4$ mm. The solid blue curve indicates the quasi-TEM mode.

Figure 7: Comparison of the analytical solution from fundamental theory with simulated results with real pin structure and those with PMC boundary condition at the bottom. Note that the thickness of the substrate h_s keeps a constant of 0.3 mm in this subsection.
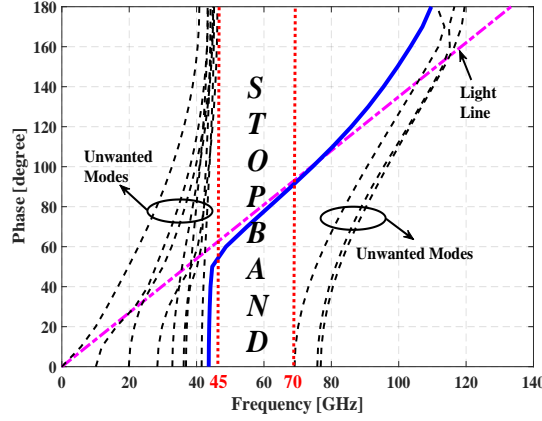
Figure 8: The dispersion diagram produced by the IMGW with geometrical dimensions: $d = 1.1$ mm, $l = 0.4$ mm, $h_p = 1.1$ mm, $h_s = 0.4$ mm and $h_g = 0.25$ mm. The solid blue curve indicates the quasi-TEM mode.

The dispersion diagram of the Ka-band structure produced by CST is illustrated in Fig. 6, where only the quasi-TEM mode propagates through the stopband from 26 to 41 GHz. Fig. 7 illustrates the comparison between the present analytical solution and the simulated results with PMC boundary condition at bottom and that by adding real pin structure, where the substrate thickness $h_s = 0.3$ mm and the width w is varied. In Fig. 7 we can see that the analytical solution has very good agreements with simulated results when the width of the IMGW is larger than 0.3 mm, while the analytical solution is bigger than simulated results when the width of

the IMGW is smaller than 0.3 mm.

Fig. 8 shows the stopband of the model of V-band, which is from 45 to 70 GHz covering the whole 60-GHz link band (57—66 GHz). The similar appearance to the
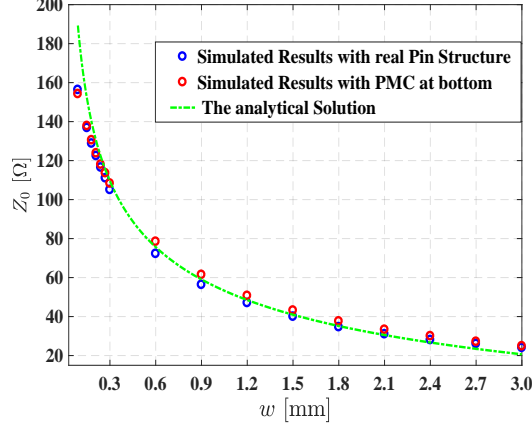
Figure 9: Comparison of the analytical solution from fundamental theory with simulated results with real pin structure and those with PMC boundary condition at the bottom. Note that the thickness of the substrate h_s keeps a constant of 0.4 mm in this subsection.

Ka-band model also occurs here: the analytical solution agrees with the simulated results when $w \geq 0.2$mm. Fig. 10 shows the stopband of E-band model which is
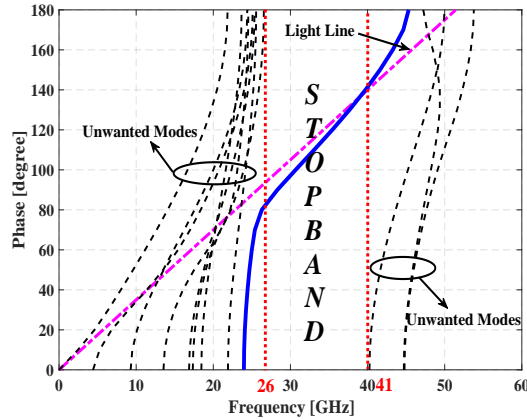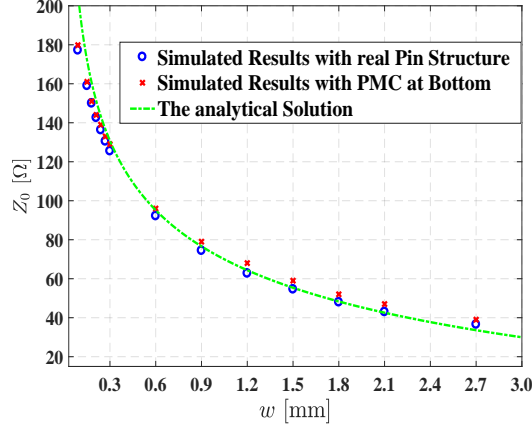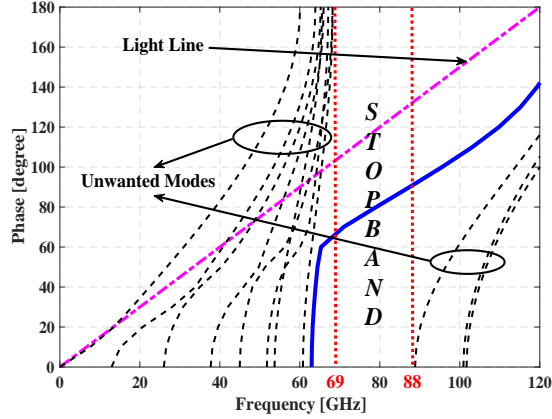

Figure 10: The dispersion diagram produced by the IMGW with geometrical dimensions: $d = 0.8$ mm, $l = 0.3$ mm, $h_p = 0.55$ mm, $h_s = 0.2$ mm and $h_g = 0.15$ mm. The solid blue curve indicates the quasi-TEM mode.

from 69 - 88 GHz. The analytical impedance agrees with the simulated ones very well when the width of the IMGW is bigger than 0.1 mm, as shown in Fig. 11.

Figure 11: Comparison of the analytical solution from fundamental theory with simulated results with real pin structure and those with PMC boundary condition at the bottom. Note that the thickness of the substrate h_s keeps a constant of 0.15 mm in this subsection.
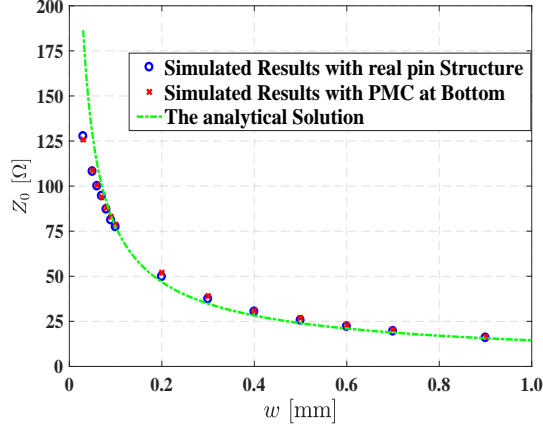
In all three cases the analytical values are bigger than simulated ones when the width of the IMGW is very small. The main reason for this is that the approximate electronic charge density in (3) is not accurate when the width of the IMGW is very small. When the microstrip of the IMGW is wide, the electrons are usually concentrated on the corners at both sides of the microstrip because of the Coulomb's force among the electrons. Therefore, the electron density varies rapidly along the microstrip to its edge. However, the electron density distribution will be more uniform when the width of the microstrip is very small. Since we are not dealing with the IMGW with a very small microstrip width w, the presentation for cases of very small w is skipped here.

3.2 Theoretical and simulated Attenuations

The attenuation analysis is carried out on the V-band model, as defined in Figs. 3-5 and TABLE I, with $w = 1$mm and varied h_s from 0.2 mm to 1 mm. The theoretical dielectric losses of the covered microstrip line and the IMGW are depicted in Fig. 12. From the figure, the dielectric loss of the covered microstrip line increases with the thickness of the substrate, while that value of the IMGW is almost constant versus the thickness of the substrate. This is due to that there is almost no propagating field inside the substrate for the IMGW. According to the Fig. 12, dielectric loss of the covered microstrip line is around 10 times bigger than that value of the IMGW when the thickness of the substrate is 0.4 mm. Similarly, the conductor losses of the covered microstrip line and the IMGW according to (23) are evaluated and the corresponding outcomes are illustrated in Fig. 13. As is depicted, the conductor losses of the IMGW and the covered microstrip line are around $0.1dB/cm$. Nevertheless,

the conductor loss of the IMGW is still $0.02dB$ lower than the value of the covered microstrip line. These outcomes confirm that the IMGW has much lower losses than the covered microstrip line because the PMC boundary condition at the bottom of the substrate drives the electromagnetic energy to distribute in the air gap. Thus, the IMGW has large advantages in high-gain high-efficiency array antenna design [17] than normal micostrip line or the covered microstrip line [33] in mmWs.

In order to verify our present analysis, a straight IMGW and a covered mi-

Figure 12: Analytically calculated dielectric losses α_d of the V-band model of the covered microstrip line and the IMGW versus the substrate thickness h_s. Other dimensions are defined in TABLE I.
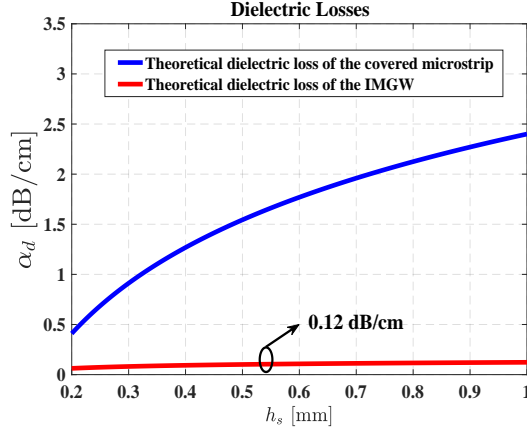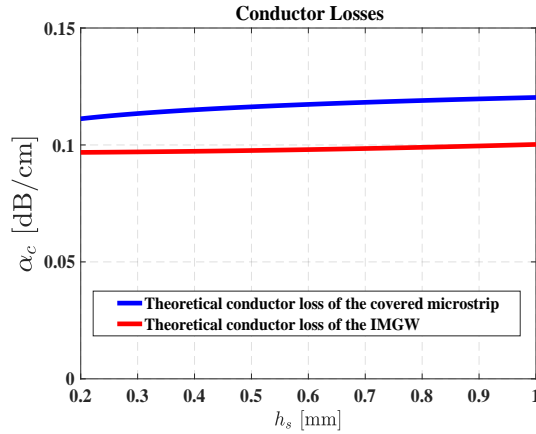

Figure 13: Analytically calculated conductor losses α_c of the V-band model of the covered microstrip line and the IMGW versus the substrate thickness h_s. Other dimensions are defined in TABLE I.

crostrip line with the same substrate and dimensions have been modeled in CST

(a)   (b)
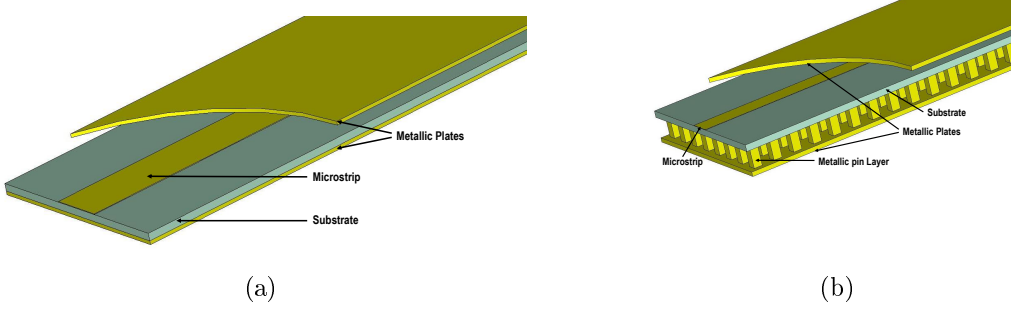
Figure 14: The simulated structures of the covered microstrip line and the IMGW in order to compare their conductor losses and dielectric losses. Both of them have the same thickness of the substrate $h_s = 0.4$ mm, length $L = 10$ mm and the width of the microstrip $w = 1$ mm. (a) The covered microstrip line and (b) The IMGW.

Microwave studio, as illustrated in Fig. 14. Transmission coefficients S_{21} with lossless materials (PEC and ideal substrate) of two structures are firstly simulated. Then they are simulated again with lossy strip (Copper) and metallic plates (Aluminum) so that the difference of the two scenarios is the conductor loss. As depicted in Fig. 15, the conductor loss of the covered microstrip line is around 0.16 dB/cm and that of the IMGW is about 0.12 dB/cm. Furthermore, the similar strategy is utilized to ideal metallic strip and lossy substrate to certify the dielectric losses of two structures. As illustrated in Fig. 16, the comparisons of transmission coefficients S_{21} in
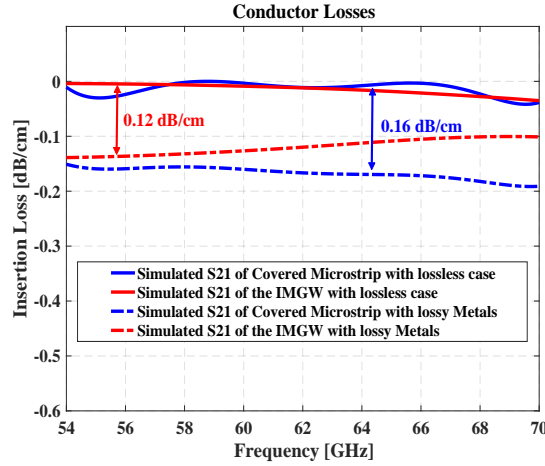
Figure 15: Simulated conductor losses of the covered microstrip line and the IMGW. For the covered microstrip line: 0.16 dB/cm. For the IMGW: 0.12 dB/cm.

the lossless case and lossy case certify that the covered microstrip line has as 5 times dielectric loss as that value of the IMGW. Note that the loss tangent value $\tan\delta$ has
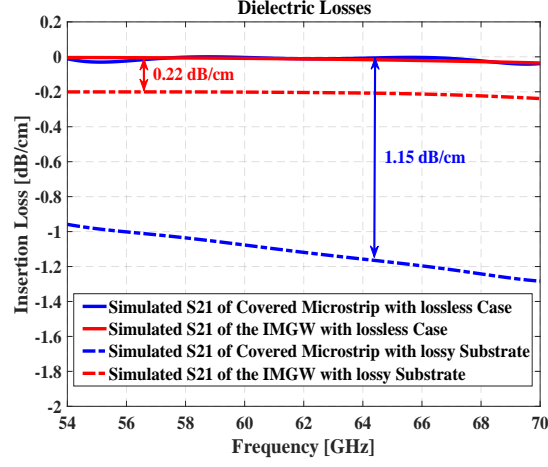
Figure 16: Simulated dielectric losses of the covered microstrip line and the IMGW. For the covered microstrip line: 1.133 dB/cm. For the IMGW: 0.22 dB/cm.

been changed as 0.01 in CST Microwave Studio at 60 GHz according to the Rogers [34]. The simulated value of the IMGW is bigger than the theoretical one in the Fig. 12. The main reason for this appearance is that the metallic pin surface provides an approximately PMC boundary condition and therefore some electromagnetic energy has been lost in the gaps between metallic pins. However, the IMGW still has a very low dielectric loss than normal covered microstrip line in mmWs.

4 Conclusion

The variational method has been applied to IMGW for determining its characteristic impedance, conductor loss and dielectric loss. The analytical solutions have good agreements with the simulated values in CST Microwave Studio, stating that the inverted microstrip gap waveguide technology can be a good candidate for high-gain high-efficient array antennas in mmWs communication based on its low dielectric loss property.

References

[1] T. S. Rappaport, J. N. Murdck, and F. Gutierrez, "State of the art in 60-GHz integrated circuits and systems for wireless communications, " *Proc. IEEE*, vol. 99, no. 8, pp. 1390-1436, Aug. 2011.

[2] B. Maurizio, P. Marco, P. Luca and K. Wu, "On the losses in substrate-integrated waveguides and cavities, " *International Journal of Microwave and Wireless Technologies*, (Oct 2009): 395-401.

[3] P.-S. Kildal, E. Alfonso, A. Valero-Nogueira, and E. Rajo-Iglesias, "Local metamaterial-based waveguides in gaps between parallel metal plates, " *IEEE Antennas Wireless Propag. Lett.*, vol. 8, pp. 84-87, 2009.

[4] A. Valero-Nogueira, E. Alfonso, J. I. Herranz, P.-S. Kildal, "Experimental demonstration of local quasi-TEM gap modes in singlehard-wall waveguides, " *IEEE Antennas Wireless Propag. Lett.*, vol. 19, no. 9, pp. 536-538, Sep. 2009.

[5] P.-S. Kildal, "Three metamaterial-based gap waveguides between parallel metal plates for mm/submm waves, " in *3rd European Conference on Antennas and Propagation, EuCAP 2009*, pp. 28-32.

[6] H. Raza, J.Yang and P.-S. Kildal "Resemblance between gap waveguides and hollow waveguides " in *IET Microwaves, Antennas and Propagation*, vol. 15, no. 7, pp. 1221-1227, 2013.

[7] P.-S. Kildal, "Artificially soft and hard surfaces in electromagnetics, " *IEEE Trans. Antennas Propag.*, vol. 28, no. 10, pp. 1537-1544, 1990.

[8] H. Raza, J. Yang, P.-S. Kildal, and E. Alfonso, "Microstrip-ridge gap waveguide - study of losses, bends, and transition to WR-15, " *IEEE Trans. Microw. Theory Tech.*, vol. 62, no. 9, pp. 1943-1952, 2014.

[9] A. Vosoogh, A. A. Brazalez and P.-S.Kildal, "A V-Band inverted microstrip gap waveguide end-coupled bandpass filter, " *IEEE Microwave and Wireless Components Letters*, vol. 26, no. 4, April, 2016.

[10] A. U. Zaman, P.-S. Kildal and A. A. Kishk, "Narrow-Band Microwave Filter Using High-Q Groove Gap Waveguide Resonators With Manufacturing Flexibility and No Sidewalls, "*IEEE Transactions on Components, Packaging and Manufacturing Technology*, vol. 2, issue: 11, Nov. 2012.

[11] M. Rezaee, A. U. Zaman and P.-S. Kildal, "V-band groove gap waveguide diplexer, "*Antennas and Propagation (EuCAP), 2015 9th European Conference on*, pp. 1 - 4, 2015.

[12] A. U. Zaman, M. Alexanderson, T. Vukusic and P.-S. Kildal "Gap Waveguide PMC Packaging for Improved Isolation of Circuit Components in High-Frequency Microwave Modules, "*IEEE Transactions on Components, Packaging and Manufacturing Technology*, vol. 4, issue: 1, Jan. 2014.

[13] D. Zarifi, A. Farahbaksh, A. Uz Zaman and P.-S. Kildal, "Design and fabrication of a wideband high-gain 60-GHz corrugated slot antenna array with ridge gap waveguide distribution layer, "*IEEE Trans. Antennas Propag.*, vol. 64, no. 7, pp. 2905-2913, July, 2016.

[14] A. U. Zaman and P.-S. Kildal "Wide-Band Slot Antenna Arrays With Single-Layer Corporate-Feed Network in Ridge Gap Waveguide Technology, "*IEEE Trans. Antennas Propag.*, vol. 62, issue: 6, June, 2014.

[15] A. Vosoogh and P.-S. Kildal, "Corporate-Fed planar 60-GHz slot array made of three unconnected metal layers using AMC pin surface for the gap waveguide, "*IEEE Antennas and Wireless Propagation Letters*, December, 2015.

[16] J.L. Liu A. Vosoogh A. U. Zaman and J. Yang, "Design and Fabrication of a High Gain 60-GHz Cavity-backed Slot Antenna Array fed by Inverted Microstrip Gap Waveguide, "*IEEE Trans. Antennas Propag.*, vol. 65, issue: 4, April, 2017.

[17] O. Heaviside, *Electromagnetic Theory,* Vol. 1, 1893. Reprinted by Dover, New York, 1950.

[18] S. B. Cohn, "Shielded coupled strip transmission line ", *IRE Trans. Microwave Theory Tech.*,vol. MTT-3, pp. 29-38, Oct. 1955.

[19] H. A. Wheeler, "Transmission-line properties of parallel strips separated by a dielectric sheet, "*IEEE Trans. Microwave Theory Tech.*, vol. MTT-13, pp. 172-185, 1965.

[20] D. Park, "Planar transmission lines, "*IRE Trans. Microwave Theory Tech.*, vol. MTT-3, part I, pp. 8-12, Apr. 1955; part II, pp. 7-11, Oct. 1955.

[21] K. Foster, "The characteristic impedance and phase velocity of high-q triplate line, "*Journal of the British Institution of Radio Engineers*, vol. 18, issue: 12, Dec. 1958.

[22] R. E. Collin, "Characteristic impedance of a slotted coaxial line, "*IRE Trans. Microwave Theory Tech.*, vol. MTT-4, pp. 4-8, Jan. 1956.

[23] E. Yamashita and R. Mittra, "Variational method for the analysis of microstrip lines, "*IEEE Trans. Microwave Theory Tech.*, vol. MTT-16, pp. 251-256, 1968.

[24] E. Yamashita and K. Atsuki, "Strip line with rectangular outer conductor and three dielectric layers,"*IEEE Trans. Microwave Theory Tech.*, vol. MTT-18, no. 5, May, 1970.

[25] T. Itoh and R. Mittra, "Spectral domain approach for calculating the dispersion characteristics of microstrip lines,"*IEEE Trans. Microwave Theory Tech.*, vol. MTT-21, pp. 496-499, 1973.

[26] T. Itoh, "Spectral domain immitance approach for dispersion characteristics of generalized printed transmission lines,"*IEEE Trans. Microwave Theory Tech.*, vol. MTT-28, pp. 733-736, July, 1980.

[27] R. H. Jansen, "The spectral-domain approach for microwave integrated circuits,"*IEEE Trans. Microwave Theory Tech.*, vol. MTT-33, pp. 1043-1056, 1985.

[28] E. F. Kuester and D. C. Chang, "Theory of dispersion in microstrip of arbitrary width,"*IEEE Trans. Microwave Theory Tech.*, vol. MTT-28, pp. 259-265, 1980.

[29] B. E. Kretch and R. E. Collin, "Microstrip dispersion including anisotropic substrates,"*IEEE Trans. Microwave Theory Tech.*, vol. MTT-35, pp. 710-718, 1987.

[30] R. E. Collin, *Field Theory of Guided Waves*, Wiley-IEEE Press, New York, Dec. 1990.

[31] J. L. Liu, A. Uz Zaman and P.-S. Kildal, *Optimizing numerical port for inverted microstrip gap waveguide in full-wave simulators,* Antennas and Propagation (EUCAP), Proceedings of the 10th European Conference on, 10-15 April 2016.

[32] J. Wu, Y. J. Cheng, and Y. Fan, "A wideband high-gain high-efficiency hybrid integrated plate array antenna for V-Band inter-satellite links, " *IEEE Trans. Antennas Propag.*, vol. 63, no. 4, pp. 1225-1233, Apr. 2015.

[33] Based on Communication with Rogers Data Sheet RO4003 Series High Frequency Circuit Materials at 60 GHz.

Paper 2

Design and Fabrication of a High Gain 60-GHz Cavity-backed Slot Antenna Array fed by Inverted Microstrip Gap Waveguide

Jinlin Liu, Abbas Vosoogh, Ashraf Uz Zaman, and Jian Yang

The layout of this paper has been revised in order to comply with the rest of the thesis.

Design and Fabrication of a High Gain 60-GHz Cavity-backed Slot Antenna Array fed by Inverted Microstrip Gap Waveguide

Jinlin Liu, Abbas Vosoogh, Ashraf Uz Zaman, and Jian Yang

Abstract

This paper deals with the design of a 16×16 slot array antenna fed by inverted microstrip gap waveguide (IMGW). The whole structure designed in this work consists of radiating slots, a groove gap cavity layer, a distribution feeding network and a transition from standard WR-15 waveguide to the IMGW. Firstly, a 2×2 cavity-backed slot sub-array is designed with periodic boundary condition to achieve good performances of radiation pattern and directivity. Then a complete IMGW feeding network with a transition from WR-15 rectangular waveguide to the IMGW has been realized to excite the radiating slots. The complete antenna array is designed at 60-GHz frequency band and fabricated using Electrical Discharging Machining (EDM) technology. The measurements show that the antenna has a 16.95% bandwidth covering 54-64 GHz frequency range. The measured gain of the antenna is more than 28 dBi with the efficiency higher than 40% covering 54-64 GHz frequency range.

1 Introduction

Recently, considerable attention has been paid to 60-GHz frequency band. Communications distances at the frequency band are limited by a high attenuation caused by the atmosphere absorption. Thereby, high gain and wide bandwidth characteristics are required for the antennas. Among all antenna types a slot array is suitable for the realization at 60-GHz band. The target of this work is to design a planar slot array based on inverted microstrip gap waveguide (IMGW) technology, which is recently introduced as a suitable guiding structure for millimeter wave (mmW) systems. The conception of the IMGW can be modeled for theoretical analysis by two parallel plates, a top Perfect Electric Conductor (PEC) layer and a bottom Perfect Magnetic Conductor (PMC) layer, with a metallic strip placed in the bottom PMC layer. This structure stops all modes propagating in all directions except for a quasi-TEM mode along the strip over a specific frequency band (stopband) when the gap between PEC and PMC plates is smaller than quarter wavelength at an operation frequency [1]. Besides IMGW there are also other three different versions of

gap waveguide — groove, ridge [2] and microstrip-ridge gap waveguides [3]. Many research works have been published on the gap waveguide technology in fields of antennas [4-8], microwave filters [9-10] and the packaging for microwave circuits [11-12]. In this paper, we systematically present a 16×16 slot antenna array designed with IMGW corporate feeding networks. In section II, we elaborate the design of a 2×2 sub-array at 60-GHz. The corporate feed networks based on IMGW technology is explained in section III. Section IV is devoted to the simulated and measured results of whole antenna structure. Finally, summary and conclusions are presented in section V.

2   Design for 2×2 Sub-array

The gap waveguide technology uses a parallel-plate stopband over a specific frequency range. The dimensions of the pins of the bed of nails at the bottom should be chosen correctly to achieve a stopband which covers as much as 60-GHz frequency band [13]. We carried out a numerical parametric analysis in this work of the IMGW whose structure is illustrated in Fig. 1(a). The corresponding dispersion diagram of the

(a)   (b)
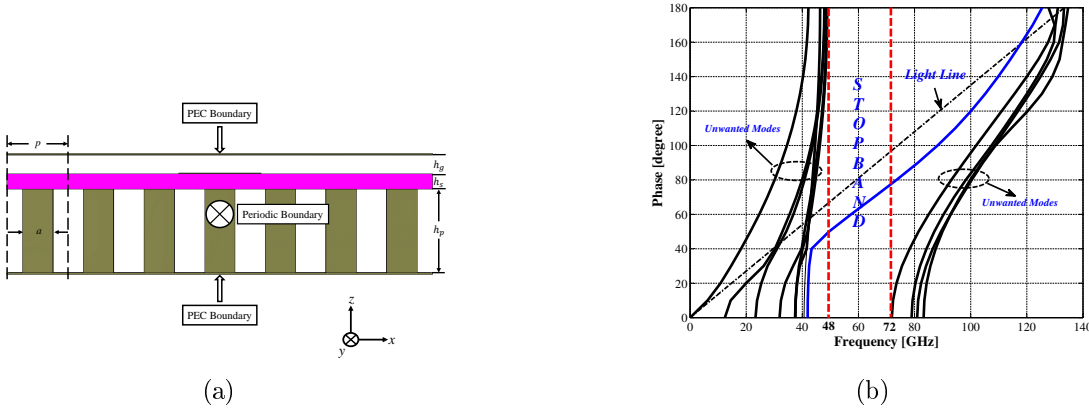
Figure 1: (a) 2-dimensional view of the unit cell. (b) Dispersion diagram of the unit cell utilized in (a) [h_s = 0.2 mm, h_g = 0.25 mm, h_p = 1.2 mm, a = 0.4 mm and p = 0.8 mm]. The blue line indicates the quasi-TEM mode.

structure is shown in Fig. 1(b), which indicates that only the quasi-TEM mode can propagate along the inverted microstrip line but the other modes are stopped in the frequency band from 48 to 72 GHz. The substrate material is Rogers RO4003 with relative permittivity ε_r = 3.55, loss tangent $tan\delta$ = 0.0027 (specified at 10 GHz by Rogers) and thickness h_s = 0.2 mm. The motivations to select RO4003 are that it has a lower loss value than traditional PCB substrate FR4 and is mechanically rigid enough for our case.

The configuration of a 2×2-element sub-array is firstly designed using periodic
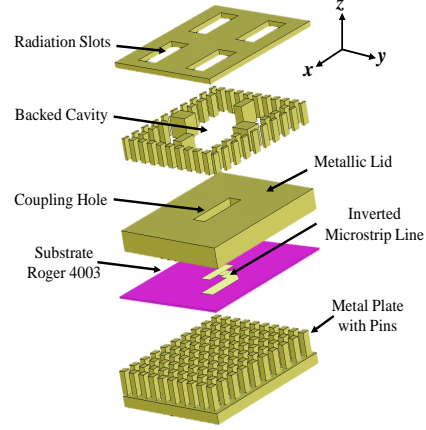
Figure 2: Detailed 3-D view of 2 × 2 slots sub-array.

(a)   (b)

(c)   (d)
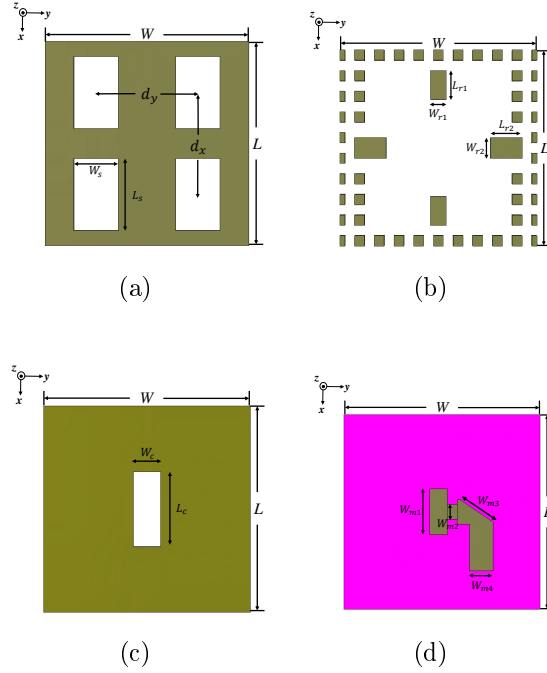
Figure 3: Geometrical parameters of a 2×2 slots array. (a) Top radiation slots layer. (b) Backed cavity layer. (c) Coupling hole layer. (d) Feed distribution networks layer.

boundary condition in CST Microwave Studio in order to evaluate the radiation pattern and directivity of the whole array antenna, as shown in Fig. 2. It consists of a radiating slot layer, a cavity layer, a PCB microstrip layer and a bed of nails at the bottom. Instead of a normal hollow rectangular waveguide cavity, we have utilized a groove gap cavity here for easy manufacture. The groove gap cavity is partitioned
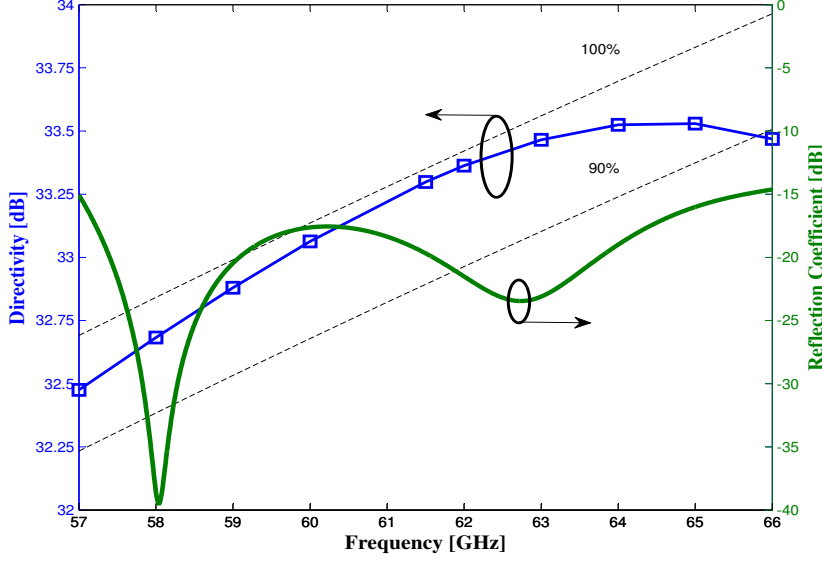
Figure 4: The simulated directivity and reflection coefficient of the 2×2 sub-array.

into four spaces by two sets of metallic blocks extending in the x and y directions. The PCB microstrip layer feeds the four spaces of groove gap cavity with identical phase and amplitude by the center coupling hole in the cavity layer.

The slots are uniformly spaced in both x and y directions with a spacing smaller than one wavelength in order to avoid grating lobes in a large broadside array. The highest frequency for this work is 66 GHz and the corresponding wavelength λ is about 4.5 mm. Therefore, the slot space d_s in this work is chosen as 4 mm. On the other hand, the value W and L should be integer times of the pins period, namely $W = Mp$ and $L = Np$. Given the above-mentioned considerations, we select $W = L = 10p = 8$ mm. The detailed geometrical demonstrations of the antenna sub-array are shown in TABLE I. In Fig. 4 the green line shows the reflection coefficient of the sub-array and an 14.5% impedance bandwidth (over 57-65.7 GHz) with the input reflection coefficient below -15 dB is achieved. The blue line with square mark in the figure illustrates the simulated directivity of the 16×16 slot array in infinite array environment. The simulated antenna efficiency is higher than 90% from 57 to 65.9 GHz.

3   Design of Feeding Distribution Network

Compared with the groove and the ridge gap waveguide structures [2], the feeding distribution network based on the IMGW technology has some obvious advantages.

Table 1: Dimensional Parameters of 2×2 unit cell referring to Fig. 3

Substrate Material	Rogers 4003 (ε^*=3.55)
W	8 mm
L	8 mm
d_x	4 mm
d_y	4 mm
W_s	1.748 mm
L_s	2.832 mm
W_{r1}	0.637 mm
L_{r1}	1.111 mm
W_{r2}	0.811 mm
L_{r2}	1.277 mm
W_c	1.071 mm
L_c	2.742 mm
W_{m1}	1.883 mm
W_{m2}	0.607 mm
W_{m3}	1.642 mm
W_{m4}	1.05 mm

First of all, it has a uniform bed of nails while the others do not. This uniform pin structure makes the fabrication much easier and cheaper. Secondly, fabrication of microstrip circuitry on PCB by etching is accurate and very low cost. Thirdly, theories and design principles of traditional inverted microstrip technique are matured so we can directly utilize them with little modifications. For these reasons, the IMGW structure is attractive in feeding networks for slot antenna arrays at mmW frequencies.

Despite its advantages, there are still challenges in design of IMGW feeding distribution networks. In [5] a planar horn array fed by an IMGW feeding network has been already expounded. Since the metallic pin surface can be modeled approximately by PMC boundary condition, the distribution network in [5] was designed with an ideal PMC condition instead of the real metallic pin structure located at the bottom plate. Differently, the corporate-feed network in the present work is designed by applying the real pin structure in the design process because there exists evanescent electromagnetic fields in the substrate and the pin structure, which though small affects the propagation of the quasi-TEM mode and losses. Therefore, assuming an ideal PMC condition to replace the metallic pins structure may give rise to a significant error in the design of feeding distribution networks. As shown in Fig. 5(a) *left*, a simple straight IMGW structure is firstly modeled in CST Microwave Studio with PMC boundary condition at the bottom plate. Then we also modeled the periodic
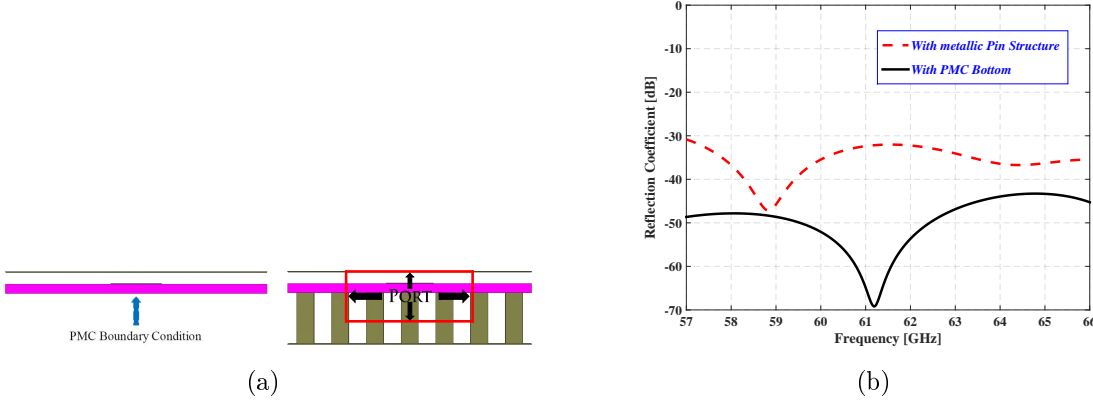
(a)   (b)

Figure 5: Discrepancy between the ideal model and the realistic model. (a) The left figure illustrates a covered microstrip line with PMC boundary condition at the bottom. In the right one the PMC boundary condition is replaced by metallic pins. (b) The black solid line shows the simulated reflection coefficient with the PMC boundary condition at the bottom. The red dash line indicates the reflection coefficient with the metallic pins at the bottom in the first structure.

pins structure in Fig. 5(a) *right* in order to see the effect of the real pin structure. The corresponding results as shown in Fig. 5(b) for both models verified the existing error in [5]. Therefore, we utilize the real pin structure in the present design of the whole feeding network to obtain accurate performances.

The IMGW feeding element for the 2×2 sub-array is present in Section II. T-junction power dividers with matching circuits are used in our feeding network. Essentially a T-junction power divider is a simple three-port network that can be utilized for power division or combining. Thereby, the T-junction is a central component in the distribution network for feeding the antenna array. In this work we designed a T-junction power divider with metallic pins at the bottom in CST Microwave Studio, as shown in Fig. 6. In order to obtain correct transition performance an optimized numerical port [14] has been utilized during the entire design procedure. The T-junction then has been optimized for the minimum reflection coefficient and the corresponding S-parameters are shown in Fig. 7, in which the reflection coefficient S_{11} is below -30 dB from 57 to 66 GHz. Also, for the determination of the loss caused by the substrate, aluminum pins and copper strip we have twice simulated the T-junction. The transmission coefficients of the lossy case are around 0.2 dB lower than these values of the lossless case and the leakage loss is a negligible value of 0.02 dB.

The aim of the matching networks is to eliminate the reflection effect on the distribution networks. In this work we apply a classical second order binomial impedance transformer for impedance matching. All characteristic impedances and load impedances have been obtained from optimized numerical ports introduced in [14]. Here we should notice that part 1 of matching microstrip in Fig. 8 has been
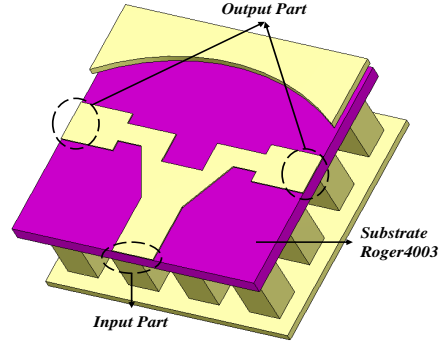
Figure 6: 3-dimensional view for the T-junction with metallic pins at the bottom.
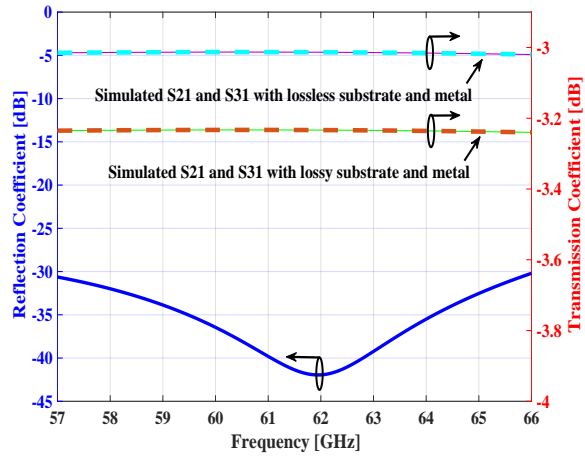

Figure 7: Simulated S-parameters of single T-junction in Fig. 6 for both lossy and lossless cases.
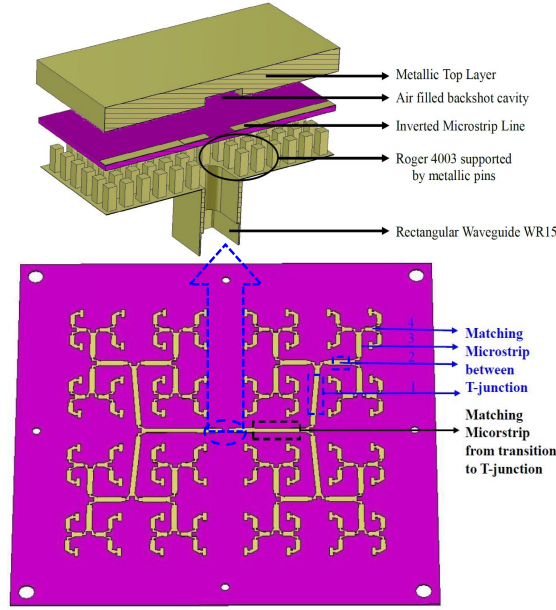
Figure 8: Illustration for the whole feeding networks including T-junction power dividers, matching microstrips and a transition power divider from WR-15 to the IMGW structure.

designed in a shape of parallelogram in order to remove its mutual coupling to the nearest coupling holes.

The input port of the array antenna is required to be WR-15 rectangular waveguide. A novel power divider transition in [15] was applied in this work. The simulated reflection coefficient of the transition is below -20 dB and the phases of the output ports have 180 degree difference. The complete corporate-feed network consists of two 32-way power dividers connected to the transition of WR-15 in the center. Due to the out-of-phase output of the transition, the two 32-way power dividers are in a mirror geometry in order to have the same phase excitations for all slots. The final designed structure of the feeding distribution network is shown in Fig. 8. Finally, the whole distribution network is optimized by genetic algorithm in CST Microwave Studio.

4   Simulated and experimental Results

The numerical model and the final manufactured prototype of the 16×16 slot array antenna are shown in Fig. 9. The metallic parts of the antenna are fabricated by Electrical Discharging Machining (EDM) Technology, where the prototype is etched by recurring electric discharges between the workpiece and electrodes. The designed array aperture dimension is $64 \times 64 \; mm^2$.

The simulated and measured input reflection coefficients of the antenna are shown

(a)   (b)
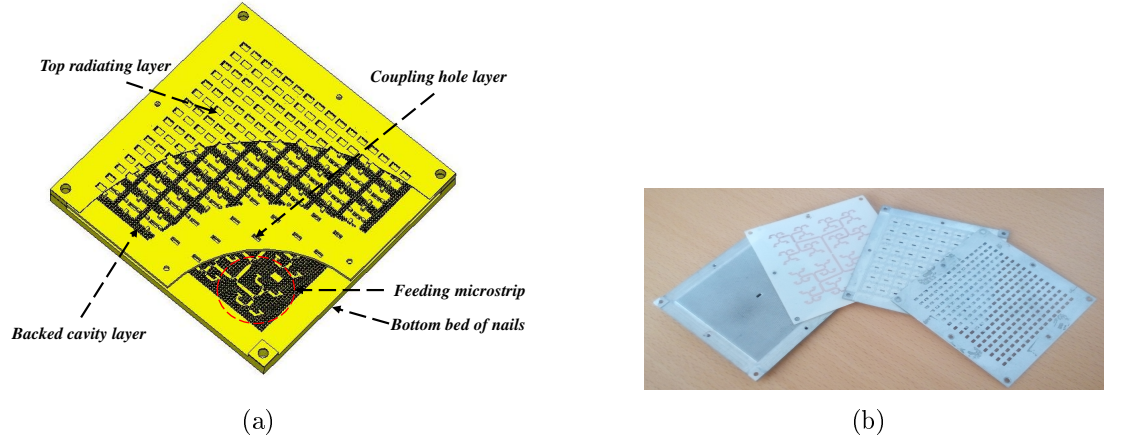
Figure 9: (a) Numerical model of the proposed array antenna in CST Microwave studio . In order to observe the microstrip and waveguide open details the substrate is hidden. (b) Photogragh of the proposed 16×16 array antenna fabricated by EDM technology.
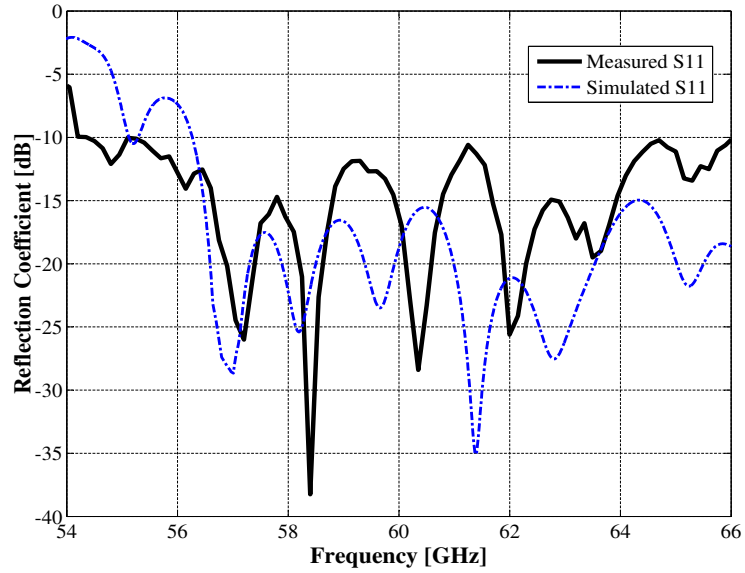

Figure 10: Comparison of simulated and measured reflection coefficient of the proposed 16×16 slot array antenna.

(a)

(b)

(c)

(d)

Figure 11: Measured and simulated radiation patterns of the proposed array antenna in E-plane at (a) 57 GHz. (b) 60 GHz. (c) 61 GHz and (d) 66 GHz.

in Fig. 10. The measured S_{11} is a bit higher than the simulation one. However, it is still below -10 dB from 54.5 to 66 GHz (19.2% impedance bandwidth). As discussed in [13], the dispersion diagram of the whole structure is affected by dimensions of metallic pins, the thickness of substrate and the height of air gap. Therefore, any manufacture tolerances of the bed of nails and the height change of air gap will cause a shift for the parallel stopband [16].

The radiation patterns of the proposed antenna were measured in an anechoic chamber in University of Karlsruher. The simulated and measured normalized radiation patterns in both E- and H-planes at four frequencies of 57, 60, 61 and 66 GHz are shown in Figs. 11 and 12. The measured co-polarized radiation patterns show a very good agreement with the simulated results. The simulated and measured radiation patterns are symmetrical, and the first relative side-lobe levels in both E- and H-planes are around -13 dB. The measured grating lobes of the fabricated array
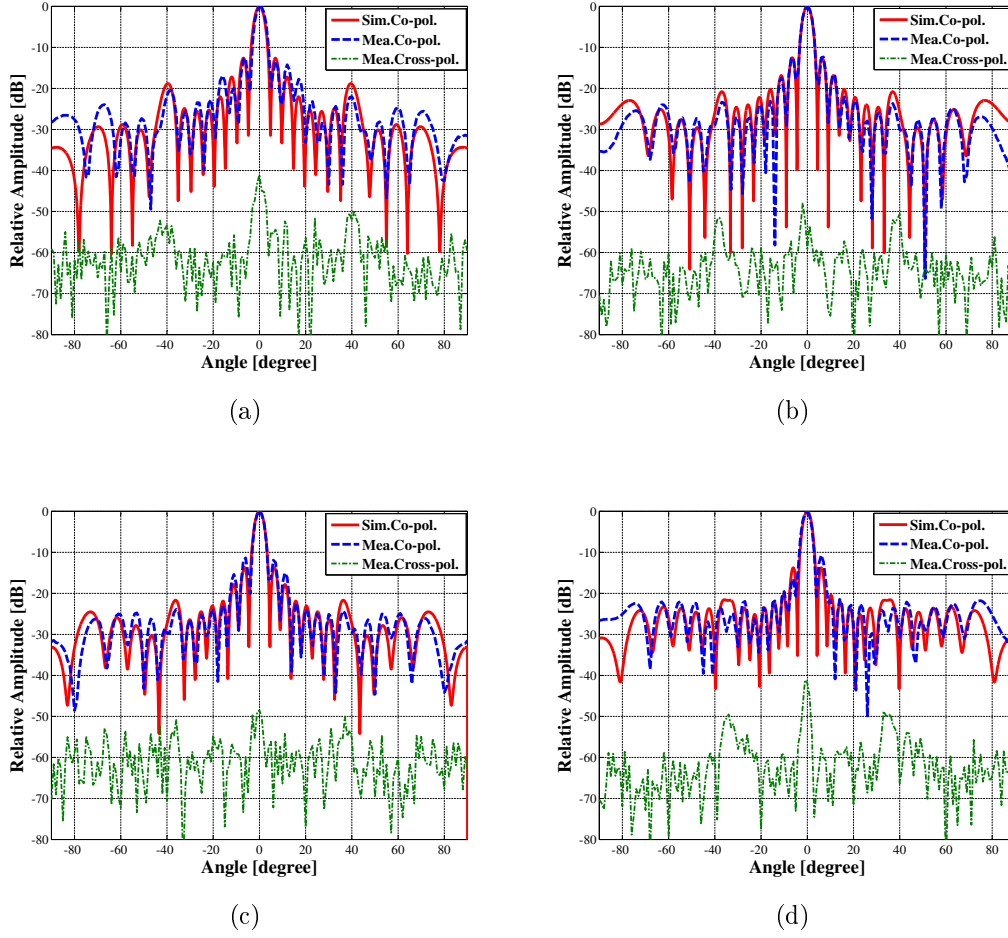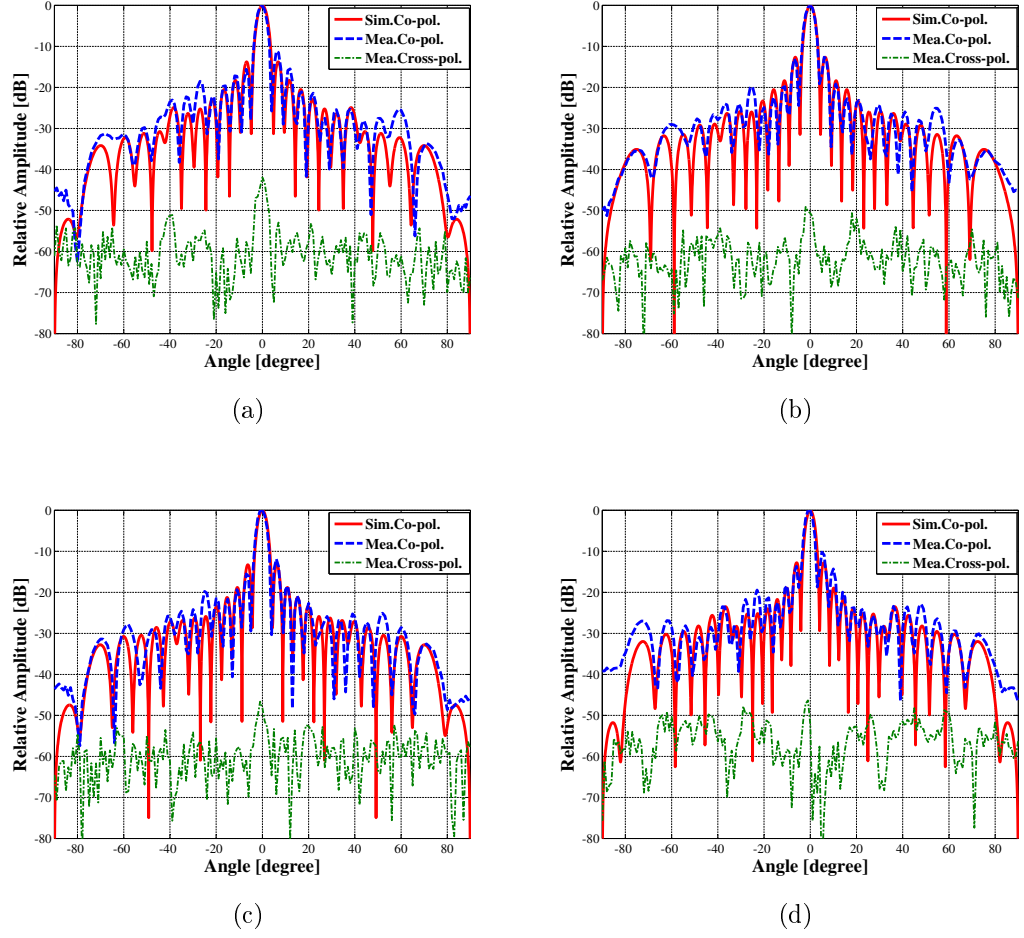
Figure 12: Measured and simulated radiation patterns of the proposed array antenna in H-plane at (a) 57 GHz. (b) 60 GHz. (c) 61 GHz. and (d) 66 GHz.

in both E- and H-planes are below -20 dB over the desired frequency band. The cross-polarized values are below -40 dB at all frequencies.

The simulated and the measured gains of the array antenna are shown in Fig. 13. The pink solid line in Fig. 13 indicates the simulated gain after setting up the modified loss tangent of the substrate (The loss tangent value of RO4003 is manually modified as 0.01 at 60-GHz in CST model). This modification helps us accurately predict the real gain of the antenna. The blue dash line in Fig. 13 shows the mea-

Table 2: COMPARISON BETWEEN THE PROPOSED AND REPORTED 60-GHz PLANAR ANTENNA ARRAYS

Performance	Ref.[19]	Ref.[4]	Present Work
Technology	Plate Laminated	Ridge Gap Waveguide	IMGW
Size [cm]	6.7 × 6.7	7 × 6.4	6.4 × 6.4
Number of Elements	256	256	256
Frequency Band [GHz]	59-64	56-65.7	54.5-64
Bandwidth	8%	16%	17%
Max Gain [dBi]	33	33	30.5
Min Efficiency	80%	70%	40%

sured gain, illustrating above 40% total aperture efficiency over the frequency band

Figure 13: Measured gain and simulated directivity of the present 16 × 16 slot array antenna.

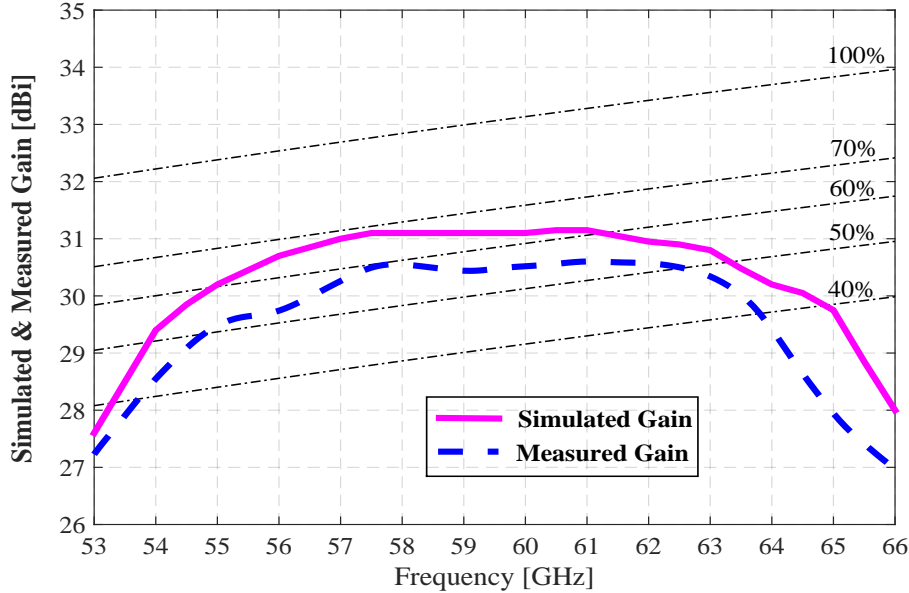54-64 GHz. What we should notice in Fig. 13 is that the measured gain drops very rapidly starting from 64 GHz, though our design target is 57-66 GHz. The similar phenomena have been also reported in [17] and [18]. The probable explanation for the reduced antenna gain is that the true loss tangent of the substrate may rapidly become larger with the increasing of the frequency and is probably even higher than 0.01 at higher frequency band. The other possible reason for the gain reduction is that the top radiating layer is very thin and therefore any assembly tolerance could cause its deformation which leads to large leakage loss at high frequency.

We summarize structural characteristics and performances of several 60-GHz high-gain antenna arrays, reported in references and compare them with our work in Table II. Compared with the designs in [17] and [18], our work exhibits wide impedance bandwidth, higher aperture efficiency and low cost on fabrication. However, because of the dielectric loss in the substrate of the feeding distribution network, the realized gain of our work is lower than those reported in [4], [6] and [19]. Thereby, there are still some work to do for the further improvements.

5   Conclusion

A high gain and wide bandwidth slot array antenna based on the IMGW technology at 60-GHz has been presented in this paper. The proposed antenna consists of four unconnected layers without any conductive contact between them. The designed prototype is manufactured by EDM technology. The simulated and measured results of the whole antenna structure show very good agreements in radiation patterns in both E- and H-plane. The measured realized gain is higher than 28 dBi over the entire operation bandwidth from 54.5 to 64 GHz, corresponding to efficiency larger than 45%. This work shows that the IMGW technology is an excellent candidate for array antennas in millimeter wave communications.

References

[1] A. Valero-Nogueira, E. Alfonso, J. I. Herranz and P.-S. Kildal, "Experimental demonstration of local quasi-TEM gap modes in singlehard- wall waveguides, " *IEEE Antennas Wireless Propag. Lett.*, vol. 19, no. 9, pp. 536-538, Sep. 2009.

[2] P.-S. Kildal, "Three metamaterial-based gap waveguides between parallel metal plates for mm/submm waves, " in *3rd European Conference on Antennas and Propagation, EuCAP 2009*, pp. 28-32.

[3] H. Raza, J. Yang, P.-S. Kildal and E. Alfonso, "Microstrip-ridge gap waveguide - study of losses, bends, and transition to WR-15, " *IEEE Trans. Microw. Theory Tech.*, vol. 62, no. 9, pp. 1943-1952, 2014.

[4] D. Zarifi, A. Farahbaksh, A. Uz Zaman and P.-S. Kildal, "Design and fabrication of a wideband high-gain 60-GHz corrugated slot antenna array with ridge gap waveguide distribution layer, " *IEEE Trans. Antennas Propag.*, vol. 64, no. 7, pp. 2905-2913, July, 2016.

[5] E. Pucci, E. Rajo-Iglesias, Vazquez-Roy and P.-S. Kildal, "Planar dual-mode horn array with corporate-feed network in inverted microstrip gap waveguide, " *IEEE Trans. Antennas Propag.*, vol. 62, no. 7, pp. 3534-3542, July, 2014.

[6] A. Vosoogh and P.-S. Kildal, "Corporate-Fed planar 60-GHz slot array made of three unconnected metal layers using AMC pin surface for the gap waveguide, " *IEEE Antennas and Wireless Propagation Letters*, December, 2015.

[7] A. Vosoogh and P.-S. Kildal, "High Efficiency 2 × 2 cavity-backed slot sub-array for 60-GHz planar array antenna based on gap technology, " *2015 International Symposium on Antennas and Propagation (ISAP)*, pp. 1 - 3, Nov. 2015.

[8] A. U. Zaman, P.-S. Kildal and A. A. Kishk, "Narrow-Band Microwave Filter Using High-Q Groove Gap Waveguide Resonators With Manufacturing Flexibility and No Sidewalls, " *IEEE Transactions on Components, Packaging and Manufacturing Technology* , Volume: 2, Issue: 11, Nov. 2012.

[9] A. Vosoogh, A. A. Brazalez and P.-S. Kildal, "A V-Band inverted microstrip gap waveguide end-coupled bandpass filter," *IEEE Microwave and Wireless Components Letters*, vol. 26, no. 4, April, 2016.

[10] A. U. Zaman, M. Alexanderson, T. Vukusic and P.-S. Kildal, "Gap Waveguide PMC Packaging for Improved Isolation of Circuit Components in High-Frequency Microwave Modules," *IEEE Transactions on Components, Packaging and Manufacturing Technology*, vol. 4, Issue: 1, Jan. 2014.

[11] E. Rajo-Iglesias, P. S. Kildal, A. U. Zaman, and A. Kishk, "Bed of springs for packaging of microstrip circuits in the microwave frequency range," *IEEE Transaction on Components, Packaging and Manufacturing Technology*, vol. 2, no. 7, July, 2012.

[12] E. Rajo-Iglesias and P.-S. Kildal, "Numerical studies of bandwidth of parallel-plate cut-off realized by a bed of nails, corrugations and mushroom-type electromagnetic bandgap for use in gap waveguides," *IET Microw.Antennas Propag.*, vol. 5, Iss. 3, pp. 282-289, 2011.

[13] J. L. Liu, A. Uz Zaman and P.-S. Kildal, "Optimizing numerical port for inverted microstrip gap waveguide in full-wave simulators," *Antennas and Propagation (EUCAP), Proceedings of the 10th European Conference on*, 10-15 April 2016.

[14] J. L. Liu, A. Uz Zaman and P.-S. Kildal, "Design of transition from WR-15 to inverted microstrip gap waveguide," *2016 Global Symposium on Millimeter Waves (GSMM) Technology and Applications*, 6-8 June 2016.

[15] A. A. Brazález, E. Rajo-Iglesias, J. L. Vázquez-Roy, A. Vosoogh, and P.-S. Kildal, "Design and validation of microstrip gap waveguides and their transitions to rectangular waveguide for millimeter-wave applications," *IEEE Transactions on Microwave Theory and Techniques*, vol. 63, no. 12, Dec, 2015.

[16] Y. Li and K.-M. Luk, "60-GHz substrate integrated waveguide fed cavity-backed aperture-coupled microstrip patch antenna arrays," *IEEE Trans. Antennas Propag.*, vol. 61, no. 3, pp. 1075-1085, Jan. 2015.

[17] J. Wu, Y. J. Cheng, and Y. Fan, "A wideband high-gain high-efficiency hybrid integrated plate array antenna for V-Band inter-satellite links," *IEEE Trans. Antennas Propag.*, vol. 63, no. 4, pp. 1225-1233, Apr. 2015.

[18] Y. Miura, J. Hirokawa, M. Ando, Y. Shibuya and G. Yoshida, "Doublelayer full-corporate-feed hollow-waveguide slot array antenna in the 60 GHz band," *IEEE Trans. Antennas Propag.*, vol. 59, no. 8, pp. 2844-2851, Aug. 2011.

Paper 3

Low sidelobe Slot Array Antenna based on Inverted Microstrip Gap Waveguide at 28 GHz

Jinlin Liu, Jian Yang, and Ashraf Uz Zaman

The layout of this paper has been revised in order to comply with the rest of the thesis.

Low sidelobe Slot Array Antenna based on Inverted Microstrip Gap Waveguide at 28 GHz

Jinlin Liu, Jian Yang, and Ashraf Uz Zaman

Abstract

In this work, a novel low sidelobe array antenna is designed at 28 GHz. The proposed array antenna is fed by classic full-corporate double-layer distribution networks based on newly introduced inverted microstrip gap waveguide. In order to achieve low sidelobe property, a classic Taylor synthesis method is adopted in this work. In the distribution network, a couple of unequal power dividers with identical output phases are applied for the low sibelobe in this work. The fundamental radiator is 2×2 slot sub-array, and the entire array antenna is constructed by 8×8 of such kind sub-arrays. The simulated radiation patterns show that the first sidelobe levels, front-back ratio of both E-plane and H-plane from 26.5 GHz to 29.5 GHz are very well improved compared with traditional ones with the equal amplitude and phase distribution networks. The input impedance bandwidth is about 12% with the reflection coefficient below -10 dB, and the gain is more than 29 dBi from 26.5 GHz to 29.5 GHz.

1 Introduction

Recently, millimeter waves (mmWs) frequency bands are attractive because of the saturation of low frequency bands below 20 GHz. The new transmission line for mmWs is still a challenge for wireless communications. As is well-known, substrate-integrated-waveguide [1] is recently very well developed in passive components, integration of active component and various of array antennas in mmWs [2]-[3]. However, the geometry suffers from the high dielectric loss due to the utilization of substrate as increasing of the frequency. Newly introduced gap waveguide technology[4] is another good candidate for mmWs system. This novel gap waveguide has a big competition in low loss properties compared to the microstrip line and the hollow waveguide [5]. Recently, fruitful outcomes of different high-gain high-efficiency slot array antennas based on gap waveguide technology have been reported in [6]-[9]. In [10], a novel W-band low-profile monopulse slot array antenna based on gap waveguide has been reported. In addition, passive filters and novel transition structures based on gap waveguide technology have been reported in [11]-[12]. Low sidelobe array antenna is usually strictly defined in industrial and commercial applications in order to minimize the interference. However, the finished mmWs array antenna before briefly focus on

the full corporate-feed distribution networks with the equal power and the identical phases. This type of array antenna has unqualified radiation patterns on the E-plane. One method to improve this situation is the tilting of the array antenna so that the diagonal plane or 45-degree plane of uniformly excited slots can be utilized [13]-[14]. Nevertheless, such a method has a limitation on the application because the principle E-plane still has a unqualified radiation pattern. On the other hand, [15] introduces an effective method to suppress the E-plane sidelobes by using continuous transverse stub array on the top of the slot array antenna. However, it requires high accurate fabrication process. As is well-known, Taylor distribution method is a traditional approach to realize low sidelobe array design. A low sidelobe slot array antenna based on Taylor distribution method in Ku-band has been introduced in [16], in which an unequal power divider based on hollow waveguide has been introduced. However, the fabrication process for the unequal power divider becomes much more difficult as the operating frequency increased. Secondly, it is very difficult to obtain a large output power ratio with the corresponding identical output phases. In this paper, we briefly introduce a novel unequal power divider with the large output power ratio and the identical output phases and its application on the low sidelobe array antenna based on inverted microstrip gap waveguide at 28 GHz.
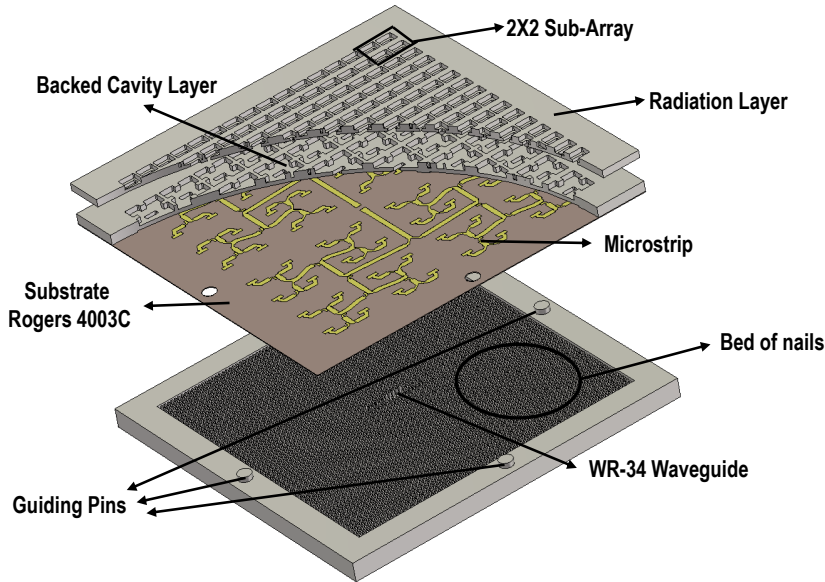

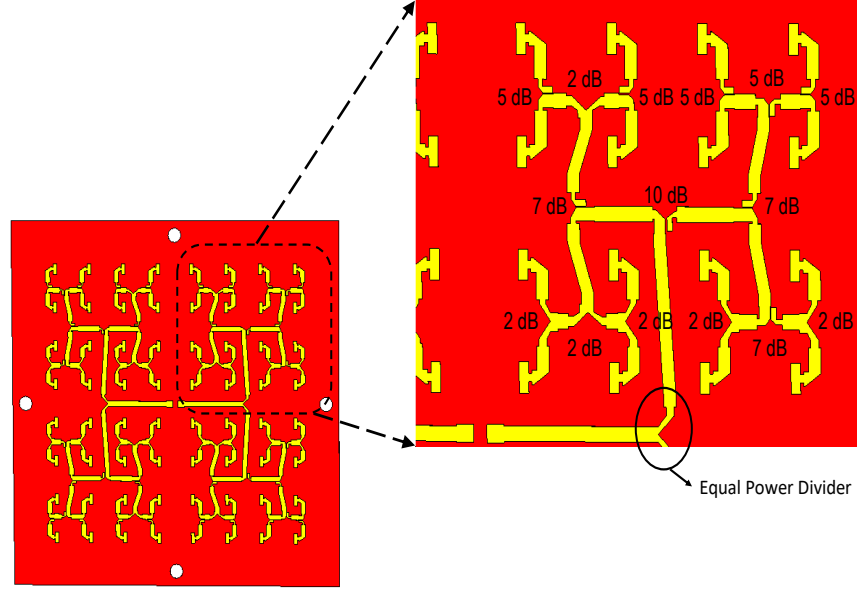Figure 1: Brief view for the proposed 16×16 array antenna.

Figure 2: Top view of the corporate-feed distribution network in the proposed work.

2   Antenna Geometry

In the Fig. 1, a double-layer corporate-feed slot array layer antenna based on inverted microstrip gap waveguide is illustrated. And its layout of microstrip is depicted in Fig. 2. In this work, four types of unequal power dividers are required for the power distribution criterion: 2 dB, 5 dB, 7 dB and 10 dB. The 3-D view for the unequal power divider is shown in Fig. 3. The detailed geometrical sizes of the unequal power divider is shown in Fig. 4. For realizing the big power ratio, the proposed unequal power divider is asymmetric. The required power ratios in this work have been obtained by the offset value T_a. The phase balance between two output ports are mainly controlled by P_a. The input and the output impedance are mainly affected by the width of microstrip W. In this work, those values are selected identical so that the matching networks between any two of them are avoided. The simulated outcomes of the 10 dB power ratio divider is shown in Fig. 5. As is shown, the reflection coefficient is below -25 dB from 26 to 30 GHz, and the output phases are almost identical. Furthermore, the analysis of the power amplitude difference and the phase difference of two output ports is shown in Fig. 6. The power ratio varies from 9 dB to 12 dB from 26 to 30 GHz. The Phase difference is very well controlled within 2 degrees.
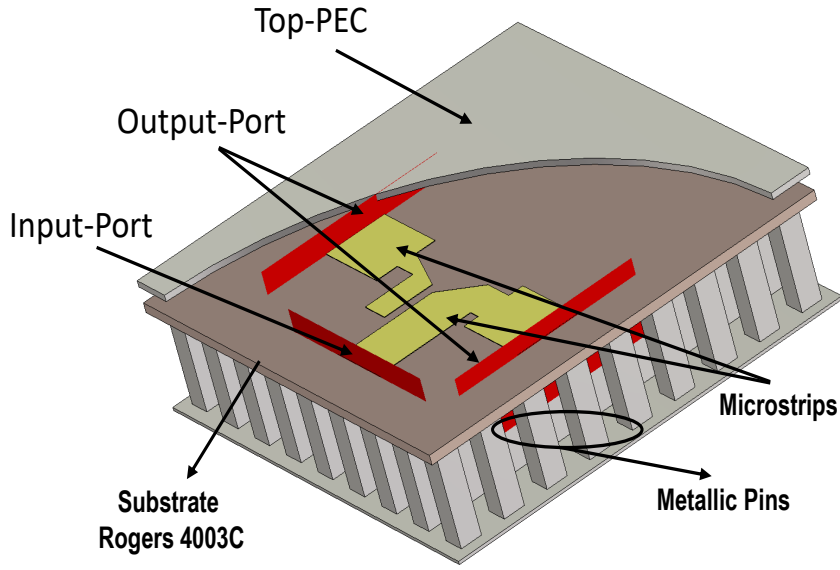
Figure 3: The unequal power divider based on inverted microstrip gap waveguide in this work.

Figure 4: Top view of the proposed unequal power divider. The top metallic plate and the substrate have been hidden.

3 Radiation Patterns and Gain

The final fabricated proposed array antenna is depicted in Fig. 7. The antenna is fabricated by CNC milling process. The proposed antenna characterizes low profile compared with the parabolic reflector antenna. The simulated normalized radiation
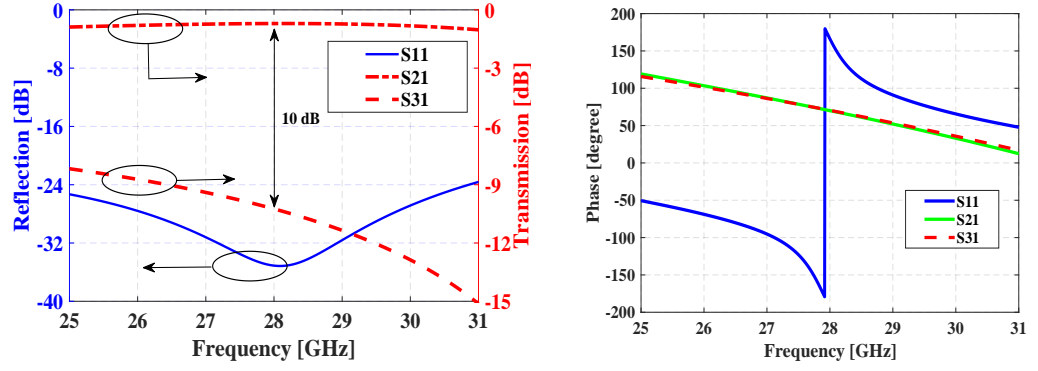
Figure 5: The simulated power amplitude and the simulated phase of the unequal power divider.
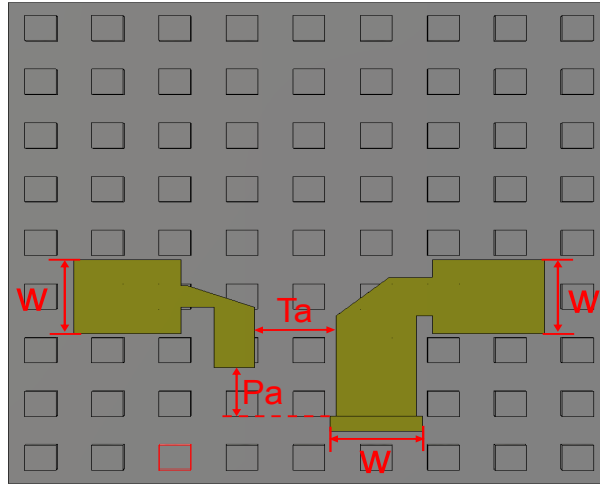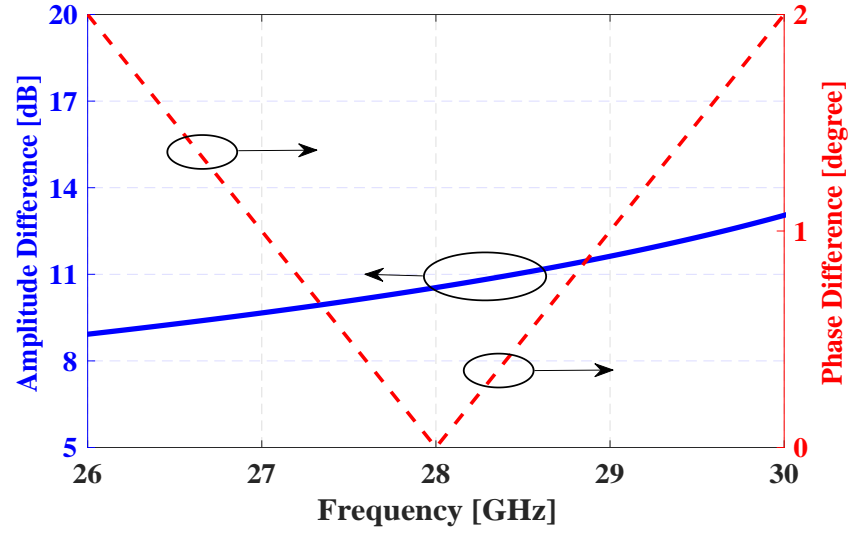

Figure 6: The simulated output power ratio and the phase ratio of the unequal power divider.

Table 1: COMPARISON BETWEEN THE PROPOSED AND REPORTED 60-GHz PLANAR ANTENNA ARRAYS

	Proposed Work	Ref.[6]
First Sidelobe Level on E-Plane	-24 dB	-13.2 dB
First Sidelobe Level on H-Plane	-21 dB	-13.2 dB
Grating Lobes Level on E-Plane	-31 dB	-21 dB
Grating Lobes Level on H-Plane	-25 dB	-26 dB
Front-Back-Ratio on E-Plane	37 dB	25 dB
Front-Back-Ratio on H-Plane	40 dB	40 dB

Figure 7: Photogragh of final fabricated array antenna.

(a)   (b)
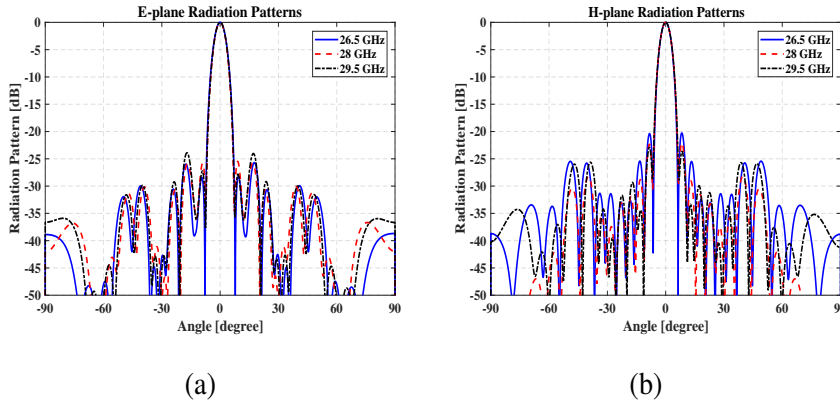
Figure 8: The simulated radiation patterns of the 16×16 array antenna in both E-plane and H-plane.

patterns in both E- and H-planes at three frequencies of 26.5, 28 and 29.5 GHz are shown in the Fig. 8. As is shown in Fig. 8, the E-plane radiation patterns are very well improved. The first sidelobe levels are belo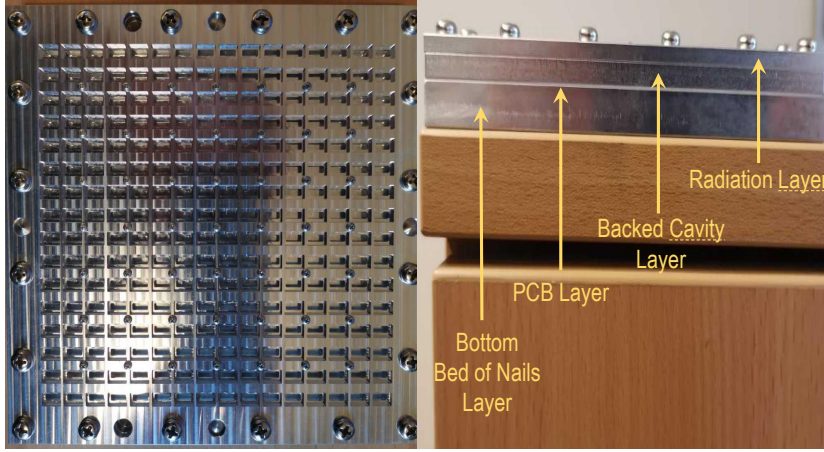w -20 dB, and those values in [6] are -13.2 dB. Compared with previous awful side lobes ratio in [6], those value of the proposed work are better than 25 dB. However, the high sidelobes value are observed in the far-out region (40-50 degrees) on the H-planes. The major reason for this phenomenon is that the 16×16 radiation slots are fed by 8×8 feed networks. It is not an accurate Taylor distribution on the every H-plane. We summarize the proposed work and anther 60-GHz antenna arrays with equal power distribution networks reported in references [6] and compare them in Table I. Compared with the design in [6], the proposed work has improved the radiation patterns very well,
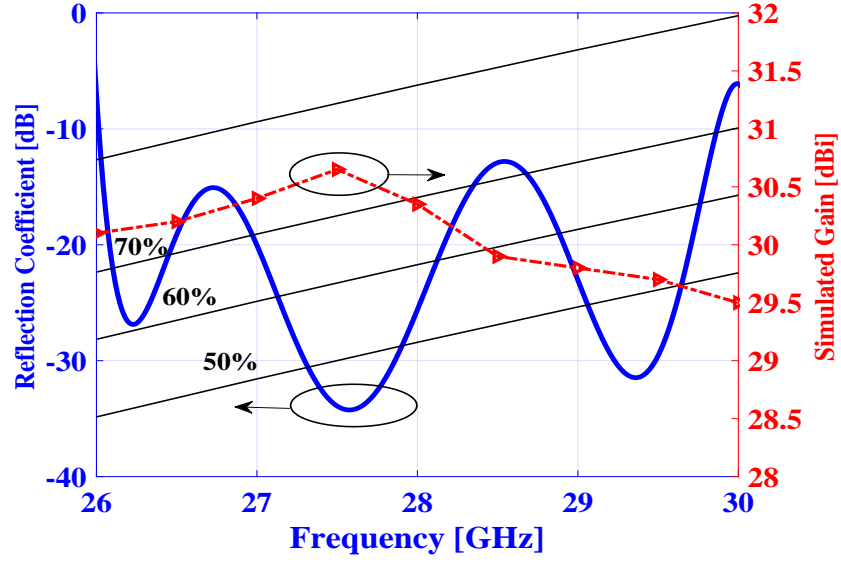
Figure 9: The simulated reflection coefficient and the simulated gain of the 16×16 array antenna.

especially on E-planes. The simulated gain and reflection coefficient are shown in Fig. 8. It is below -10 dB from 26.5 to 29.5 GHz. The simulated gain is higher than 29 dBi with 50% percent antenna efficiency.

4   Conclusion

A high-gain slot array antenna based on inverted microstrip gap waveguide has been introduced in this paper. The radiation patterns on both E- and H-planes have been very well improved because Taylor synthesis method has been utilized for the proposed antenna. To achieve this target, several different unequal power dividers with identical output phases are applied for in this work. The simulated radiation patterns show that the first sidelobe levels, front-back ratio of both E-plane and H-plane from 26.5 GHz to 29.5 GHz are much better than traditional ones with the equal amplitude and phase distribution networks. The input impedance bandwidth is about 12% with the reflection coefficient below -10 dB, and the gain is more than 29 dBi from 26.5 GHz to 29.5 GHz.

References

[1] D. Deslandes and K. Wu, "Integrated microstrip and rectangular waveguide in planar form," *IEEE Microw. Wireless Compon. Lett.*, vol. 11, no. 2, pp. 68-70, Feb. 2001.

[2] L. Wang, J. L. Gomez-Tornero and O. Quevedo-Teruel, "Substrate Integrated Waveguide Leaky-Wave Antenna With Wide Bandwidth via Prism Coupling," *IEEE Trans. Antennas Propag.*, vol. 66, no. 6, pp. 3110-3118, Jun. 2018.

[3] T. Li and Z. N. Chen, "Wideband substrate integrated waveguide (SIW)-fed end-fire metasurface antenna array," *IEEE Trans. Antennas Propag.*, vol. 66, no. 12, pp. 7032-7040, Dec. 2018.

[4] P.-S. Kildal, "Three metamaterial-based gap waveguides between parallel metal plates for mm/submm waves," *in 3rd European Conference on Antennas and Propagation, EuCAP 2009*, pp. 28-32, Mar. 2009.

[5] J. Liu, J. Yang and A. U. Zaman, "Analytical solutions to characteristic impedance and losses of inverted microstrip gap waveguide based on variational method," *IEEE Trans. Antennas Propag.*, vol. 66, no. 12, pp. 7049-7057, Dec. 2018.

[6] J. Liu, A. Vosoogh, A. U. Zaman and J. Yang, "Design and fabrication of a high gain 60-GHz cavity-backed slot antenna array fed by inverted microstrip gap waveguide," *IEEE Trans. Antennas Propag.*, vol. 65, no. 4, pp. 2117-2122, Apr. 2017.

[7] J. Liu, A. Vosoogh, A. U. Zaman and P.-S. Kildal, "Design of 8×8 slot array antenna based on inverted microstrip gap waveguide," *Antennas and Propagation (ISAP), 2016 International Symposium on*, pp. 760-761, Oct. 2016.

[8] J. Liu, A. Vosoogh, A. U. Zaman and P.-S. Kildal, "Design of a cavity-backed slot array unit cell on inverted microstrip gap waveguide *Antennas and Propagation (ISAP), 2015 International Symposium on*, pp. 1-2, Nov. 2015.

[9] J. Liu, A. Vosoogh, A. U. Zaman, and J. Yang, "A slot array antenna with single-layered corporate-feed based on ridge gap waveguide in the 60-GHz band," *IEEE Trans. Antennas Propag.*, vol. 67, no. 3, pp. 1650-1658, Mar. 2019.

[10] A. Vosoogh, A. Haddadi, A. U. Zaman, J. Yang, H. Zirath, and A. A. Kishk, "W-band low-profile monopulse slot array antenna based on gap waveguide corporate-feed network," *IEEE Trans. Antennas Propag.*, vol. 66, no. 12, pp. 6997-7009, Dec. 2018.

[11] D. Sun, and J. Xu, "Real time rotatable waveguide twist using contactless stacked air-gapped waveguides," *IEEE Microwave and Wireless Components Letters*, vol. 27, no. 3, pp. 215-217, 2017.

[12] J. Liu, A. U. Zaman and P.-S. Kildal, "Design of transition from WR-15 to inverted microstrip gap waveguide," *2016 Global Symposium on Millimeter Waves (GSMM) Technology and Applications*, 6-8 Jun. 2016.

[13] T. Tomura, J. Hirokawa, T. Hirano, and M. Ando, "A 45 linearly polarized hollow-waveguide 16×16-slot array antenna covering 71-86 GHz band," *IEEE Trans. Antennas Propag.*, vol. 62, no. 10, pp. 5061-5067, Oct. 2014.

[14] T. Tomura, Y. Miura, M. Zhang, J. Hirokawa, and M. Ando, "A 45 linearly polarized hollow-waveguide corporate-feed slot array antenna in the 60-GHz band," *IEEE Trans. Antennas Propag.*, vol. 60, no. 8, pp. 3640-3646, Aug. 2012.

[15] H. Arakawa, H. Irie, T. Tomura and J. Hirokawa, "Suppression of E-Plane sidelobes using a double slit layer in a corporate-feed waveguide slot array antenna consisting of 2×2-element radiating units," *IEEE Trans. Antennas Propag.*, vol. 67, no. 6, pp. 3743-3751, Jun. 2019.

[16] Guan-Long Huang, Shi-Gang Zhou, Tan-Huat Chio, Hon-Tat Hui, and Tat-Soon Yeo, "A low profile and low sidelobe wideband slot antenna array feb by an amplitude-tapering waveguide feed-network," *IEEE Trans. Antennas Propag.*, vol. 63, no. 1, pp. 419-423, 2015.

Paper 4

Design of Wideband Slot Array Antenna by Groove
Gap Waveguide in Millimeter Waves

Jinlin Liu, Ashraf Uz Zaman, and Jian Yang

The layout of this paper has been revised in order to comply with the rest of
the thesis.

Design of Wideband Slot Array Antenna by Groove Gap Waveguide in Millimeter Waves

Jinlin Liu, Ashraf Uz Zaman, and Jian Yang

Abstract

The newly introduced gap waveguide technology offers non-contact waveguide configurations so that the good electrical contact between different metallic layers can be avoided. Thereby, the gap waveguide structures are relatively simple to manufacture, especially at millimeter and sub-millimeter wave frequencies. This work systematically presents a high-efficiency corporate-fed slot array antenna based on groove gap waveguide in the millimeter waves. A cavity-backed slot sub-array is firstly designed in a groove gap waveguide cavity. The cavity is fed through a coupling hole from groove gap waveguide distribution network at the bottom layer. The sub-array is numerically optimized in an infinite array environment. Low side lobes are obtained in the both E- and H-planes by diagonal placement of the radiation slot rotating by 45 degrees. Furthermore, the radiation narrow slot pair is adopted so that the good cross polarization is achieved. The fabricated antenna depicts more than 25% bandwidth with input reflection coefficient better than -8 dB and the aperture efficiency higher than 60% with around 25 dBi realized gain between 70 and 90 GHz. The measured cross polarization level is below -27 dB, which satisfies the ETSI standard.

1 Introduction

Recently, the saturation of spectrum at microwave frequencies causes the consideration of higher frequency bands. Especially, the millimeter wave range between 30 GHz and 300 GHz has been paid lots of attentions [1]-[2]. Furthermore, the usage of the millimeter wave frequencies has the advantage of allowing for larger bandwidths, and thereby, achieving higher data transfer rates. In such frequency ranges, traditional hollow waveguide and microstrip lines have met up with difficulties to design antennas and passive components.Indeed, hollow waveguide are normally manufactured in two parts and then joined together. In microwave frequency band, it is still convenient to fabricate hollow waveguide because its geometrical dimensions are large. However, its fabrication becomes a big problem because its dimensions are very small in millimeter waves. Moreover, it suffers from problems of irregular rectangular shape and poor electrical contacts. Diffusion bonding and vacuum welding are probably two

manufacture technologies for hollow waveguide in millimeter waves [3]. Nevertheless, its fabrication cost is relatively high. On the other hand, microstrip lines or covered microstrip lines are able to integrate the active components, but still present high dielectric losses in millimeter waves. Thereby, new technologies in millimeter waves are still demanded.

Substrate integrated waveguide (SIW) is a appropriate candidate in millimeter waves. Nevertheless, it exhibits undesired dielectric losses in the substrate at increasing frequencies. As is well known, the loss tangent value of substrate increases versus the frequency. Thereby, the dielectric loss in SIW is unacceptable above 60 GHz so that the antenna efficiency is affected [4]-[5]. In such a situation, there is still need to find new technological solutions for waveguides that have low losses and are cheap to manufacture. The recently introduced gap waveguide technology [6] constitutes a new type of guiding structure that shows lot of potential to overcome the issues of conventional technologies, and become a suitable approach at millimeter wave frequencies. First of all, the gap waveguide shows low loss compared with microstrip, covered microstrip and SIW. Secondly, unlike the conventional manufacture of hollow waveguide, the gap waveguide structure is very flexible to be manufacture. Most importantly, the electrical contact between the building blocks is not needed in this new guiding structure so that expensive fabrication technologies, such as vacuum welding and diffusion bonding, can be avoided in millimeter waves. Until now four different variety of gap technology, ridge gap waveguide, groove gap waveguide, microstrip-gap
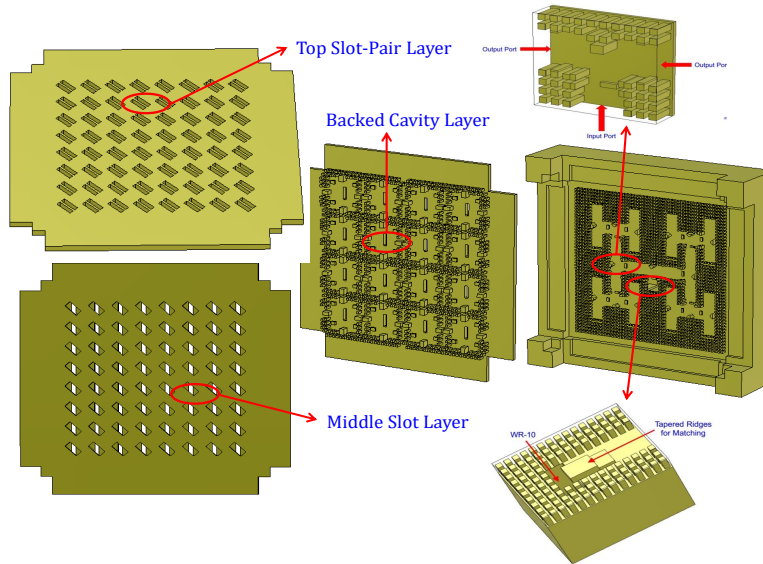

Figure 1: Configuration of the proposed corporate-feed slot array antenna based on groove gap waveguide.

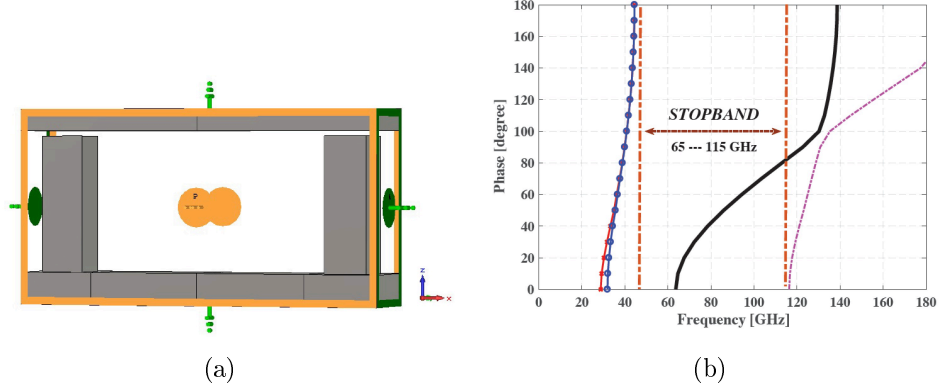<div style="text-align:center">(a)   (b)</div>

Figure 2: (a) A groove gap waveguide unit cell for determination of dispersion diagram. (b) The corresponding dispersion diagram.

waveguide, and inverted microstrip-ridge gap waveguide have been already investigated. In [7]-[9] slot array antennas based on gap waveguide technology have been finished. They are able to achieve characteristics of high-gain and high-efficiency because of low loss property. In [10]-[11] filter and duplexer have been developed. In addition, gap waveguide is also able to be applied for microwave circuits packaging [12].

In this work, we Initially introduce a 45° linearly polarized corporate-feed groove gap waveguide slot array antenna covering 71.5 to 90 GHz. As depicted in Fig. 1, the whole slot array antenna consists of the distribution feeding networks, the backed cavity layer, the middle slot layer and the top radiation slot layer. The feeding part is composed of equally-split H-plane T-junctions and a vertical transition from WR-10 standard hollow waveguide from its back. In order to satisfy the radiation pattern of ETSI standard, the radiation slots in this work have been 45° rotated [13]-[14]. Given the rising of the cross polarization level caused by 45° degree rotation, a narrow-slot pair configuration on the top is designed to suppress the cross-polarization. The proposed antenna has been fabricated by computerized numerical control (CNC) milling machine. The measured reflection coefficient and far-field radiation patterns are discussed in the end.

2 Design of Sub-array

The pin dimensions of bed of nails at both distribution networks and backed cavities should be chosen correctly to achieve a parallel plate stopband which covers as much as the operating frequency. As depicted in Fig. 2 (a), the design unit cell of proposed groove gap waveguide is built with PEC, periodic and PEC boundary conditions in x-, y- and z-axis in CST Microwave Studio, respectively. Correspondingly, the dispersion diagram of the structure is shown in Fig. 2(b), which is obtained by utilizing the

eigenmode solver in CST Microwave Studio. The obtained stopband is from 65 to 115 GHz. The proposed 2×2 sub-array is illustrated in Fig. 3. The sub-array consists of four layers — the top pair radiation layer, the middle slot layer, the backed cavity layer and the bottom distribution feed networks layer. An air-filled cavity formed by pins, feeds four radiating slots with spacing smaller than 3.1 mm, which is equal
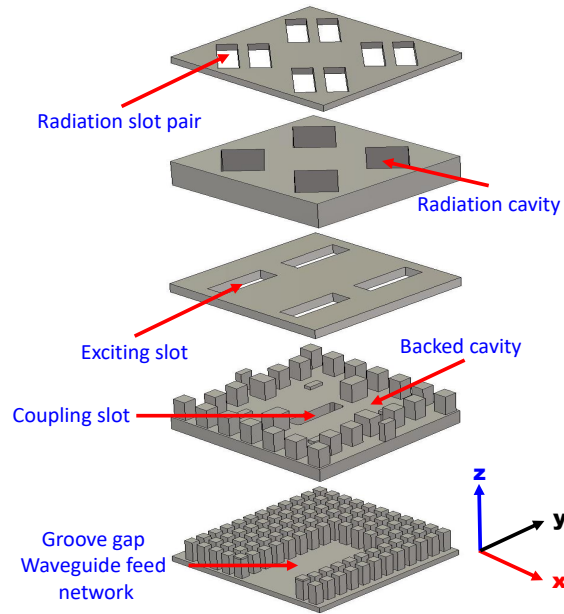
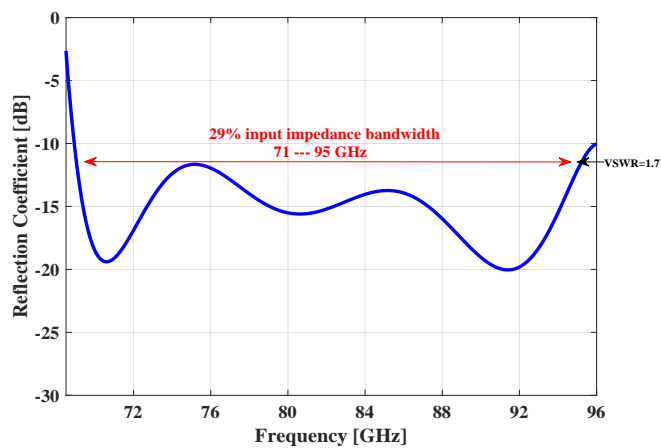Figure 3: Model for the analysis of the 2×2-element sub-array.

Figure 4: The reflection coefficient of the sub-array.

to one wavelength on the top layer. A groove gap waveguide excites the cavity via a coupling slot on the bottom layer. There is a small gap between each layers and thereby no electrical contact between the different layers. This is a manufacturing advantage of this technology. The designed sub-array has 6×6 mm^2 dimensions. The sub-array is optimized in the infinite array environment by using CST Microwave Studio where the mutual coupling between sub-arrays are automatically included. The simulated reflection coefficient of the sub-array is illustrated in Fig. 4. The sub-array bandwidth is 29% (71 — 95 GHz) with the VSWR better than 1.7. The directivity versus frequency of an array with the same aperture size is shown in Fig. 5. The blue line in the graph shows the maximum available directivity between 100% and 80% aperture efficiency, which clearly shows that the designed sub-array has high aperture efficiency. In Fig. 6, the E- and H-plane far field patterns of an array with 32×32 slots over its aperture are illustrated for different frequencies.

3 Simulation and Measurement for the 8×8 Slot Array

The fabricated 8×8 slot array antenna is illustrated in Fig. 8. The prototype is manufactured by Computerized Numerical Control (CNC) technology. The fabricated machine is Fanuc α D14B15 with fabrication tolerance 2.5 μm, and this is good enough to fabricate our array antenna. The dimensions of effective aperture are 24 $\times$ 24 mm^2 and it was fabricated by aluminium (with electric conductivity 3.6×10^7 S/m). The entire structure is simulated in CST Microwave Studio. The simulated

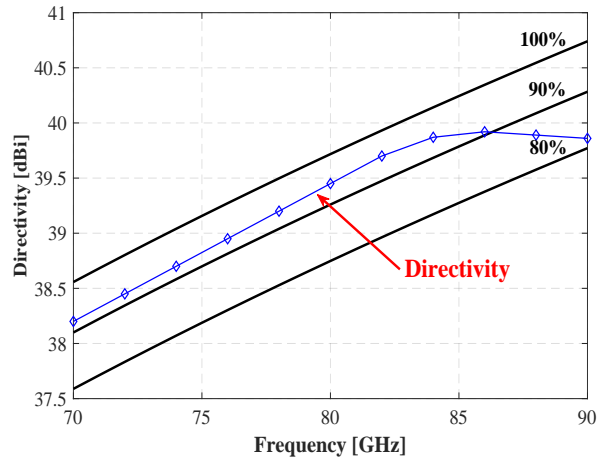Figure 5: The simulated directivity of the 32 × 32 slot array according to the periodic boundary condition.
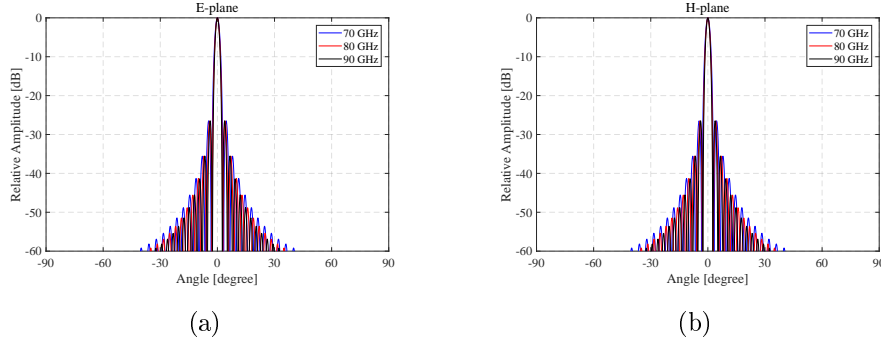
(a)   (b)

Figure 6: Normalized radiation patterns of an array with 32×32 slot aperture dimension in (a). E-plane and (b). H-plane. Infinite array approach.

reflection coefficient of complete antenna is below -10 dB from 70 to 90 GHz, as shown in Fig. 9. However, the measured reflection coefficient is a bit higher than simulated one because of the tolerances of manufacturing and assembling tolerances. Still, it covers 71.5 to 90 GHz with the VSWR better than 2.4. The simulated far-field radiation patterns of proposed antenna at 70, 80 and 90 GHz in both E- and H-planes are depicted in Fig. 9. Low sidelobe characteristics are obtained over the bandwidth investigated here. No grating lobe is observed. The simulated first sidelobe levels are less than -26 dB. The measured frequency characteristics of the gain and the cross polarization are shown in Fig. 10. The gain and the cross polarization are measured by V- and W-band far-field measurement systems for 70—75 GHz and 75—90 GHz,
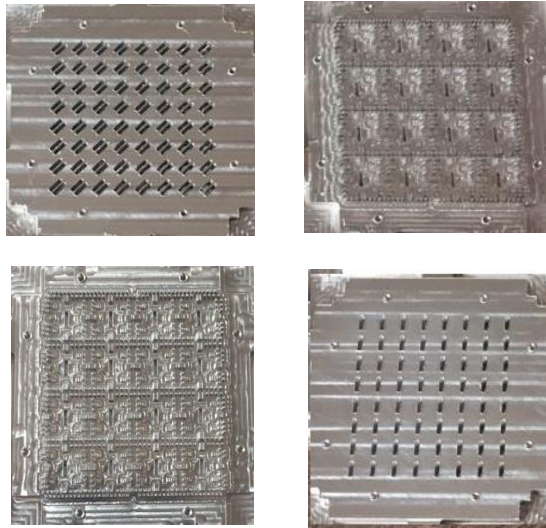

Figure 7: Picture of manufactured antenna in this work.

respectively. In the 71—89 GHz band, the gain variation is 25—26.2 dBi. The bandwidth for a gain of more than 25 dBi and the antenna efficiency of more than 60% is greatly improved. The cross polarization is suppressed below -27 dB over the full bandwidth. In [14] the the cross polarization level are very well pressed under -30 dB, but this work has not achieved the outcome. The main reason for the problem is that the assembly of the four layers array antenna always has small geometrical errors, which makes the drop of gain and the rise of the cross-polarization and the reflection coefficient.
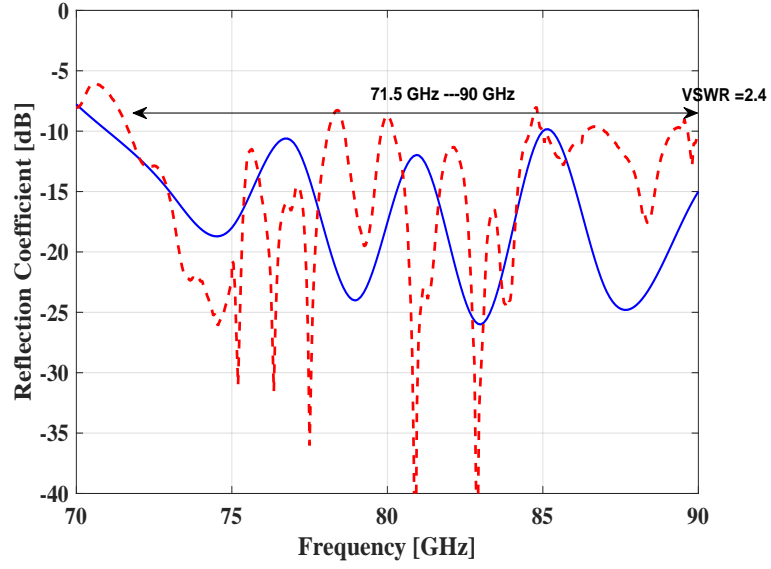

Figure 8: The simulated and the measured reflection coefficients of proposed antenna. The blue curve indicates the simulated reflection coefficient, and the red line depicts the measured one.
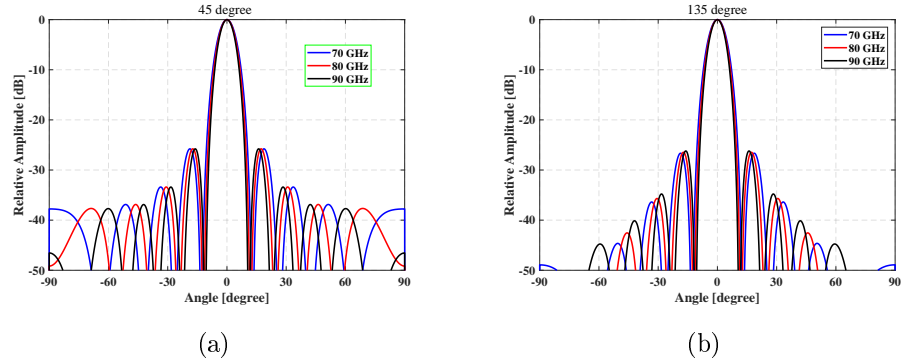

Figure 9: The simulated far-field radiation patterns of proposed antenna. (a) E-plane and (b) H-plane.
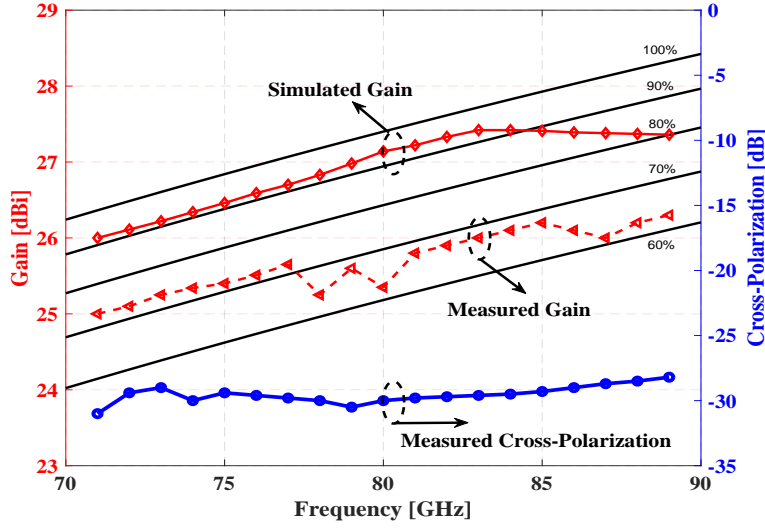
Figure 10: The simulated and measured gains of the proposed array antenna. The measured one shows the antenna efficiency is higher than 60%. The measured cross-polarization is better than -27 dB, which fulfills the ETSI standard.

4   Conclusion

In this work, we present a 45 degree 8 × 8 cavity-backed slot array antenna based on groove gap waveguide for high-gain 80 GHz. The proposed antenna consists of four layers, i.e. 45 degree radiation slot layer, middle coupling slot layer, backed cavity layer and feeding network layers without need of electrical contact between layers. This presents manufacturing advantages in particular at millimeter wave. The array antenna can be directly connected with standard WR-10 interface. The measured gain is higher than 25 dBi from 71 to 90 GHz, correspondingly the antenna efficiency larger than 60%.

5   Acknowledgement

The authors would like to thanks Dr. Kuikui Fan at Southeast University in Nanjing for the measurement of the reflection coefficient and Shanghai Academy of Spaceflight Technology for the measurement of the gain and cross polarization level.

References

[1] P. Smulders, "Exploring the 60-GHz band for local wireless multimedia access: Prospects and future directions," *IEEE Commun. Mag.*, vol. 40, no. 1, pp. 40-147, Jan. 2002.

[2] T. S. Rappaport, J. N. Murdck, and F. Gutierrez, "State of the art in 60-GHz integrated circuits and systems for wireless communications," *Proc. IEEE*, vol. 99, no. 8, pp. 1390-1436, Aug. 2011.

[3] Y. Miura, J. Hirokawa, M. Ando, Y. Shibuya and G. Yoshida, "Doublelayer full-corporate-feed hollow-waveguide slot array antenna in the 60 GHz band," *IEEE Trans. Antennas Propag.*, vol. 59, no. 8, pp. 2844-2851, Aug. 2011.

[4] Y. Li and K.-M. Luk, "Low-cost high-gain and broadband substrate integrated-waveguide-fed patch antenna array for 60-GHz band," *IEEE Trans. Antennas Propag.*, vol. 62, no. 11, pp. 5531-5538, Nov. 2014.

[5] Y. Li and K.-M. Luk, "60-GHz substrate integrated waveguide fed cavity-backed aperture-coupled microstrip patch antenna arrays," *IEEE Trans. Antennas Propag.*, vol. 63, no. 3, pp. 1075-1085, Mar. 2015.

[6] P.-S. Kildal, "Three metamaterial-based gap waveguides between parallel metal plates for mm/submm waves," in proceeding of *3rd European Conference on Antennas and Propagation, EuCAP 2009*, pp. 28-32.

[7] A. Vosoogh, P.-S. Kildal and Vessen Vassilev, "Wideband and high-gain corporate-fed gap waveguide slot array antenna with ETSI Class II radiation pattern in V-Band," *IEEE Trans. Antennas Propag.*, vol. 65, no. 4, pp. 1823 - 1831, April, 2017.

[8] J. L. Liu, A. Vosoogh, A. U. Zaman and J. Yang, "Design and fabrication of a high gain 60-GHz cavity-backed slot antenna array fed by inverted microstrip gap waveguide," *IEEE Trans. Antennas Propag.*, vol. 65, no. 4, pp. 2117 - 2122, April, 2017.

[9] J. L. Liu, A. Vosoogh, A. Uz Zaman and P.-S. Kildal, "Design of 8 × 8 slot array antenna based on inverted microstrip gap waveguide," *Antennas and Propagation (ISAP), 2016 International Symposium on*, 24-28, October, 2016.

[10] E. Rajo-Iglesias, P. S. Kildal, A. U. Zaman, and A. Kishk, "Bed of springs for packaging of microstrip circuits in the microwave frequency range," *IEEE Trans. Compon. Packag. Manuf. Technol.*, vol. 2, no. 7, pp. 1623 - 1628, July, 2012.

[11] A. U. Zaman, P.-S. Kildal and A. A. Kishk, "Narrow-Band microwave filter using High-Q groove gap waveguide resonators with manufacturing flexibility and no sidewalls," *IEEE Trans. Compon. Packag. Manuf. Technol.*, vol. 2, no. 11, pp. 1882 - 1889, Nov. 2012.

[12] A. U. Zaman, M. Alexanderson, T. Vukusic and P.-S. Kildal, "Gap waveguide PMC packaging for improved isolation of circuit components in high-frequency microwave modules," *IEEE Trans. Compon. Packag. Manuf. Technol.*, vol. 4, no. 1, pp. 16 - 25, Jan. 2014.

[13] T. Tomura, Y. Miura, M. Zhang, J. Hirokawa, and M. Ando, "A 45 degree linearly polarized hollow-waveguide corporate-feed slot array antenna in the 60-GHz band, " *IEEE Trans. Antennas Propag.*, vol. 60, no. 8, pp. 3640-3646, Aug. 2012.

[14] T. Tomura, Y. Miura, M. Zhang, J. Hirokawa, and M. Ando, "A 45 Linearly Polarized Hollow-Waveguide 16 × 16-Slot Array Antenna Covering 71—86 GHz Band," *IEEE Trans. Antennas Propag.*, vol. 62, no. 10, pp. 5061-5067, Aug. 2014.

Paper 5

A Slot Array Antenna With Single-Layered Corporate-Feed Based on Ridge Gap Waveguide in the 60 GHz Band

Jinlin Liu, Abass Vosoogh, Ashraf Uz Zaman, and Jian Yang

The layout of this paper has been revised in order to comply with the rest of the thesis.

A Slot Array Antenna With Single-Layered Corporate-Feed Based on Ridge Gap Waveguide in the 60 GHz Band

Jinlin Liu, Abass Vosoogh, Ashraf Uz Zaman, and Jian Yang

Abstract

This paper presents an 8×8-element slot array antenna with single-layered corporate-feed based on the ridge gap waveguide technology in the 60-GHz band. As is well-known, a corporate-feed slot array antenna usually has backed cavities to increase the bandwidth and provide a space for its distribution network, and therefore three layers in total: one layer for radiating slots and two layers for feed network with one layer of back cavities and one of power dividers. The antenna in this work is designed by utilizing only two separate metallic layers – a corporate-feed network layer and a radiating slot layer. Compared with the conventional three-layered slot array antennas, the proposed antenna avoids the utilization of the backed cavity layer so that its complexity and manufacture cost decrease. In order to solve the problem of the narrow bandwidth caused by taking away the backed cavities we utilize double-ridged radiating slots instead of the conventional rectangular ones. A compact transition power divider from standard waveguide WR-15 to the ridge gap waveguide is introduced to excite the proposed array antenna. The 8×8-element slot array antenna has been fabricated by computerized numerical control machining technique. The measured results demonstrate that the -10 dB reflection coefficient has around 17% bandwidth covering 56.5 − 67 GHz frequency range, and the measured gain is better than 26 dBi with more than 70% antenna efficiency over 58 − 66 GHz.

Double-layered slot array, ridge gap waveguide, single-layered corporate-feed network, 60-GHz frequency band.

1   Introduction

Recently, the current saturation of spectrum at microwave frequencies causes new attention to the millimeter waves (mmWs). Hence, the unlicensed 60-GHz band (from 57 to 66 GHz) has a very strong potential for high data rates wireless communications [1]-[2]. However, the communication distance at 60-GHz is strongly affected

137

by atmospheric absorption [3]. Thereby, an antenna with high-gain and wideband is theoretically required for such kind of point-to-point wireless systems. The reflector antenna is normally a conventional choice. Nevertheless, thin planar slot array antennas are more desirable in the 60-GHz frequency band due to its high efficiency and thin profile. A high-gain high-efficiency corporate-feed slot array antenna based on conventional hollow waveguide technology at 60-GHz has been achieved in [4]. However, its fabrication is complicated and the corresponding cost is high. One traditional technology, patch array, has higher dielectric loss so that it is almost impossible to realize the high efficiency planar array in mmWs [5]. Another popular technology to mmWs is the substrate integrated waveguide (SIW). Nevertheless, its dielectric loss becomes problematically significant if it is applied for designing large high-gain array antennas in the 60-GHz band [6]-[7].

The gap waveguide is a new technology recently introduced in [8]-[9]. Theoretically, this new waveguide consists of two parallel plates, a top plate of perfect electric conductor (PEC) and a bottom plate of perfect magnetic conductor (PMC). If the air gap between the parallel plates is smaller than quarter-wavelength, there is no propagating wave between the plates. However, if a wave guiding structure, such as a microstrip or ridge, is added between the PEC-PMC plates, a quasi-TEM mode is able to propagate along the guiding structure. Given the non-existence of PMC in nature, the metallic pins surface is applied to realize Artificial Magnetic Conductor (AMC) [10]. This novel gap waveguide has advantages compared to the microstrip line and the hollow waveguide. First of all, the gap waveguide can keep a planar profile as well as being low loss since the waves propagate in the air gap. Secondly, this technology can avoid the requirement of good metallic contacts between the parallel metallic plates because the metallic pins surface can create a high impedance to avoid the wave leakage. In addition, the gap waveguide makes fabrication process easy and cheap by molding or die-sink electrical discharge machining (EDM) technique. Furthermore, the AMC of gap waveguide technology can be utilized to package active components [11]-[12] and low-cost bandpass filters [13]-[14].

So far, there are four different realizations of gap waveguide technology — groove, ridge, inverted microstrip [8] and microstrip-ridge gap waveguides [15]. In [16]-[17] two high-gain high-efficiency slot array antennas in V-band on ridge gap waveguide (RGW) have been reported. Other similar works on inverted microstrip gap waveguide (IMGW) have been reported in [18]-[19]. A planar array based on groove gap waveguide (GGW) has been reported in [20]. Recently, a novel wideband and continuous beam steering flat antenna on RGW is proposed in the 60-GHz band [21]. A W-band high-gain L-probe excited substrate integrated cavity (SIC) antenna on RGW distribution networks is also proposed in [22]. In addition, a high-efficiency millimeter wave antenna array with the RGW feeding network is designed in [23]. In order to achieve wideband and provide enough space for the distribution networks, all antennas in [4]-[7] and [16]-[23] have backed cavities where four slots are fed by
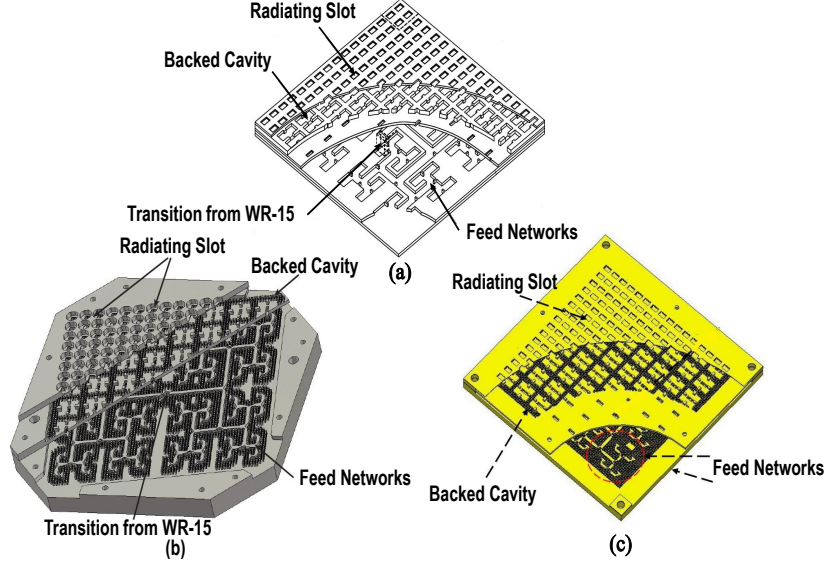
1. Introduction

Figure 1: (a) depicts a cavity-backed slot array antenna fed by hollow waveguide introduced in [4]. (b) shows a cavity-backed slot array antenna fed by ridge gap waveguide reported in [17] and a similar antenna fed by inverted microstrip gap waveguide stated in [18] is illustrated in (c). These three full corporate-feed antennas consist of three layers — distribution feed networks, backed cavity and radiation slots and their operating frequency all in the 60-GHz band.

one cavity. Therefore, such a type of antennas consist of three layers — distribution feed networks, backed cavities and radiation slots. Some typical examples are shown in Fig. 1. Unfortunately, it is inevitable to increase the manufacture cost and design complexity for designing those corporate-feed antennas. On the other hand, instead of using the corporate-feed network, a series-feed network [24]-[26] is commonly applied for a single-layered fed slot array because its structure is simple. Nevertheless, its congenital disadvantage is also obvious. The bandwidth is usually limited to several percentage because of the long line effect. Thereafter, it is much preferred to have a slot array with single-layered corporate-feed network. A successful slot array with single-layered corporate-feed network can be found in [27] in the 60-GHz using hollow waveguide manufactured by diffusion bonding technology. However, this manufacture technology is very expensive for massive production and its bandwidth is limited within 10%. In [28] a 2×2 slot antenna unit cell based on ridge gap waveguide (RGW) in Ku-band was reported. This 2×2 unit cell utilizes bend parts in ridge line to excite slots and this geometry thereby has difficulties in layout of distribution network of a large array antenna.

In this paper, we initially introduce a new slot array antenna with single-layered corporate-feed network in the 60-GHz band. This novel antenna avoids utilization of the backed-cavities by a new layout of the corporate-feed distribution network in RGW and meanwhile achieves expected radiation pattern. The shape of the radia-
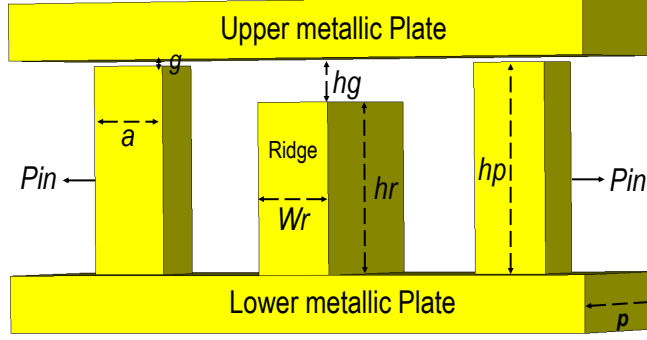
Figure 2: The geometrical dimensions of the ridge gap waveguide for the array antenna in this work.

tion slots is a modified double-ridge waveguide, which has a wider bandwidth than that of rectangular slots with a single-layered corporate-feed network.

The organization of this paper is as follows. Firstly, a novel slot unit cell is designed based on RGW, where the excitation scheme for the slot is different from those in [16]-[23]. Then the unit cell has been optimized in an infinite array environment in CST Microwave Studio for high directivity and low reflection coefficient. Thereafter, a T-junction power divider including a transformer from a standard waveguide WR-15 to the ridged gap waveguide is designed for the input port of the whole array antenna. Finally, measurement results after fabrication are presented.

2 Geometrical dimensions of RGW for stopband, transition and mutual coupling

Based on the fundamental theory in [8], a gap waveguide supplies a stopband over a specific frequency range between the two parallel-plates. Since our target is to cover the whole unlicensed 60-GHz frequency band (57 - 66 GHz), the dimensions of the

Table 1: Design Parameters of the Structure in Fig. 1

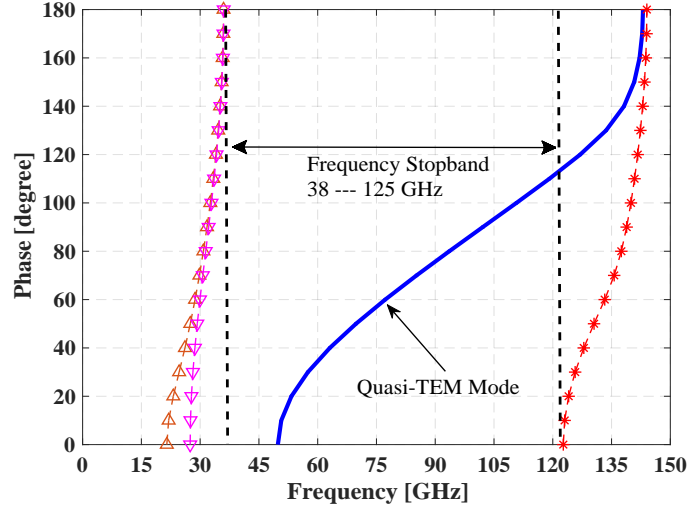|	
Height of the Ridge [h_r]	0.75 mm
Width of the Ridge [W_r]	0.55 mm
Height of the Air Gap between Pins and upper Plate [g]	0.03 mm
Height of Air Gap between Ridge and upper Plate [h_g]	0.2 mm
Height of the Pin [h_p]	0.92 mm
Width of the Pin [a]	0.4 mm
Period of the Pin [p]	1.05 mm

Figure 3: Corresponding dispersion diagram of the ridge gap waveguide depicted in Fig. 1. The blue solid line stands for the Quasi-TEM mode.

RGW should be properly chosen to cover as much of the 60-GHz frequency band as possible. A simple geometrical schematic diagram of the RGW is depicted in Fig. 2. The dimensions of the pins and the ridge line are chosen according to the method introduced in [29]. A center frequency of $f_0 = 62$ GHz is assumed in this work. Then the height of the pins should be typically selected as $\lambda_0/4$, which is equal to 1.2 mm. Nevertheless, for the easier manufacture shorter pins have been chosen in this work. Furthermore, for achieving good radiation patterns the spacing between any two slots is selected as 4.2 mm, which is equal to $0.87\lambda_0$. Having considered the layout of the distribution network, four rows of metallic pins are required for the dimension of 4.2 mm and the corresponding periodicity of metallic pins is 1.05 mm. On the other hand, the width of square metallic pins is chosen as 0.4 mm. Thereby, the spacing between two arbitrary pins is 0.65 mm, which is equal to the difference of two mentioned variables. The dispersion diagram of the ridge gap waveguide is depicted in Fig. 3. The stopband is from 38 to 125 GHz, which covers the whole V-band.

In corporate-feed array antennas in [16]-[23], the space for the layout of ridge lines is usually very limited so that the backed cavities is applied to provide more space for the distribution feed network. Therefore, it is a big challenge to lay out feed networks without backed cavities in this work. Before designing the whole array antenna, the coupling between two ridge lines with only one row of pins should be tested. Fig. 4 illustrates a simple model to examine the performance. The length of the whole structure is 10.5 mm. While the height of the metallic pins h_p is already
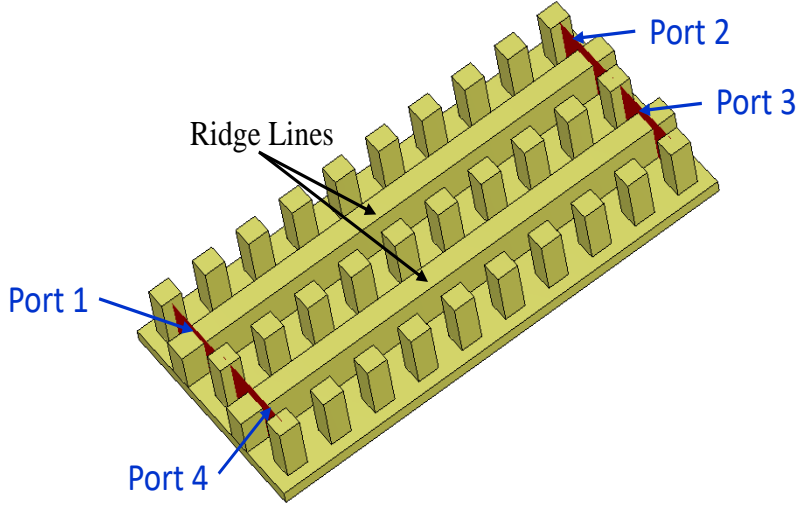
Figure 4: Top view of two parallel ridge lines with one row of pins in between. Upper flat metallic plate is hidden to illustrate the bottom plate.
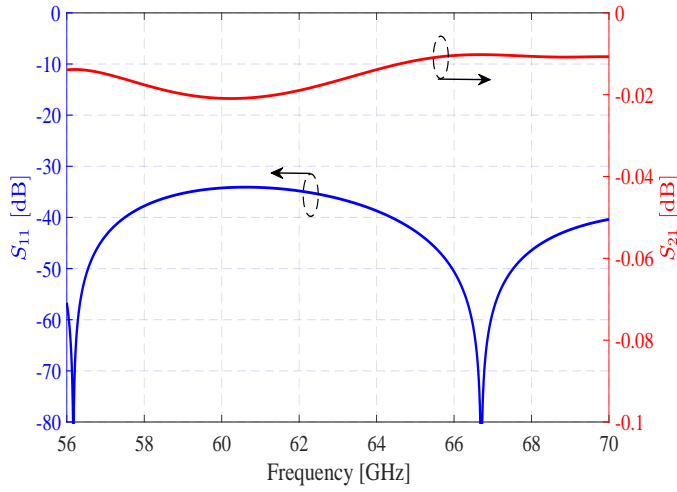

Figure 5: Simulated reflection coefficient and the transmission coefficient of the two parallel RGWs in Fig. 4.

fixed, we have to search for the optimal dimensions of air gap height g, the width W_r and the height h_r of the ridge in order to minimize the reflection coefficients and the coupling S_{31} between two ridge lines with only one row of pins. As illustrated in Fig. 5, the reflection coefficient of the straight ridge line is below -33 dB from 56 to
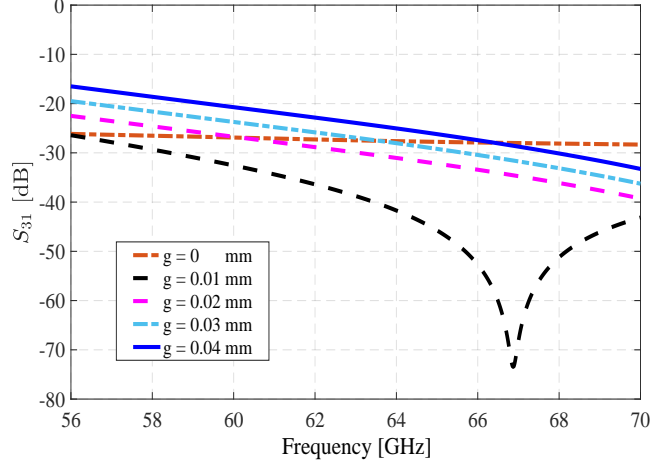
Figure 6: Mutual coupling investigation on one row pins between two straight ridge lines defined in Fig. 4. Parameter sweep for g is carried out in CST Microwave Studio.

70 GHz. This outcome is acceptable for the array antenna design in this work. The parameter sweep method is also utilized for g stated in Fig. 2 in this part in order to minimize the mutual coupling between the two ridge lines. As is shown in Fig. 6, the mutual coupling is lower than -20 dB when the air gap between the metallic pins and upper metallic plate g is smaller than 0.03 mm. This value is acceptable for designing distribution feed network based on RGW only with one row of pins [17]. Having considered the requirement of non-electrical contact, we have selected 0.03 mm in this work and it presents that the feed network has very low leakage and mutual coupling between two neighbor ridge lines with one row of pins in the 60-GHz band.

3 Design of Antenna Unit Cell

As depicted in Fig. 7, the antenna unit cell consists of a radiating slot and a ridge feeding line. This element is under periodic boundary condition defined in CST Microwave Studio. The slot in this work is designed as an '8' shape, which is actually a double ridge slot with circularly curved corners and smoothly profiled ridges. The double ridges will lower the cutoff frequency of the dominant mode and will raise the cutoff frequency of the next higher order modes in the slot [30]. Therefore, it increases the bandwidth of the array antenna compared with that by using a normal rectangular slots. To excite the electromagnetic wave in the slot, the magnetic field created by the ridge line of feed layer should rotate along the vertical direction of the double ridged slot. Then electromagnetic wave can radiate with same phase and
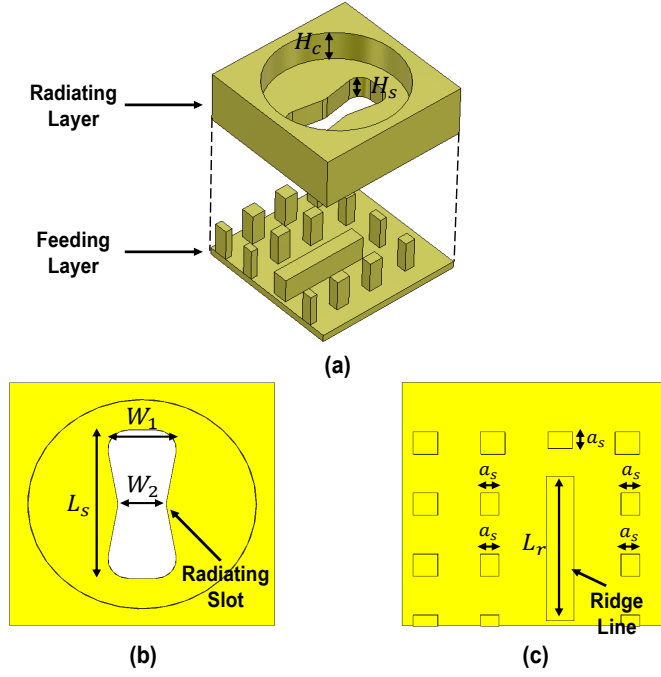
Figure 7: Proposed antenna unit cell: (a) Exploded view. (b) Radiating layer. (c) Feeding layer.
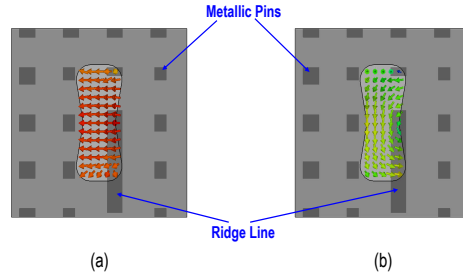

Figure 8: Illustrations for field-distributions: (a) E-filed. (b) H-field.

polarization from slot. This method is actually a magnetic coupling radiation, which is different from excitation method stated in [16]-[20] and [28]. It avoids utilization of the conventional bend ridge line and makes the feed network very compact so the layout of the feed network is possible in such limited space as in the single-layered corporate-feed network case. The length of the slot L_s is firstly chosen so that the mutual coupling to the neighbor feed line can be eliminated. If L_s is small, the slot would not extend to the neighbor ridge feed line. W_1, W_2, H_s and L_r have been optimized to achieve the minimum reflection coefficient. TABLE II lists the optimized geometrical parameters of the unit cell shown in Fig. 7. Fig. 8 depicts
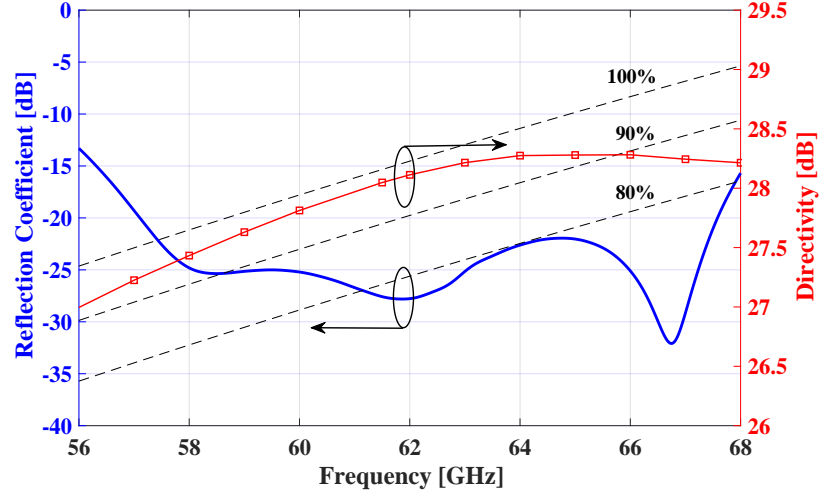
Figure 9: Simulated reflection coefficient of the single slot unit cell and directivity of an array antenna with 8×8 slot aperture dimension in infinite array environment.

the corresponding E- and H-fields distributions in the double ridged slot from CST Microwave Studio. The magnetic field is desired as predicted before. The distance between any two slots is equal to $0.87\lambda_0$, which satisfies the condition of non-grating lobes (element spacing d<$1/(1+1/8)\lambda_0$=$0.89\lambda_0$) in both E- and H-planes [31]. Fig. 9 shows corresponding reflection coefficient of the unit cell and the directivity of 8×8-element array antenna in infinite array environment. It has 20% impedance bandwidth (over 56-68 GHz) with input reflection coefficient better than -15 dB. The directivity is higher than 27.5 dBi and the aperture efficiency is better than 90% from 56 to 66 GHz. Here we have utilized the CST Microwave Studio periodic boundary condition along the lateral and longitudinal directions of 8×8-element in order to

Table 2: Design Parameters of the Structure in Fig. 6

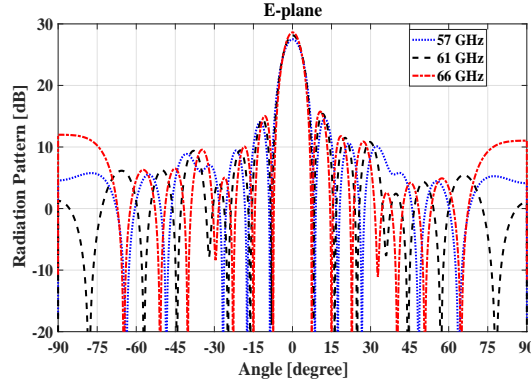|	
Width of the Slot [W_1]	1.13 mm
Width of the Slot [W_2]	0.8 mm
Length of the Slot [L_s]	2.7 mm
Length of the Ridge [L_r]	1.8 mm
Width of the smaller Pin [a_s]	0.3 mm
Height of the Slot [H_s]	0.75 mm
Height of the Circular Cavity [H_c]	1.25 mm

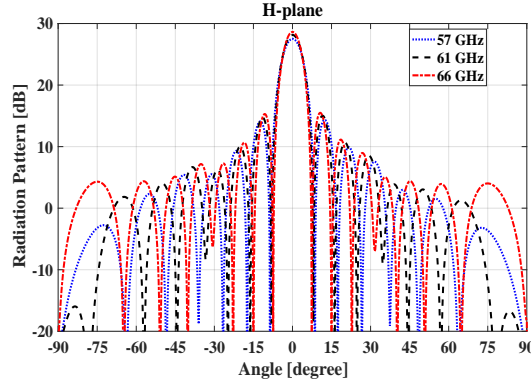Figure 10: E-plane radiation pattern of the 8×8-element array antenna with periodic boundary condition.

Figure 11: H-plane radiation pattern of the 8×8-element array antenna with periodic boundary condition.

estimate the radiation pattern of the whole structure. Fig. 10 and 11 illustrate the radiation patterns in both E- and H-planes of 8×8-element slot array antenna.

4 Corporate-Feed Network Design

The corporate-feed array antenna utilizes a T-junction power divider to feed each unit cell in the whole array antenna. The configuration of the T-junction RGW power divider used in this work is depicted in Fig. 12. In TABLE III, the geometrical parameters of the T-junction RGW power divider are listed. The corresponding simulated reflection coefficient is shown in Fig. 13, which is below -30 dB from 57 to 66 GHz. In order to have an easy massive production of the antenna by using molding technique of plastic material with metalized surface treatment, the smallest
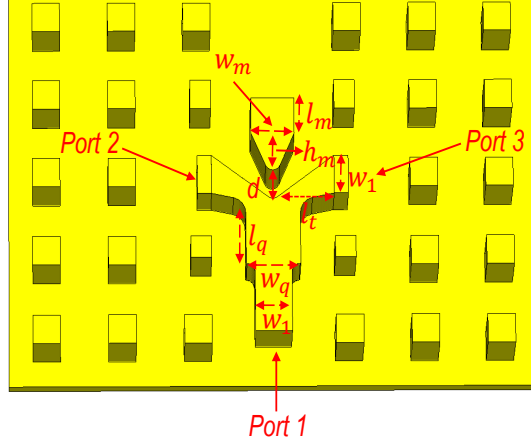
Figure 12: Geometry of the T-junction power divider based on RGW in this work. The upper metallic plate is hidden.

Table 3: Design Parameters of the Structure in Fig. 12

w_1	0.54 mm
w_q	0.8 mm
l_q	0.72 mm
l_t	0.92 mm
d	0.4 mm
w_m	0.72 mm
l_m	0.6 mm
h_m	0.47 mm

dimensions of the extruding parts (pins and ridges) are 0.4 mm.

The whole array antenna in this work is excited through a standard V-band rectangular waveguide (WR-15) at the bottom of whole structure. In this work we prefer a hybrid power divider similar as that described in [17]-[19]. The hybrid structure is illustrated in Fig. 14. The simulated S-parameters of the structure both in amplitude and phase are shown in Fig. 15. The reflection coefficient S_{11} in the whole band 56 – 68 GHz is below -20 dB. In addition, we should point out that the phases of the output ports have 180 degree difference, as shown in Fig. 15 (b). Fig. 16 shows the whole array antenna. The complete corporate-feed network consists of two 16-way RGW power dividers from central hybrid transition power divider to 64 radiating slots. The two 16-way feed networks are mirrored since the phase difference from hybrid transition part is able to be compensated. The thickness of the whole array antenna is 9.7 mm.
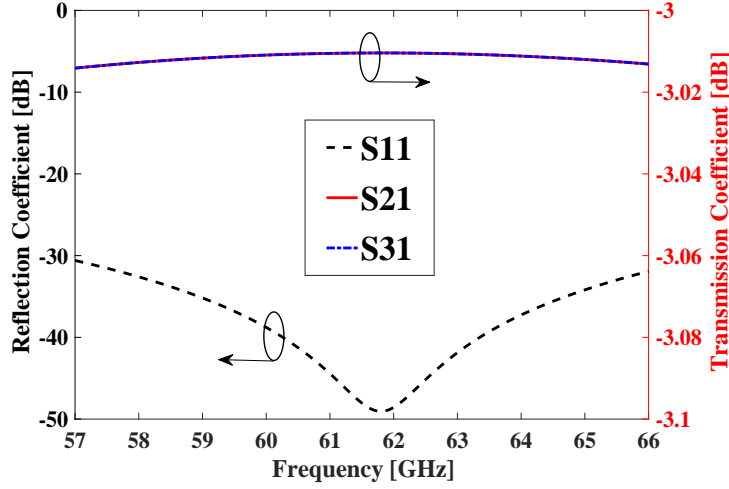
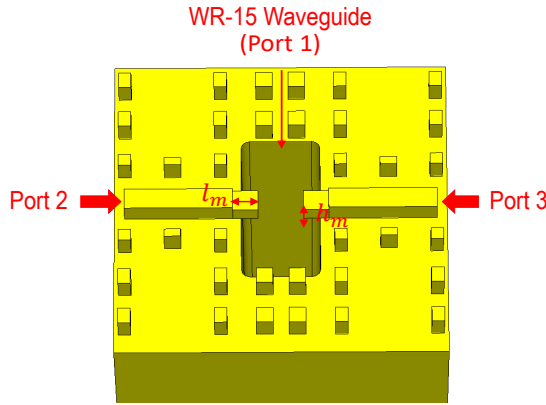Figure 13: Simulated reflection coefficient and transmission coefficient of the power divider in Fig. 12.

Figure 14: Geometrical illustration for hybrid transition from WR-15 to RGW. $l_m = 0.75$ mm and $h_m = 0.45$ mm.

5 Experimental Results

The fabricated 8×8 slot array antenna is illustrated in Fig. 17. The prototype is manufactured by Computerized Numerical Control (CNC) technology with aluminium (with electric conductivity 3.6×10^7 S/m). Planar dimension of the proposed antenna is 36 mm × 36 mm (The dimensions of effective aperture are 33.6 mm × 33.6 mm).

The entire structure is simulated in CST Microwave Studio. Since the hybrid transition, T-junction power divider and unit cell already have excellent reflection coefficients, the simulated reflection coefficient of complete antenna is below -15 dB

(a)   (b)
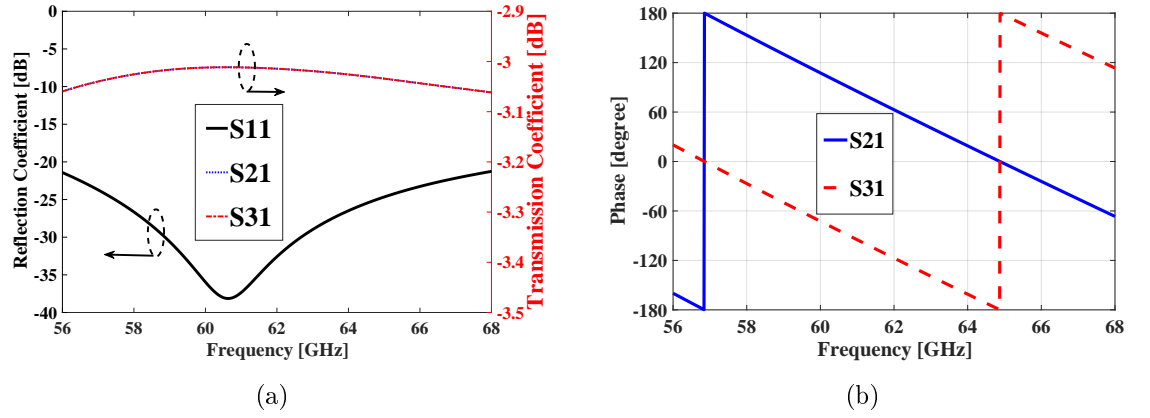
Figure 15: Simulated S-parameter results of designed hybrid transition from WR-15 to RGW. (a) Amplitude. (b) Phase.

Figure 16: Proposed single-layered corporate-feed 8×8 slot array antenna.

Figure 17: Configuration of the 8×8 slot array and photos of the fabricated antenna.

from 57 to 66 GHz without any further optimization, as shown in Fig. 18. However, the measured reflection coefficient is a bit higher than simulated one because the assembly tolerance of the proposed antenna is around 0.015 mm, which is measured

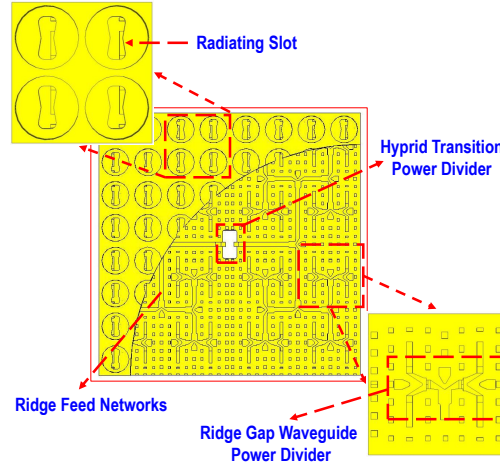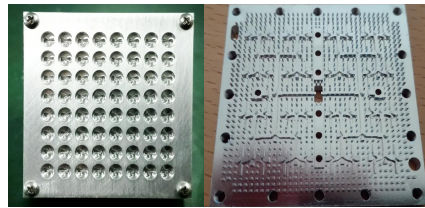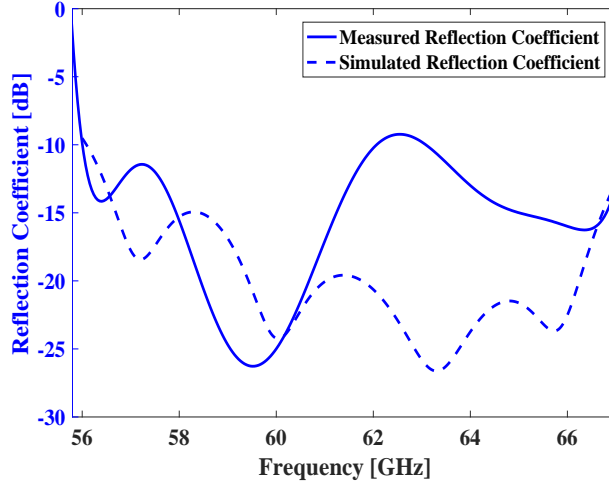Figure 18: The simulated and the measured reflection coefficients of the proposed array antenna.

by a X-ray inspection machine of Nikon, XTH 160 with a measurement tolerance of 20 nm.

The radiation patterns and the gain were measured in an anechoic chamber in China Academy of Space Technology in Shanghai. The simulated and the measured far-field radiation patterns of proposed antenna at 57, 62 and 67 GHz in both E- and H-planes are depicted in Fig. 19. The measured radiation patterns show a good agreement with the simulated results. The simulated and the measured radiation patterns are symmetrical, and the first relative side-lobe levels in both E- and H-planes are around -12 dB. These mean that the distribution network works very well with low mutual couplings among the ridge feed lines. Since the element spacing of proposed antenna is 4.2 mm and wavelength at 67 GHz is equal to 4.477 mm, so the ratio 4.2/4.477= 0.94, which is larger than the non-grating lobes condition of 0.89 at 67 GHz [31], the radiation patterns in E-plane at 67 GHz at $\pm$ 90 degree are higher than the desired.

The measured and the simulated antenna gains are shown in Fig. 20. It can be observed that the realized gain varies from 25.8 to 27 dBi over 57 to 66 GHz, whereas the antenna efficiency is more than 70% (Here the definition of antenna efficiency is defined as $e_{ant}=e_{rad} \cdot e_{pol} \cdot e_{ap}$, where e_{rad}, e_{pol} and e_{ap} are radiation efficiency, polarization efficiency and aperture efficiency, respectively). The simulated relative cross-polarization values are below -37 dB from 56 to 67 GHz, as also seen in Fig. 20.

In table IV fundamental characteristics and performances of different kinds of 60-GHz antenna arrays are listed to compare with our work. For the antennas by using conventional microstrip, the high loss and the radiation leakage are the critical issues when designing large microstrip corporate-feed networks for array antenna in mmWs
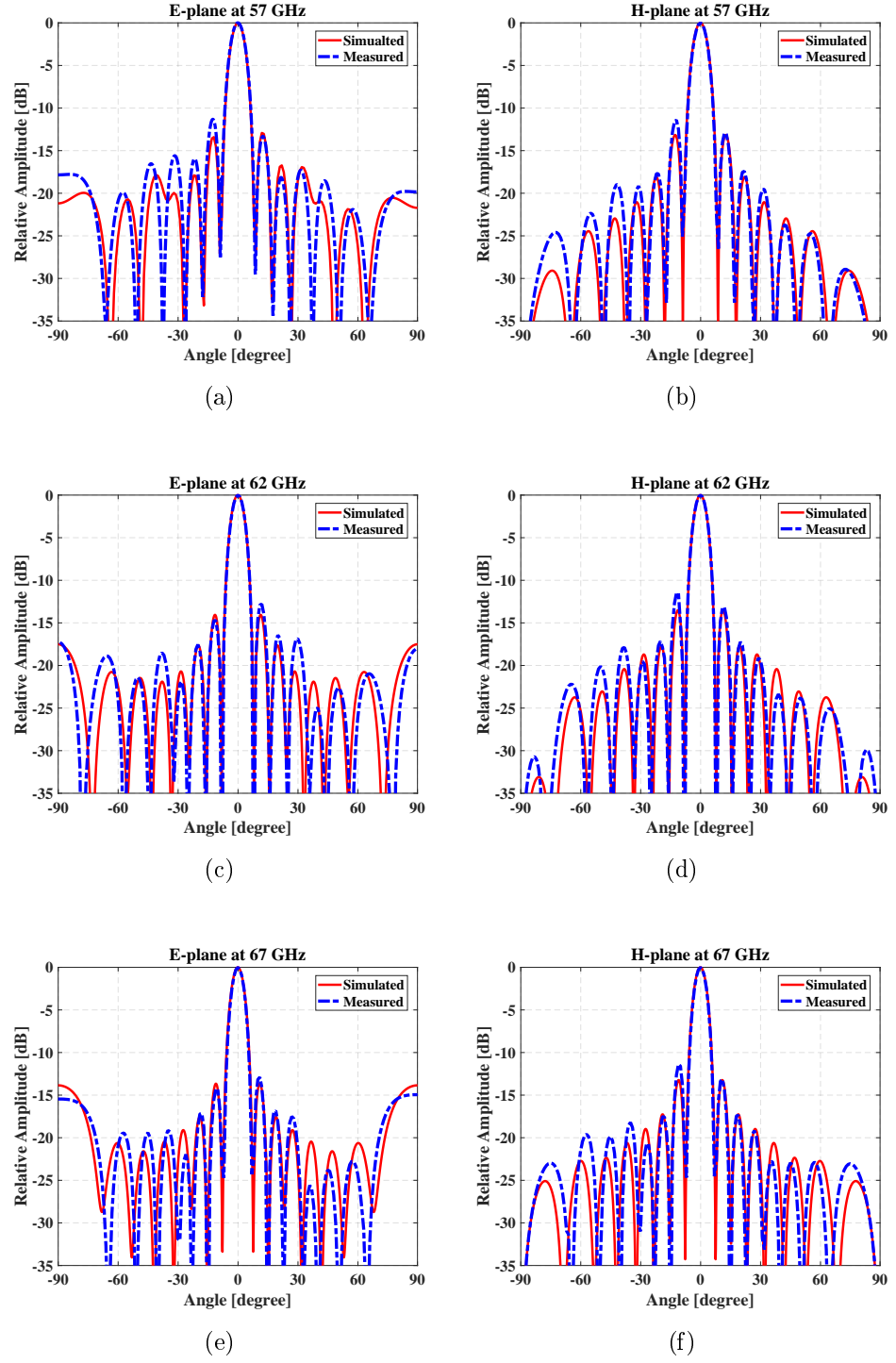
Figure 19: The simulated and the measured radiation patterns of proposed array antenna on both E-plane and H-plane at 57 GHz, 62 GHz and 67 GHz.
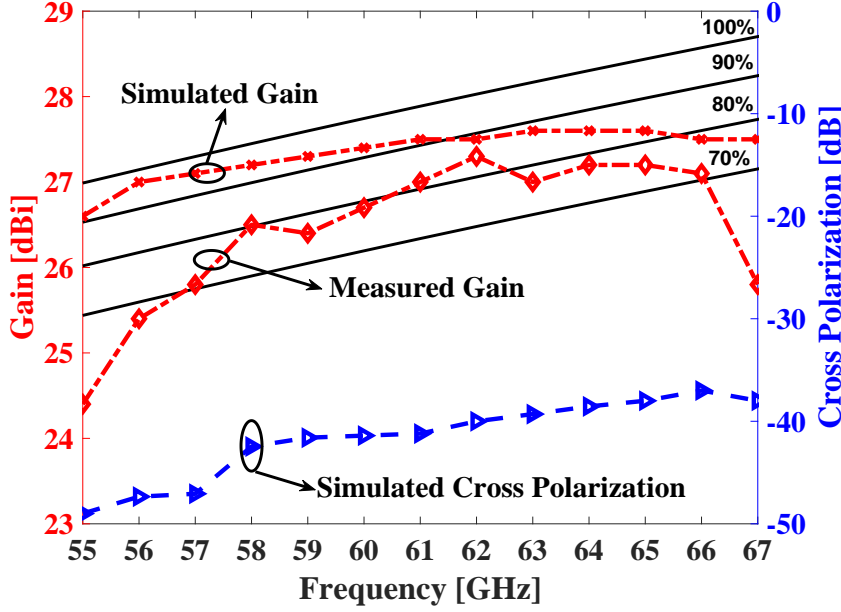
Figure 20: Red lines: simulated and measured gains of the proposed array antenna. Blue line: simulated cross-polarized value.

such as the one in [5] where the antenna efficiency is only 15% - 20%. The SIW technology also has applied the substrate to integrate with active components. Thereby, it still has high dielectric loss in mmWs. Probably utilization of low loss substrate materials is an opportunity to fabricate SIW prototypes, but such solution might increase the cost. Another transmission line including substrate materials is IMGW. However, it cannot totally avoid the dielectric loss and thereby the antenna efficiency of a large array reported in [18] is also limited within 60%. Without utilization the substrate materials, the GGW, the hollow waveguide and the RGW thereby have a huge competitive strength. Nevertheless, the GGW and the RGW still have two advantages among them. Firstly, in [4] and [27] laminated plate technology has been applied for fabrication and their cost is very expensive. Secondly, the bandwidth of the array antennas by hollow waveguide is somehow limited. On the other hand, the GGW and the RGW also sometimes have the disadvantage of expensive fabrication. However, suitable parameters for metallic pins will reduce the fabrication cost. In this work, we have realized a two-layer slot array antenna which still possesses the equal performances of other three-layer antennas in [4] and [20]. Meanwhile it reduces the fabrication cost and thereby will be very helpful for industry.

Conclusion

A single-layered corporate-feed array antenna based on RGW at 60-GHz is presented. This array antenna not only overcomes the disadvantage of narrow bandwidth from conventional single layer array with series-fed network, but also realize the advantage of wideband from three-layer slot array with backed cavity. The simpler geometry will definitely decrease the manufacture cost so that it has huge commercial potential in the future. The array antenna can be directly connected with standard WR-15 interface. An 8×8-element slot array has been designed, simulated, manufactured and measured. The measured gain is higher than 26 dBi from 58 to 66 GHz, correspondingly the antenna efficiency larger than 70%.

Acknowledgment

Table 4: COMPARISON BETWEEN THE PROPOSED AND REPORTED 60-GHz PLANAR ANTENNA ARRAYS

Performance	Ref.[5]	Ref.[6]	Ref.[17]	Ref.[18]	Ref.[20]	Ref.[27]	Present Work
Technology	Microstrip	SIW	RGW	IMGW	GGW	Hollow Waveguide	RGW
Size [cm]	24×24	1.6×1.7	6.4×6.4	6.4×6.4	7.7×7.2	6.8×6.7	3.36×3.36
Number of Elements	4096	16	256	256	256	256	64
Number of Layers	3	4	3	3	3	2	2
Frequency Band [GHz]	58-67	54-68	57-68	54.5-64	55.5-67	59-64	56.5-67
Bandwidth[S11 < -10 dB]	12%	22%	19%	17%	19%	8%	17%
Max Gain [dBi]	39	18	32	30.5	32.5	32.5	27
Antenna Efficiency	15%-20%	35%-45%	60%-70%	40%-60%	75%-85%	70%-75%	70%-85%

References

[1] P. Smulders, "Exploring the 60 GHz band for local wireless multimedia access: Prospects and future directions," *IEEE Commun. Mag.*, vol. 40, no. 1, pp. 40-147, Jan. 2002.

[2] T. S. Rappaport, J. N. Murdck, and F. Gutierrez, "State of the art in 60-GHz integrated circuits and systems for wireless communications," *Proc. IEEE*, vol. 99, no. 8, pp. 1390-1436, Aug. 2011.

[3] J. H. Van Vleck, "The absorption of microswaves by oxygen," *Phys. Rev.*, vol. 71, no. 7, pp. 413-424, 1947.

[4] Y. Miura, J. Hirokawa, M. Ando, Y. Shibuya and G. Yoshida, "Double layer full-corporate-feed hollow-waveguide slot array antenna in the 60 GHz band," *IEEE Trans. Antennas Propag.*, vol. 59, no. 8, pp. 2844-2851, Aug. 2011.

[5] J. Wu, Y. J. Cheng, and Y. Fan, "A wideband high-gain high-efficiency hybrid integrated plate array antenna for V-Band inter-satellite links," *IEEE Trans. Antennas Propag.*, vol. 63, no. 4, pp. 1225-1233, Apr. 2015.

[6] Y. Li and K.-M. Luk, "Low-cost high-gain and broadband substrate integrated-waveguide-fed patch antenna array for 60-GHz band," *IEEE Trans. Antennas Propag.*, vol. 62, no. 11, pp. 5531-5538, Nov. 2014.

[7] Y. Li and K.-M. Luk, "60-GHz substrate integrated waveguide fed cavity-backed aperture-coupled microstrip patch antenna arrays," *IEEE Trans. Antennas Propag.*, vol. 63, no. 3, pp. 1075-1085, Mar. 2015.

[8] P.-S. Kildal, "Three metamaterial-based gap waveguides between parallel metal plates for mm/submm waves," *in 3rd European Conference on Antennas and Propagation, EuCAP 2009*, pp. 28-32, Mar. 2009.

[9] A. U. Zaman and P.-S. Kildal, "Gap waveguides," in Handbook of Antenna Technologies, Z. N. Chen, D. Liu, H. Nakano, X. Qing, and T. Zwick, Eds. Singapore: Springer, pp. 3273-3347, 2016.

[10] P.-S. Kildal, "Artificially soft and hard surfaces in electromagnetics," *IEEE Trans. Antennas Propag.*, vol. 28, no. 10, pp. 1537-1544, Oct. 1990.

[11] A. U. Zaman, M. Alexanderson, T. Vukusic and P.-S. Kildal, "Gap waveguide PMC packaging for improved isolation of circuit components in high-frequency microwave modules," *IEEE Trans. Compon. Packag. Manuf. Technol.*, vol. 4, no. 1, pp. 16-25, Jan. 2014.

[12] E. Rajo-Iglesias, P. S. Kildal, A. U. Zaman, and A. Kishk, "Bed of springs for packaging of microstrip circuits in the microwave frequency range," *IEEE Trans. Compon. Packag. Manuf. Technol.*, vol. 2, no. 7, pp. 1623-1628, Jul. 2012.

[13] A. U. Zaman, P.-S. Kildal and A. A. Kishk, "Narrow-Band microwave filter using high-Q groove gap waveguide resonators with manufacturing flexibility and no sidewalls," *IEEE Trans. Compon. Packag. Manuf. Technol.*, vol. 2, no. 11, pp. 1882-1889, Nov. 2012.

[14] A. Vosoogh, A. A. Brazalez and P.-S. Kildal, "A V-Band inverted microstrip gap waveguide end-coupled bandpass filter, " *IEEE Antennas Wireless Propag. Lett.*, vol. 26, no. 4, pp. 261-263, Apr. 2016.

[15] H. Raza, J. Yang, P.-S. Kildal, and E. A. Alos, "Microstrip-ridge gap waveguide-Study of losses, bends, and transition to WR-15," *IEEE Trans. Microw. Theory Techn.*, vol. 62, no. 9, pp. 1943-1952, Sept. 2014.

[16] A. Vosoogh, and P.-S. Kildal, "Corporate-Fed planar 60 GHz slot array made of three unconnected metal layers using AMC pin surface for the gap waveguide," *IEEE Antennas Wireless Propag. Lett.*, pp. 1935-1938, Dec. 2015.

[17] A. Vosoogh, P.-S. Kildal and V. Vassilev, "Wideband and high-gain corporate-fed gap waveguide slot array antenna with ETSI class II radiation pattern in V-Band," *IEEE Trans. Antennas Propag.*, vol. 65, no. 4, pp. 1823-1831, Apr. 2017.

[18] J. Liu, A. Vosoogh, A. U. Zaman and J. Yang, "Design and fabrication of a high gain 60-GHz cavity-backed slot antenna array fed by inverted microstrip gap waveguide," *IEEE Trans. Antennas Propag.*, vol. 65, no. 4, pp. 2117-2122, Apr. 2017.

[19] J. Liu, A. Vosoogh, A. U. Zaman and P.-S. Kildal, "Design of 8×8 slot array antenna based on inverted microstrip gap waveguide," *Antennas and Propagation (ISAP), 2016 International Symposium on*, pp. 760-761, Oct. 2016.

[20] A. Farahbakhsh, D. Zarifi and A. U. Zaman, "60-GHz groove gap waveguide based wideband H-plane power dividers and transitions: for use in high-gain slot

array antenna," *IEEE Trans. Microw. Theory Techn.*, vol. 65, no. 11, pp. 4111-4121, Nov. 2017.

[21] K. Tekkouk, J. Hirokawa, R. Sauleau and M. Ando, "Wideband and large coverage continuous beam steering antenna in the 60-GHz band," *IEEE Trans. Antennas Propag.*, vol. 65, no. 9, pp. 4418-4426, Sept. 2017.

[22] B. Cao, H. Wang, Y. Huang and J. Zheng, "High-gain L-probe excited substrate integrated cavity antenna array with LTCC-based gap waveguide feeding network for W-Band application," *IEEE Trans. Antennas Propag.*, vol. 63, no. 12, pp. 5465-5474, Dec. 2015.

[23] M. S. Sorkherizi, A. Dadgarpour and A. A. Kishk, "Planar high-efficiency antenna array using new printed ridge gap waveguide technology," *IEEE Trans. Antennas Propag.*, vol. 65, no. 7, pp. 3772-3776, Jul. 2017.

[24] S. Park, Y. Tsunemitsu, J. Hirokawa and M. Ando, "Center feed single layer slotted waveguide array," *IEEE Trans. Antennas Propag.*, vol. 54, no. 5, pp. 1474-1480, May. 2006.

[25] M. Ando, J. Hirokawa, T. Yamamoto, A. Akiyama, Y. Kimura and N. Goto, "Novel single-layer waveguides for high-efficiency millimeter-wave arrays," *IEEE Trans. Microw. Theory Techn.*, vol. 46, no. 6, pp. 792-799, Jun. 1998.

[26] Y. Tsunemitsu, S. Matsumoto, Y. Kazama, J. Hirokawa, and M. Ando, "Reduction of aperture blockage in the center-feed alternating-phase fed single-layer slotted waveguide array antenna by E- to H-plane cross-junction power dividers," *IEEE Trans. Antennas Propag.*, vol. 56, no. 6, pp. 1787-1790, Jun. 2008.

[27] M. Sano, J. Hirokawa, and M. Ando, "Single-layer corporate-feed slot array in the 60-GHz band using hollow rectangular coaxial lines," *IEEE Trans. Antennas Propag.*, vol. 62, no. 10, pp. 5068-5076, Oct. 2014.

[28] A. U. Zaman and P.-S. Kildal, "Wide-band slot antenna arrays with single-layer corporate-feed network in ridge gap waveguide technology," *IEEE Trans. Antennas Propag.*, vol. 62, no. 6, pp. 2992-3001, Jun. 2014.

[29] E. Rajo-Iglesias and P.-S. Kildal, "Numerical studies of bandwidth of parallel-plate cut-off realized by a bed of nails, corrugations and mushroom-type electromagnetic bandgap for use in gap waveguides," *IET Microw.Antennas Propag.*, vol. 5, no. 3, pp. 282-289, Feb. 2011.

[30] S. Hopfer, "The design of ridged waveguides," *IRE Transaction on Microwave Theory and Techniques*, vol. 3, no. 5, pp. 20-29, Oct. 1955.

Paper 6

Design and Fabrication of a 32×32-element Slot Array Antenna based on Ridge Gap Waveguide in D-Band

Jinlin Liu, Ashraf Uz Zaman, and Jian Yang

The layout of this paper has been revised in order to comply with the rest of the thesis.

Design and Fabrication of a 32×32-element Slot Array Antenna based on Ridge Gap Waveguide in D-Band

Jinlin Liu, Ashraf Uz Zaman, and Jian Yang

Abstract

This paper presents a new design of slot array antenna based on ridge gap waveguide at 140 GHz. The proposed array antenna consists of 32×32 radiation slots, backed cavities and full-corporate distribution network based on ridge gap waveguide. In order to fabricate the proposed array antenna by Computerized Numerical Control (CNC) technology, the periodic pin structure has been chosen with an aspect ratio of 1.5:1. Since the layout space for distribution networks is very limited, a novel stepped T-junction power divider is introduced in this work. The achieved reflection coefficient is much lower than that of the previous continuous T-junction power dividers which enables easy cascading of several T-junctions for building up a very large feed network. The measured results demonstrate about 11.4% of reflection coefficient bandwidth ($|S11| <$ -10 dB) covering the 135—151 GHz frequency range, and the measured gain is larger than 37 dBi over the band with more than 50% antenna efficiency.

Slot Array Antenna, High-Gain, Ridge Gap Waveguide, Stepped T-junction Power Divider, 140 GHz.

1 Introduction

Recently, D-band (110-170 GHz) has gained lots of attention for wireless applications, such as radar and wireless communication systems [1]-[2]. As seen in Fig. 1, the frequency band 135-155 GHz has the lowest air attenuation over the whole D-band. It is very advantageous to utilize this frequency band for high data rate wireless links. Due to several limitations in commercially available D-band electronics such as output power, Local oscillator leakage and packaging losses, the high-gain and high-efficiency antenna plays a very important role for the point-to-point wireless links. Usually, a parabolic reflector antenna is a classic choice for such a radio links system. Take one example in [2], a reflector antenna has been utilized at 122 GHz. Nevertheless, its antenna diameter is about 450 mm, and such a bulky dimension makes it not convenient for integration with front-end planar circuits. In [3], a 32 by 32 and a 16 by
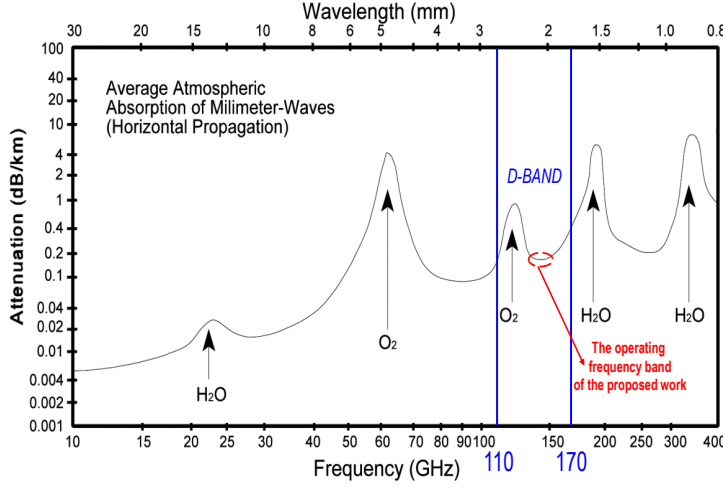
Figure 1: Average atmospheric absorption of millimeter-waves at sea level.

16 hollow waveguide antenna arrays fabricated by diffusion bonding technology have been introduced at 125 GHz, respectively. Those two slot arrays demonstrate the characteristics of high-gain, high-efficiency and low profile. However, the diffusion bonding technology needs around 1000 degree with precise thermal control and high mechanical pressure which makes this technology rather expensive. In past few years, substrate integrated waveguide (SIW) [4] and its applications for array antennas have been explored [5]-[10]. However, the substrate is a fundamental component and its dielectric loss is becoming problematically significant versus the frequency. In [11]-[12], two array antennas based on SIW backed cavities and low temperature co-fired ceramic (LTCC) distribution networks have been reported. However, unbearable dielectric losses at 140 GHz affects the antenna efficiency and the manufacture cost of LTCC is not cheap in such a high frequency band.

Recently introduced gap waveguide technology [13] has low losses [14] and low cost for manufacture in millimeter-waves if the metallic pins dimensions are correctly selected. In [14]-[22], several different slot array antennas based on groove gap waveguide (GGW), ridge gap waveguide (RGW) and inverted microstrip gap waveguide have been reported. A novel W-band low-profile monopulse slot array antenna on RGW has been reported in [23]. A novel leaky wave antenna on GGW has been recently presented in [24]. The other applications, such as detector, multi-beam and phased array, have been reported in [25]-[28].

In this work, we present a slot array antenna based on RGW at 140 GHz. The major challenges are stated as follows. As described in [13], the pin dimensions significantly decrease up to that level which becomes very challenging to fabricate by using conventional CNC milling or molding technique. The pins size had been chosen as $0.4 \times 0.4 \ mm^2$ with an aspect ratio of 3.25:1 in the every slot array antenna from [14]-

162

[22] which by scaling becomes 0.15×0.15 mm^2 at 140 GHz. In this work, relatively larger pins are selected for 140 GHz array antenna so that the fabrication technology such as the CNC milling can be used for fabricating the antenna. Secondly, the conductor loss at 140 GHz becomes much greater then that of lower frequency band because of the skin effect and surface roughness. Thereby, the insertion losses of the sub-array, T-junction power divider and the other transition parts should be minimized so that the antenna efficiency is guaranteed. This high-gain antenna could be an alternative to reflector, lens or slot array by diffusion bonding technology in wireless link systems.

2   Antenna Design

2.1   Design for Sub-Array

According to the fundamental theory in [13], an arbitrary gap waveguide is able to provide a stopband over a specific frequency range between the two plates of Perfect
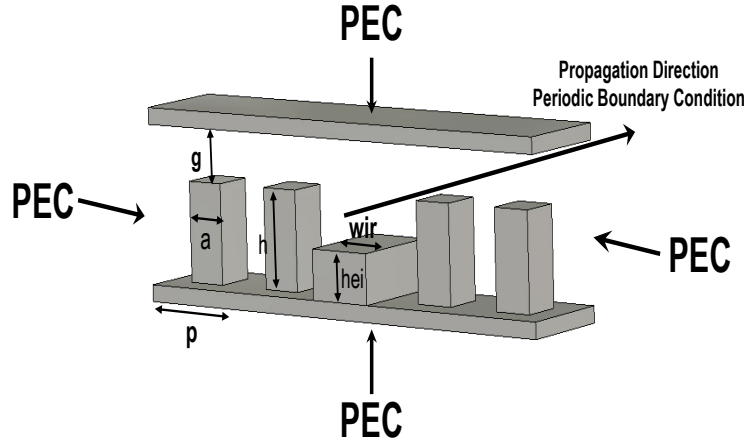

Figure 2: Infinite periodic unit cell based on RGW structure.

Table 1: Design Parameters of the Structure in Fig. 2

wir	0.45 mm
hei	0.3 mm
p	0.72 mm
h	0.58 mm
a	0.38 mm
g	0.05 mm

Electric Conductor(PEC) and Perfect Magnetic Conductor (PMC). Since our design target is from 135-150 GHz, the dimensions of metallic pins are theoretically smaller than 0.15 mm according to the previous experience [14]-[22]. In [29], a new approach of designing metallic pins has been introduced where low aspect ratio pins can create a wider frequency band. The width of the metallic pins are appropriately selected in this work so that the proposed array antenna is able to be fabricated by CNC milling technology. A center frequency of $f_0 = 140$ GHz is assumed in this work. Then the height of the pins is determined as $\lambda_0/4$, which is equal to 2.2 mm. Thereby, the height of metallic pins is selected as $h = 0.58$ mm in this work. Furthermore, for achieving good radiation patterns the spacing between any two slots is selected as 1.8 mm, which is equal to $0.81\lambda_0$. Having considered the layout of the distribution network, five rows of metallic pins are required for the dimension of 3.6 mm and the corresponding periodicity of metallic pins is 0.72 mm. The dispersion diagram of the ridge gap waveguide is depicted in Fig. 3. The obtained stopband is from 100 to 180 GHz, which covers our design target 135-150 GHz. The corresponding geometrical parameters of the proposed RGW are listed in TABLE I.

As illustrated in Fig. 4, the configuration of a 2×2-element sub-array is first designed using periodic boundary condition in CST Microwave Studio. The top of the entire sub-array is the radiation layer, which contains radiation slots with rectangular flare. The function of the flared slot is to suppress mutual coupling between slots and improve the bandwidth of the sub-array. Just below the slot layer, a gap waveguide cavity layer is placed. The electromagnetic coupling to the cavity through a hole aperture, which is excited via a ridge gap waveguide feeding line. The distribution
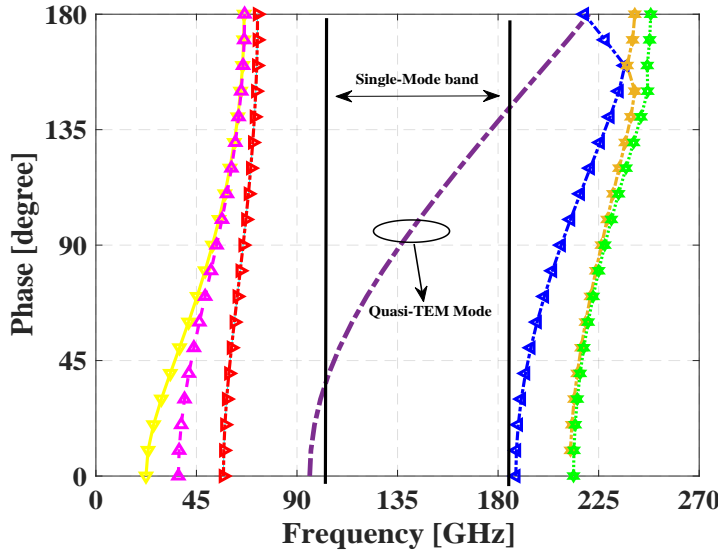

Figure 3: Dispersion diagram for the infinite periodic unit cell including a ridge in RGW.
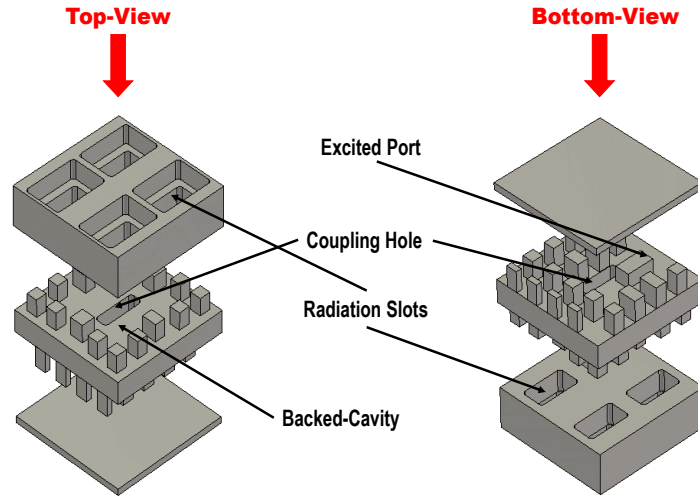
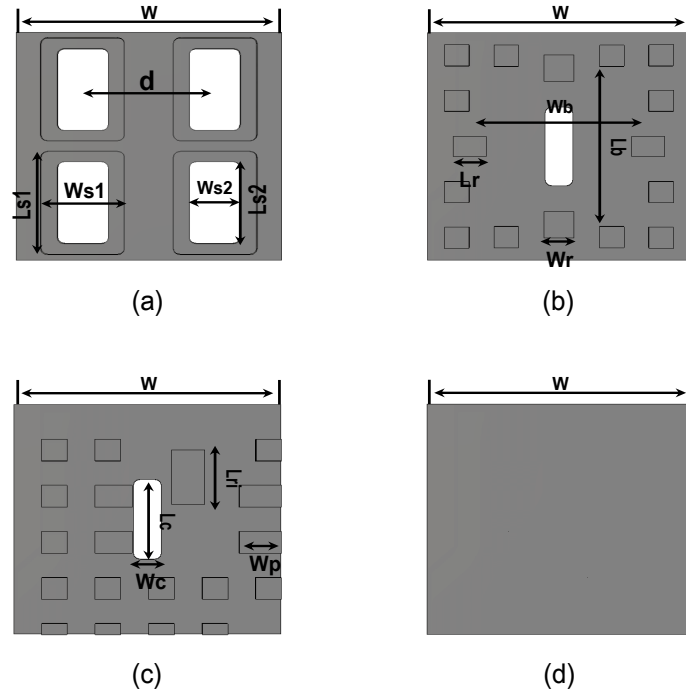Figure 4: Distributed view of the proposed 2×2 cavity-backed slot sub-array.

Figure 5: Geometrical parameters of a 2×2 slots array. (a) Top radiation slots layer. (b) Backed cavity layer. (c) Distribution network layer. (d) Bottom metallic layer.

Table 2: Design Parameters of the Structure in Fig. 5

W	3.6 mm
d	1.8 mm
$Ls1$	1.75 mm
$Ws1$	1.15 mm
$Ls2$	1.4 mm
$Ws2$	0.72 mm
Wb	2.59 mm
Lb	2.68 mm
Wr	0.45 mm
Lr	0.46 mm
Wc	0.4 mm
Lc	1.32 mm
Wp	0.55 mm
Lri	0.81 mm
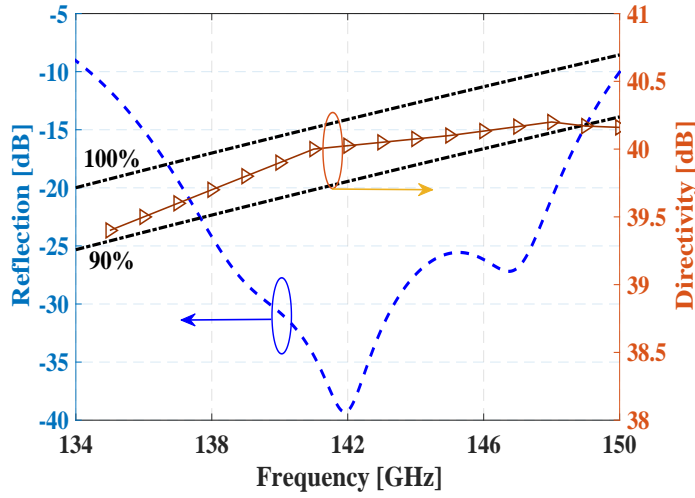
Figure 6: Simulated directivity and reflection coefficient of the 2×2 sub-array.

network is placed on the back side of the cavity layer. The major reason for this design is to reduce the misalignment error between the separate cavity layer and the feed layer which becomes very tricky at D-band and which effects the operating bandwidth of the sub-array used previously in [14]-[22]. Thereby, the bottom waveguide layer is a smooth metallic plate. Because all three layers are separated by a small gap, there is no electrical contact between the different layers. The designed sub-array is 3.6

mm by 3.6 mm in both E- and H-planes. Fig. 5 illustrates the detailed geometrical parameters of the 2 by 2 sub-array, and the corresponding values are listed in TABLE II. The geometry is optimized by setting periodic boundary conditions in the CST Microwave Studio. In Fig. 6, the blue line shows the reflection coefficient, and an 11.5% impedance bandwidth (over 134-150 GHz) with the input reflection coefficient below -10 dB is achieved. The yellow line with triangle marks depicts the simulated directivity of the 32 by 32 slot array in infinite array environment. The simulated antenna efficiency is higher than 90% from 135 to 148 GHz.

2.2   Design for Distribution Networks

T-junction power divider on RGW in the V-band have been explored very well, as stated in [15]-[16]. Because the periodic length p is selected as 1.1 mm and a as 0.4 mm in the previous design of V-band, there are enough space for the layout of the bend ridges. In this work, the periodic length is so small that the T-junction power divider with continuous bend ridge is impossible to fit in. For this reason, we have developed a stepped T-junction power divider, as depicted in Fig. 7. In Table III, the geometrical parameters of the T-junction RGW power divider are listed. The corresponding simulated reflection coefficient is shown in Fig. 8, which is below -40 dB from 134 to 152 GHz. This performance is much better than the previous designs in [15]-[16]. Furthermore, it is easy to be fabricated so that it can be found more applications in the other frequency bands.   The whole array antenna in this paper is excited through a standard D-band rectangular waveguide (WR-6) at the bottom of the whole structure. Then, a hybrid power divider similar to those described in [15]-[17] is designed, and its geometry is illustrated in Fig. 9. The simulated S-parameters of the structure both in amplitude and phase are shown in Fig. 10. The reflection
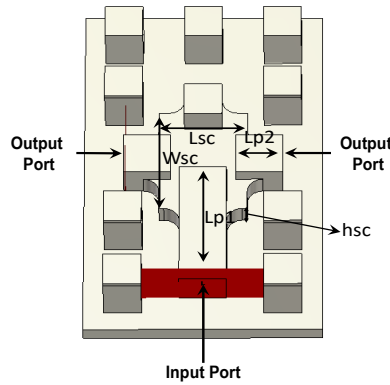

Figure 7: Geometry of the discontinuous T-junction power divider based on RGW in this work. The upper metallic plate is hidden.
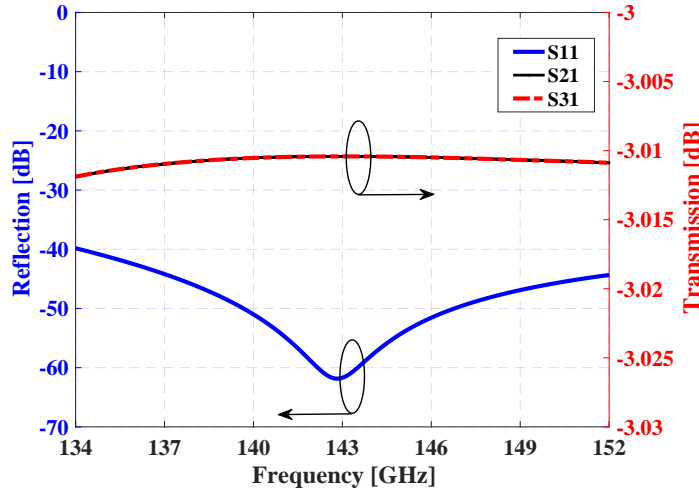
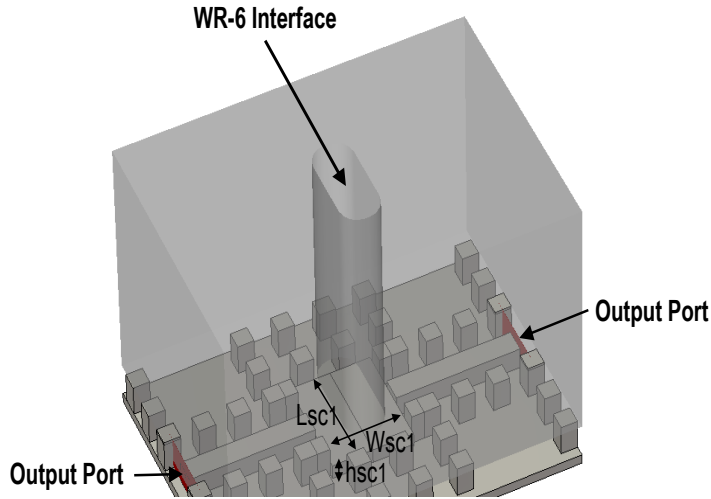Figure 8: Simulated reflection coefficient and transmission coefficient of the power divider in Fig. 7.

Figure 9: Geometrical illustration for hybrid transition from WR-6 to RGW.

coefficient is below -27 dB in the whole band 134-150 GHz. The corresponding design parameters are listed in TABLE III. In addition, such a hybrid structure is essentially a differential feeding geometry so that the phases of the output ports have 180 degree difference, as shown in Fig. 10(b). In order to compensate the difference of the output phases, the two distribution networks are in a mirror geometry. The final numerical designed antenna is shown in Fig. 11. The thickness of the whole array antenna is 7.7 mm.

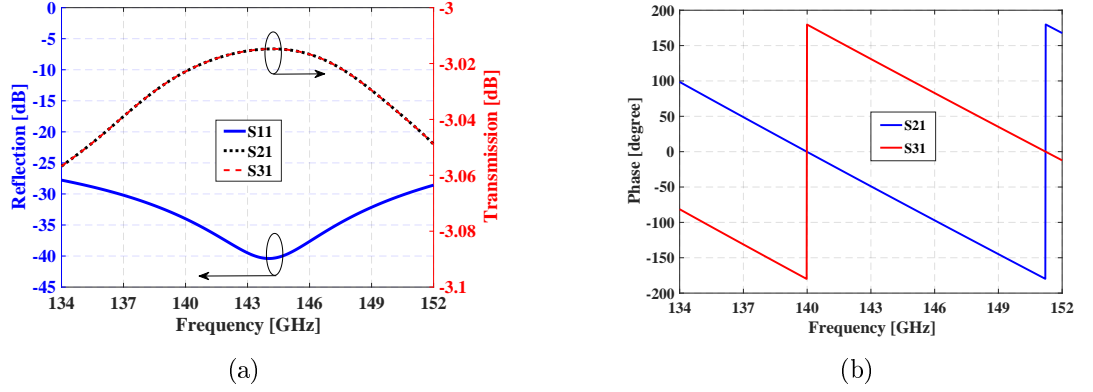(a)   (b)

Figure 10: Simulated S-parameter results of designed hybrid transition from WR-6 to RGW. (a) Amplitude. (b) Phase.

Table 3: DESIGN PARAMETERS OF THE STRUCTURES IN FIGS. 7 AND 9

$Lp1$	1.35 mm
hsc	0.27 mm
Wsc	1.16 mm
Lsc	0.84 mm
$Lp2$	0.45 mm
$Lsc1$	2.05 mm
$Wsc1$	1.77 mm
$hsc1$	0.30 mm

3   Experimental Results

The fabricated prototype of the 32×32 slot array antenna has been done by DMG MORI CNC Milling machine with aluminum (with electric conductivity $3.6{\times}10^7$ S/m), which is illustrated in Fig. 12. The manufacture tolerance of the machine is 1 μm, which is accurate enough for the designed antenna. The planar dimension of the proposed antenna is 65 mm × 65 mm (the dimensions of effective aperture are 57.6 mm × 57.6 mm). The entire structure is simulated in CST Microwave Studio, and the simulated reflection coefficient of the completed antenna is below -10 dB from 135 to 150 GHz without any further optimization, as shown in Fig. 13. Nevertheless, the measured one is a bit higher than the simulated one. This phenomenon occurred in the previous works [15]-[18]. The misalignment of three antenna layers from assembling is always a problem for such a high frequency band. In addition, the extra ohmic losses caused by ridge surface roughness from CNC milling fabrication should be also considered for the difference of reflections. The radiation patterns and the gain were measured by a near-field measurement setup in
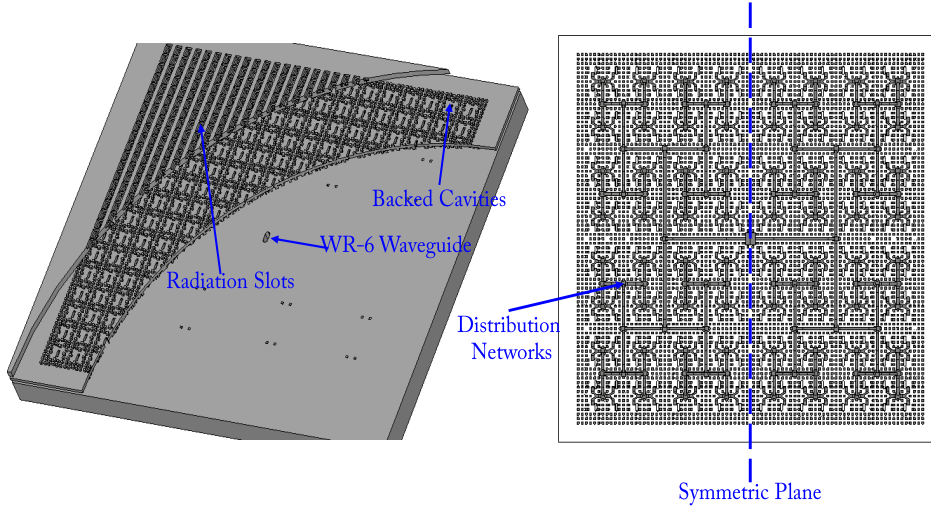
Figure 11: The proposed 32×32 slot array antenna and its full corporate-feed distribution networks.
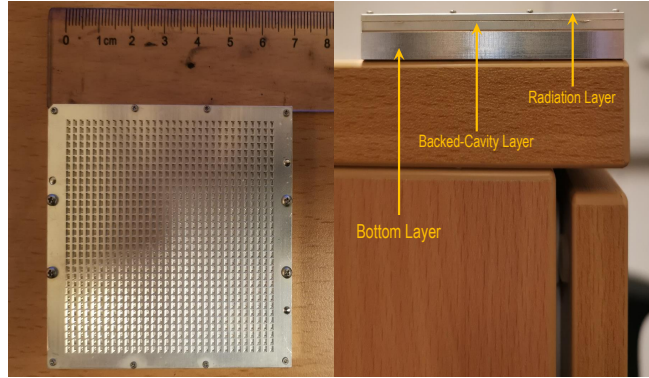

Figure 12: Photograph of the final fabricated 32×32 slot array antenna.

an anechoic chamber at Southeast University in Nanjing, China, as shown in Fig. 14. The simulated and the measured radiation patterns of the fabricated antenna at 135, 140, 145 and 150 GHz in both E- and H-planes are depicted in Fig. 15 and Fig. 16. The measured radiation patterns have reasonable agreements with the simulated ones while the measured side lobes are a little bit higher than simulated ones. Nevertheless, the measured radiation patterns are symmetrical, and their first side lobes both in E- and H-planes are lower than -13 dB. The measured gain is higher than 37 dBi with the measured antenna efficiency higher than 50% from 136 to 150 GHz, as depicted in Fig. 17. There are big differences between the measured and the simulated gains in the whole frequency band. In Table IV, fundamental characteristics and performances
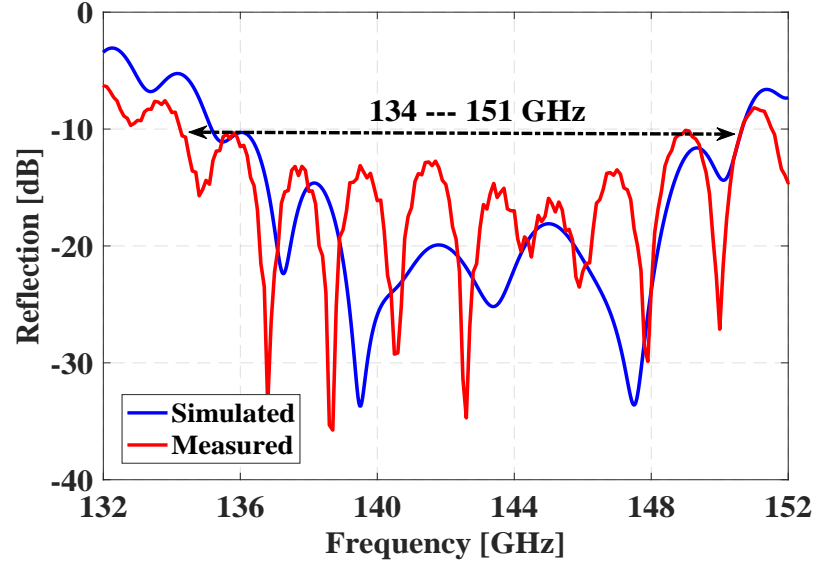
Figure 13: Simulated and the measured reflection coefficients of the proposed array antenna.
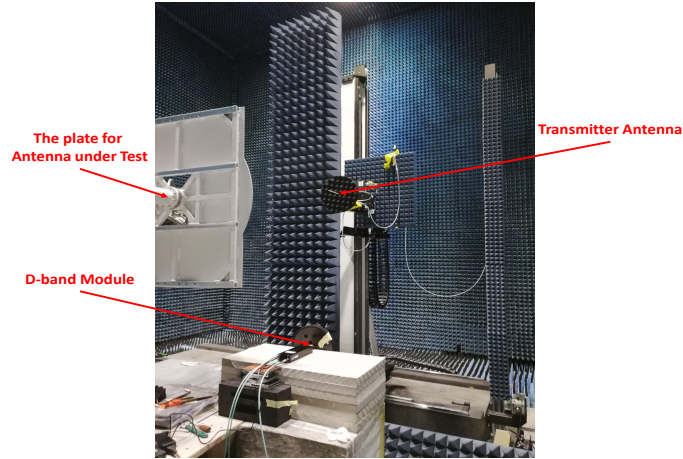

Figure 14: Photograph of the measurement setup for the gain and the radiation pattern test.

of different kinds of D-band antenna arrays are listed for comparison with our work. The technologies for array antenna focus on hollow waveguide by diffusion bonding, LTCC and SIW in the past years. The performance of array antenna in [3] is high-gain, high-efficiency and low profile. However, its fabrications cost is much higher than traditional CNC milling technology. LTCC and SIW technology is popular in recent years. Nevertheless, the loss tangent value of the substrate linearly increases versus the frequency [14]. Thereby, the dielectric loss of SIW structure in the D-

Figure 15: The simulated and the measured radiation patterns of proposed array antenna on E-plane at (a) 135 GHz, (b) 140 GHz, (c) 145 GHz and (d) 150 GHz.

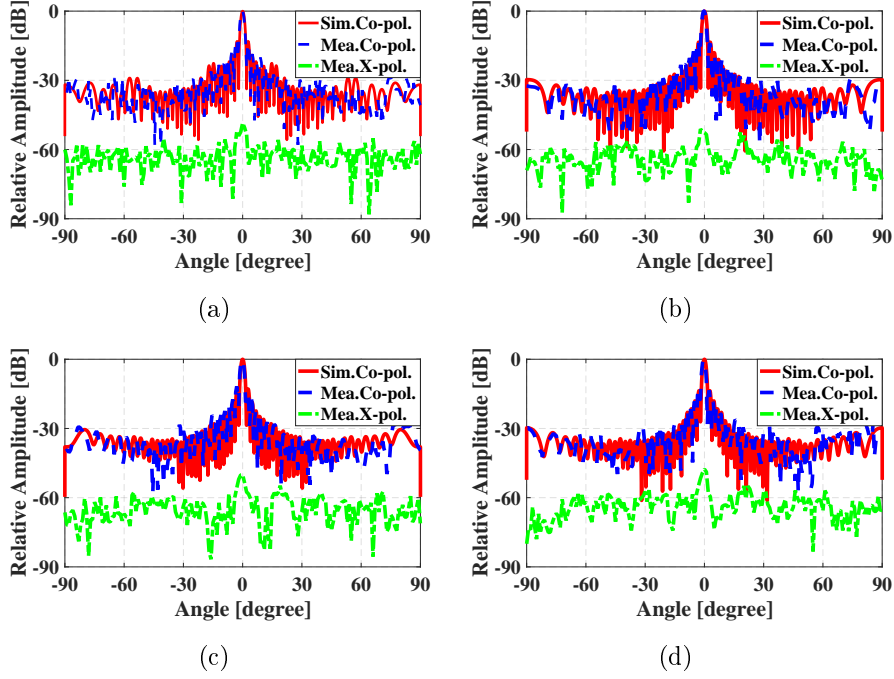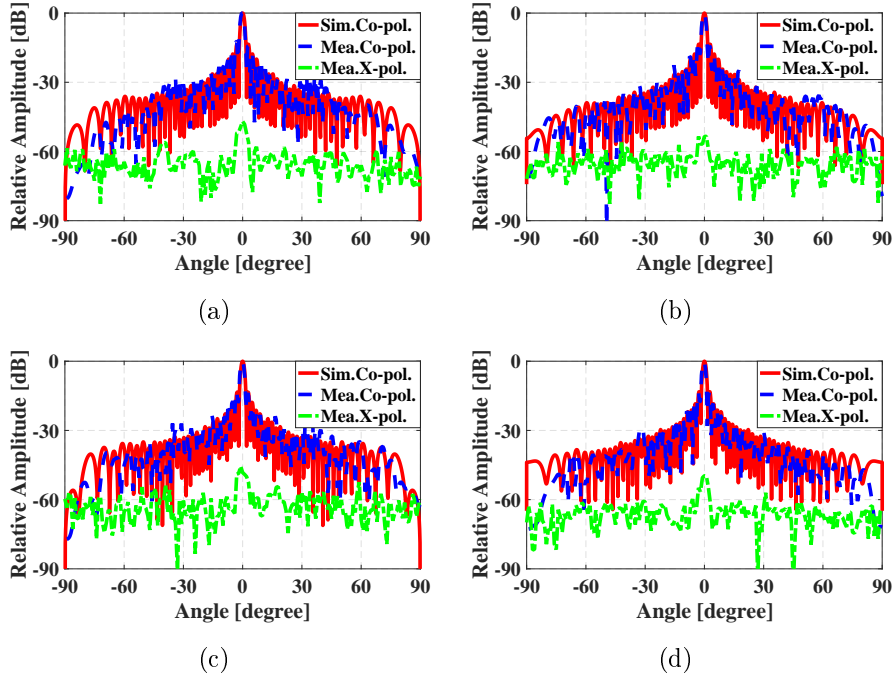

Figure 16: The simulated and the measured radiation patterns of proposed array antenna on H-plane at (a) 135 GHz, (b) 140 GHz, (c) 145 GHz and (d) 150 GHz.
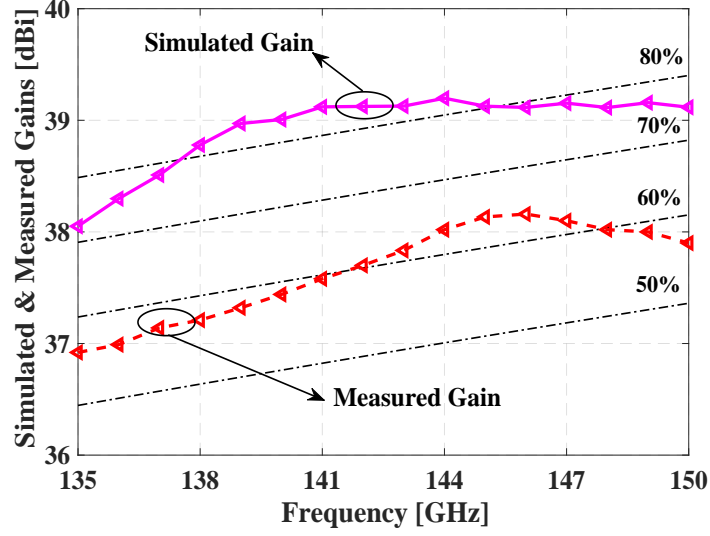
Figure 17: Simulated and measured gains of the proposed array antenna.

band is a critical and unavoidable issue. Secondly, the manufacture of the small via holes is also a big challenge for SIW technology. In addition, the manufacture cost of the distribution networks by LTCC in the D-band is also much higher than that of CNC milling technology. In this paper, we have realized a slot array antenna based on RGW with low cost, high-gain, high-efficiency and low profile. This type of slot array antenna is very practical for D-band high speed wireless links.

4 Conclusion

A 32×32 corporate-feed array antenna based on RGW in D-band is presented in this work. The simpler geometry will definitely decrease the manufacturing cost so that it has huge commercial potential in the future. The array antenna can be directly connected with standard WR-6 interface. The measured gain is higher than 37 dBi from 135 to 150 GHz, correspondingly the antenna efficiency larger than 50%.

Table 4: COMPARISON BETWEEN THE PROPOSED AND REPORTED D-band PLANAR ANTENNA ARRAYS

Performance	Ref.[3]	Ref.[11]	Ref.[12]	Present Work
Technology	Hollow Waveguide	LTCC and SIW	LTCC and SIW	RGW
Size [cm]	6.72 × 6.72	15 × 11	9.6 × 8.6	5.76 × 5.76
Number of Elements	1024	64	64	1024
Frequency Band [GHz]	120-134	127-148	131-145	135-151
Bandwidth[$|S11| < $-10 dB]	11.8%	15%	11.3%	11.2%
Max Gain [dBi]	39	21	20	38.2
Antenna Efficiency	50%-70%	15%-25%	25%-35%	55%-63%

References

[1] T. Jaeschke, C. Bredendiek, S. Kueppers and N. Pohl, "High-precision D-band FMCW-radar sensor based on a wideband SiGe-transceiver MMIC," *IEEE Trans. Microw. Theory Tech.*, vol. 62, no. 12, pp. 3582-3597, Dec. 2014.

[2] A. Hirata et al., "120-GHz-band wireless link technologies for outdoor 10-Gbit/s data transmission," *IEEE Trans. Microw. Theory Techn.*, vol. 60, no. 3, pp. 881-895, Mar. 2012.

[3] D. Kim, J. Hirokawa, M. Ando, J. Takeuchi, and A. Hirata, "64×64-element and 32×32-element slot array antennas using double-layer hollow-waveguide corporate-feed in the 120 GHz band," *IEEE Trans. Antennas Propag.*, vol. 62, no. 3, pp. 1507-1512, Mar. 2014.

[4] D. Deslandes and K. Wu, "Integrated microstrip and rectangular waveguide in planar form," *IEEE Microw. Wireless Compon. Lett.*, vol. 11, no. 2, pp. 68-70, Feb. 2001.

[5] L. Wang, J. L. Gomez-Tornero, and O. Quevedo-Teruel, "Substrate integrated waveguide leaky-wave antenna with wide bandwidth via prism coupling," *IEEE Trans. Microw. Theory Techn.*, vol. 66, no. 6, pp. 3110-3118, Jun. 2018.

[6] T. Li and Z. N. Chen, "Control of beam direction for substrate-integrated waveguide slot array antenna using metasurface," *IEEE Trans. Antennas Propag.*, vol. 66, no. 6, pp. 2862-2869, Jun. 2018.

[7] T. Li and Z. N. Chen, "A dual-band metasurface antenna using characteristic mode analysis," *IEEE Trans. Antennas Propag.*, vol. 66, no. 10, pp. 5620-5624, Oct. 2018.

[8] H. J.-Zarmehri and M. H. Neshati, "Design and development of high-gain SIW H-plane horn antenna loaded with waveguide, dipole array, and reflector nails using thin substrate," *IEEE Trans. Antennas Propag.*, vol. 67, no. 4, pp. 2813-2818, Apr. 2019.

[9] J. Xu, W. Hong, Z. H. Jiang and H. Zhang, "Wideband, Low-profile patch array antenna with corporate stacked microstrip and substrate integrated waveguide feeding structure" *IEEE Trans. Antennas Propag.*, vol. 67, no. 2, pp. 1368-1373, Feb. 2019.

[10] Y. F. Wu and Y. J. Cheng, "Proactive conformal antenna array for near-field beam focusing and steering based on curved substrate integrated waveguide," *IEEE Trans. Antennas Propag.*, vol. 67, no. 4, pp. 2354-2363, Apr. 2019.

[11] J. Xu, Z. N. Chen, X. Qing, and W. Hong, "140-GHz TE20-mode dielectric-loaded SIW slot antenna array in LTCC," *IEEE Trans. Antennas Propag.*, vol. 61, no. 4, pp. 1784-1793, Apr. 2013.

[12] J. Xiao, X. Li, Z. Qi and H. Zhu, "140-GHz TE340-Mode substrate integrated cavities-fed slot antenna array in LTCC, " *IEEE Access*, vol. 7, pp. 26307-26313, Feb. 2019.

[13] P.-S. Kildal, "Three metamaterial-based gap waveguides between parallel metal plates for mm/submm waves," in *3rd European Conference on Antennas and Propagation (EUCAP)*, Berlin, Germany, Mar. 2009, pp. 28-32.

[14] J. Liu, J. Yang and A. U. Zaman, "Analytical solutions to characteristic impedance and losses of inverted microstrip gap waveguide based on variational method," *IEEE Trans. Antennas Propag.*, vol. 66, no. 12, pp. 7049-7057, Dec. 2018.

[15] J. Liu, A. Vosoogh, A. U. Zaman, and J. Yang, "A slot array antenna with single-layer corporate-feed based on ridge gap waveguide in the 60-GHz band, "*IEEE Trans. Antennas Propag.*, vol. 67, no. 3, pp. 1650-1658, Mar. 2019.

[16] A. Vosoogh, and P.-S. Kildal, "Corporate-Fed planar 60 GHz slot array made of three unconnected metal layers using AMC pin surface for the gap waveguide," *IEEE Antennas Wireless Propag. Lett.*, pp. 1935-1938, Dec. 2015.

[17] J. Liu, A. Vosoogh, A. U. Zaman and J. Yang, "Design and fabrication of a high gain 60-GHz cavity-backed slot antenna array fed by inverted microstrip gap waveguide," *IEEE Trans. Antennas Propag.*, vol. 65, no. 4, pp. 2117-2122, Apr. 2017.

[18] A. Farahbakhsh, D. Zarifi and A. Uz Zaman, "60-GHz groove gap waveguide based wideband H-plane power dividers and transitions: for use in high-gain slot array antenna, "*IEEE Trans. Microw. Theory Techn.*, vol. 65, no. 11, pp. 4111 - 4121, Nov. 2017.

[19] J. Liu, A. Vosoogh, A. Uz Zaman and P.-S. Kildal, "Design of 8×8 slot array antenna based on inverted microstrip gap waveguide, "*Antennas and Propagation (ISAP), 2016 International Symposium on*, 24-28, October, 2016.

[20] Y. Al-Alem, and A. A. kishk, "High-Gain 60-GHz Slot Antenna with Symmetric Radiation Characteristics, "*IEEE Trans. Antennas Propag.*, vol. 67, no. 5, pp. 2971-2982, Feb. 2019.

[21] M. Ferrando-Rocher, J. I. Herranz-Herruzo, A. Valero-Nogueira, B. Bernardo-Clemente, A. U. Zaman and J. Yang, "8×8 Ka-Band Dual-Polarized Array Antenna Based on Gap Waveguide Technology, "*IEEE Trans. Antennas Propag.*, vol. 67, no. 7, pp. 4579-4588, Jul. 2019.

[22] Z. Talepour and A. Khaleghi, "Groove Gap Cavity Slot Array Antenna for Millimeter Wave Applications, "*IEEE Trans. Antennas Propag.*, vol. 67, no. 1, pp. 659-664, Jan. 2019.

[23] A. Vosoogh, A. Haddadi, A. U. Zaman, J. Yang, H. Zirath, and A. A. Kishk, "W-band low-profile monopulse slot array antenna based on gap waveguide corporate-feed network,"*IEEE Trans. Antennas Propag.*, vol. 66, no. 12, pp. 6997-7009, Dec. 2018.

[24] L. Wang, E. Rajo-Iglesias, J. L. Gmez-Tornero and O. Quevedo-Teruel, "Low-dispersive Leaky-wave antenna integrated in gap waveguide technology,"*IEEE Trans. Antennas Propag.*, vol. 66, no. 11, pp. 5727-5736, Nov. 2018.

[25] S. Y. Jun, B. S. Izquierdo, E. A. Parker, "Liquid Sensor/Detector Using an EBG Structure, "*IEEE Trans. Antennas Propag.*, vol. 67, no. 5, pp. 3366-3373, May. 2019.

[26] Y. Shi et al. "Novel W -Band LTCC Transition From Microstrip Line to Ridge Gap Waveguide and its Application in 77/79 GHz Antenna Array, "*IEEE Trans. Antennas Propag.*, vol. 67, no. 2, pp. 915-924, Feb. 2019.

[27] Q. Wu, J. Hirokawa, J. Yin, C. Yu, H. Wang, and W. Hong, "Millimeter wave multi-beam endfire dual-circularly polarized antenna array for 5G wireless applications,"*IEEE Trans. Antennas Propag.*, vol. 66, no. 9, pp. 4930-4935, Sep. 2018.

[28] M. M. M. Ali and A.-R. Sebak , "2-D Scanning Magnetoelectric Dipole Antenna Array Fed by RGW Butler Matrix,"*IEEE Trans. Antennas Propag.*, vol. 66, no. 11, pp. 6313-6321, Sep. 2018.

[29] F. Fan, J. Yang, V. Vassilev, and A. U. Zaman, "Bandwidth investigation on half-height pin in ridge gap waveguide," *IEEE Trans. Microw. Theory Techn.*, vol. 66, no. 1, pp. 100-108, Jan. 2018.